New Kludge scheme for the construction of approximate waveforms for extreme-mass-ratio inspirals

Carlos F. Sopuerta and Nicolás Yunes

Phys. Rev. D **84**, 124060 — Published 30 December 2011

DOI: 10.1103/PhysRevD.84.124060

New Kludge Scheme for the Construction of Approximate Waveforms for Extreme-Mass-Ratio Inspirals

Carlos F. Sopuerta[1] and Nicolás Yunes[2, 3, 4]

[1] *Institut de Ciències de l'Espai (CSIC-IEEC), Facultat de Ciències, Campus UAB, Torre C5 parells, Bellaterra, 08193 Barcelona, Spain.*
[2] *Department of Physics, Montana State University, Bozeman, MT 59717, USA.*
[3] *Department of Physics and MIT Kavli Institute, 77 Massachusetts Avenue, Cambridge, MA 02139, USA.*
[4] *Princeton University, Physics Department, Princeton, NJ 08544, USA.*

We introduce a new kludge scheme to model the dynamics of generic extreme mass-ratio inspirals (stellar compact objects spiraling into a spinning super-massive black hole) and to produce the gravitational waveforms that describe the gravitational wave emission of these systems. This scheme combines tools from different techniques in General Relativity: It uses a a multipolar, post-Minkowskian expansion for the far-zone metric perturbation (which provides the gravitational waveforms, here taken up to mass hexadecapole and current octopole order) and for the local prescription of the self-force (since we are lacking a general precription for it); a post-Newtonian expansion for the computation of the multipole moments in terms of the trajectories; and a BH perturbation theory expansion when treating the trajectories as a sequence of self-adjusting Kerr geodesics. The orbital evolution is thus equivalent to solving the geodesic equations with *time-dependent* orbital elements, as dictated by the multipolar post-Minkowskian radiation-reaction prescription. To complete the scheme, both the orbital evolution and wave generation require to map the Boyer-Lindquist coordinates of the orbits to the harmonic coordinates in which the different multipolar post-Minkowskian quantities have been derived, a mapping that we provide explicitly in this paper. This new kludge scheme is thus a combination of approximations that can be used to model generic inspirals of systems with extreme mass ratios to systems with more moderate mass ratios, and hence can provide valuable information for future space-based gravitational-wave observatories like the Laser Interferometer Space Antenna and even for advanced ground detectors. Finally, due to the local character in time of our multipolar post-Minkowskian self-force, this scheme can be used to perform studies of the possible appearance of transient resonances in generic inspirals.

PACS numbers: 04.30.-w,04.50.Kd,04.25.-g,04.25.Nx

I. INTRODUCTION

Gravitational waves (GWs) hold the promise to provide detailed information about astrophysical bodies that are obscure in the electromagnetic spectrum, such as binary black hole (BH) systems. Moreover, such waves will allow for the first studies of the nature of the gravitational interaction and of the validity of General Relativity (GR) in the strongest regimes [1, 2]. An accurate modeling of such GWs is essential for the extraction and characterization of weak signals buried in detector noise. This is because waveform templates act as an optimal linear filter that maximizes the signal-to-noise ratio (SNR) in the presence of stochastic noise. The absence of such templates for certain GW sources renders suboptimal any GW search strategy. Therefore, the construction and modeling of GWs to construct accurate templates for data analysis is of paramount importance in the blossoming of GW astrophysics.

One of the staple GW sources of the planned space-based observatory *Laser Interferometer Space Antenna* (LISA) [3, 4] that require accurate templates for their detection and analysis are extreme-mass-ratio inspirals (EMRIs) [5]. These events consist of a small compact object (SCO), such as a stellar-mass BH or neutron star (NS), spiraling in a generic orbit into a spinning, (super)massive black hole (MBH), whose evolution is GW dominated. In such inspirals, the SCO spends up to millions of cycles in close orbits around the MBH, possibly with large pericenter velocities and eccentricities, sampling the strong gravitational field of the MBH.

Many astrophysical scenarios predict the existence of such EMRIs. One such scenario postulates that the SCO exchanges energy and angular momentum with other stars in a stellar core/cusp near a MBH at a galactic center, via two-body relaxation and dynamical friction [5]. If so, the SCO can be swung sufficiently close to the MBH to be gravitationally captured [5, 6], at which point it would slowly inspiral until being swallowed by the MBH. Of course, such a scenario is complicated by mass segregation [7], triaxial density profiles [8], resonant relaxation [9], etc. Other channels of EMRI formation include binary tidal separation [10] (where a binary is disrupted with one component captured by the MBH) and massive star capture or production in accretion discs [11], where the stellar-mass BH is directly formed in the accretion disk of the MBH. It turns out that the EMRI GWs produced by EMRIs in each astrophysical mechanism have distinct characteristic that may be use to distinguish them from EMRI observations [12].

The inspiral is by far the dominant GW phase for EMRI data analysis purposes. This can be understood

rather easily (see, e.g. [13, 14]). The number of cycles accumulated in the inspiral scales with the inverse of the mass ratio $m_\star/M_\bullet$, while in the plunge and merger it scales with the MBH mass $M_\bullet$ only. Since the mass ratio for EMRIs is in the range $\mathcal{O}(10^{-4})$-$\mathcal{O}(10^{-6})$, the characteristic duration and cycle accumulation during the inspiral phase is several orders of magnitude larger than during plunge and merger. In turn, the SNR is in the range $\mathcal{O}(10)$-$\mathcal{O}(10^2)$ for EMRIs at realistic distances and it scales linearly with the total number of cycles. Thus, the contribution of the plunge and merger to the SNR is reduced by a factor of $\mathcal{O}(m_\star/M_\bullet)$ relative to the inspiral contribution. In addition, there is no detectable ringdown for EMRIs, as the SCO barely perturbs the background geometry as it crosses the MBH's event horizon. Since the SCO is not disrupted in EMRI plunges, the SCOs internal structure is erased or *effaced* almost completely, without affecting the inspiral signal.

A positive consequence of the large number of EMRI GW cycles is that these waves carry a detailed map of the MBH geometry, so that we expect to determine the EMRI physical parameters with high precision [15]. This information will be very useful, in particular to test the spacetime geometry of MBHs [16, 17] and even alternative theories of gravity (see, e.g. [17–20]). Moreover, given that the expected even rate is in the range $10-10^3$ EMRIs/yr [7, 21], EMRI observations will allow us to understand better the stellar dynamics near galactic nuclei, populations of stellar BHs, etc. (for a review see [5]), and it also possible that they will tell us about cosmology [22].

Although one is left to model the inspiral phase of EMRIs, this task remains a gargantuan endeavor for several reasons. First, the accuracy requirements for EMRI templates are much more stringent than for comparable-mass binaries. For detection and parameter estimation one usually demands an absolute accuracy of better than 1 and SNR^{-1} radians in the GW phase respectively over the entire time of observation. In a one year inspiral, a typical EMRI can have 10^5 cycles in-band, which then translates into a relative radian accuracy of $\mathcal{O}(10^{-6})$ and $\mathcal{O}(10^{-8})$ for detection and parameter estimation respectively. It is important to note that these precision requirements are just simple estimates that do not take into account data analysis strategies that may relax them (see, e.g. [21]). In contrast, the above relative measure becomes of $\mathcal{O}(10^{-2}/\mathrm{SNR})$ for ground-based data analysis of comparable-mass plunge-merger-ringdowns with current numerical relativity simulations, because these accumulate only $\mathcal{O}(10)$ GW cycles in these phases. In between EMRIs and comparable mass inspirals, there are Intermediate-Mass-Ratio Inspirals (IMRIs), which can be potential sources for both space-based detectors (where an Intermediate-Mass BH (IMBH) inspirals into a MBH) and advanced ground-based detectors (where a SCO inspirals into an IMBH).

The extreme mass ratios involved in the problem also lead to the appearance of two different spatial and time scales. The two different spatial scales are represented by the very different sizes of the MBH and the SCO, $m_\star/M_\bullet \ll 1$, whereas the different time scales are the orbital one and the one associated with the *radiation reaction* effects, $T_{\mathrm{Orbital}}/T_{\mathrm{RR}} \sim m_\star/M_\bullet \ll 1$. An illustration of how this complicates the EMRI problem is the recent work of Lousto and Zlochower [23], who evolved the first $1:100$ mass-ratio binary over the last two orbits before merger and plunge; this simulation took approximately 100 days of computational time using full numerical relativity. This means that with present numerical relativity techniques, full numerical simulations are out of the question for EMRI modeling.

Another key reason for the difficulty of EMRI modeling is their intrinsic strong-relativistic nature. In the interesting part of the EMRI dynamics, the SCO is moving around the strong-field region of the MBH, acquiring large pericenter velocities and even sampling regions inside the ergosphere, leading to large relativistic Γ-factors over tens of thousands of GW cycles. Approximate techniques employed in the comparable-mass regime, such as low-velocity expansions in the post-Newtonian (PN) approximation, are then ill-suited for EMRIs. So neither numerical relativity nor PN theory are, for very different reasons, suitable schemes to model EMRIs.

A better-suited framework that exploits the extreme mass ratios involved is BH perturbation theory, where one treats the SCO as a small perturbation of the MBH background geometry. In this context, the inspiral can be described as the action of a *self-force*. This local vector force is made out of the regularized metric perturbations generated by the SCO, after eliminating divergences due to the particle description of the SCO. The SCO's motion is then governed by the MiSaTaQuWa equation of motion equation, derived in [24, 25] (see also Sec. II). The MiSaTaQuWa equation is considered the foundation of a self-consistent scheme to describe EMRIs in an *adiabatic* way by coupling it to the partial differential equations that describe the perturbations produced by the SCO. For recent discussions on these issues see [26–28] and for general reviews see [29–31].

At present, the gravitational self-force has been computed for the case of a non-rotating MBH using time-domain techniques [32] (see also [33–35] for the study of the physical consequences of the self-force) and progress is being made towards calculations for the more astrophysically relevant case of a spinning MBH [36]. In the meantime, a number of new techniques in the frequency and time domains are being developed to produce accurate and efficient self-force calculations [37]. In any case, given the amount of cycles required for EMRI GWs and the present complexity of self-force calculations, we cannot expect to generate complete waveform template banks by means of full self-force calculations. Instead, the goal of these studies should be to understand all the details of the structure of the self-force so that we can formulate efficient and precise algorithms to create the waveforms needed for LISA data analysis, perhaps complementing some of the existent approximating schemes

that we review below.

A. Existent EMRI Waveform Models

In parallel to the efforts to make progress in the self-force program, there has also been some efforts to build certain less-reliable approximation schemes to model EMRIs. These are very useful, for instance, for parameter estimation studies. We compare and contrast these in Table I, ordered by level of complexity from simplest (top) to most complex (bottom), where we also include the new Kludge scheme at the bottom for comparison.

The simplest model is that of Peters and Mathews [38], in which the SCO is assumed to be moving on Keplerian ellipses. The orbital elements of this ellipse evolve according to leading-order (Newtonian), dissipative radiation-reaction, ie. the quadrupole formula for the loss of energy and angular momentum. Waveforms are then computed also to leading order via the quadrupole formula [44].

A better model was introduced by Barack and Cutler [15], the so-called *Analytical Kludge* waveform model. This model is based on the Peters & Mathews [38] model, but it is enhanced via different PN formulae in order to account for all the relativistic effects, both dissipative and conservative, present in a generic EMRI event. It has the advantage that the orbital evolution is decoupled from the evolution of the additional relativistic effects (which evolve effectively in the radiation-reaction time scale), and hence EMRI waveforms, also prescribed via the quadrupole formula [44], can be computed very fast. For this reason, it has become the method of choice for many LISA parameter estimation and data analysis studies (see, e.g. [45]).

A more sophisticated approach was proposed by Babak, et. al. [39] and is sometimes referred to as the *Numerical Kludge* waveform model. In this setup, the orbital motion is given by geodesics around a Kerr BH and the *radiative* effects are prescribed via PN evolution equations for orbital elements (from 2PN expressions for the fluxes of energy and angular momentum) calibrated to more accurate Teukolsky fluxes with 45 fitting parameters [46]. The waveforms are then modeled again via a multipolar expansion [47], but this time taken to next-to-leading order (quadrupole plus octopole).

Recently, a new hybrid scheme has been proposed by Yunes, et. al. [14, 40, 41] based on effective-one-body (EOB) techniques [48]. In this approach, the SCO-MBH, two-body system is mapped to an effective one-body system: a Kerr BH perturbed by a small effective object. The orbital motion is obtained by solving the Hamilton equations for the Hamiltonian of the effective system. When neglecting conservative self-force corrections, this reduces to solving the geodesic equations in the Kerr background. The radiation-reaction comes from the short-wavelength approximation of Isaacson's [49], where the waveform is constructed from an orbit-averaged, but resummed PN expression [50]. This radiation-reaction force is then enhanced through the addition of very high PN order point-particle results [51, 52] and expressions that account for the flux of energy and angular momentum into the MBH's horizon [52, 53]. Although shown to be accurate for equatorial, circular orbits [40] relative to Teukolsky waveforms, the EOB scheme has not yet been tested for eccentric or inclined orbits.

Another approach is the *Teukolsky*-based scheme of Hughes and others [42, 43, 54–63] have developed. In this model, one prescribes the inspiral as a sequence of *slowly*-changing geodesics. The mapping between them is given by the orbit-averaged evolution of orbital elements, which in turn is obtained by a balance law relating averaged fluxes at the boundaries of spacetime and at the location of the SCO. These averaged fluxes at a given geodesic or point in orbital phase space are computed by solving the Teukolsky equation at that point. Therefore, the construction of any single waveform requires the mapping of the entire orbital phase space, which in turn is computationally prohibitive for truly generic EMRIs. Moreover, this scheme has numerical (and conceptual) difficulties when modeling EMRIs in regimes of spacetime where the evolution deviates from adiabaticity, such as in or close to plunge, around rapidly spinning MBHs ($a/M_\bullet > 0.9$), or highly eccentric inspirals.

B. The New Kludge Scheme

In this paper, we devise a new kludge approximation scheme (relative to numerical kludge) that combines seemingly disparate ingredients from BH perturbation theory and the multipolar post-Minkowskian formalism of Blanchet and Damour [64]. We shall here combine two different approximation schemes, BH perturbation theory (which assumes only that the mass-ratio is small) and the multipolar post-Minkowskian formalism (which assumes the gravitational field strength is small), together with other ingredients related to the choice of coordinate system and waveform construction method.

In the new kludge scheme, the orbital motion is prescribed as a spacetime trajectory that is piecewise geodesic (with respect to the MBH geometry) and such that the different geodesic intervals are connected via the SCO's local, self-acceleration (due to its own gravity in the presence of the MBH). In this sense, each geodesic interval can be chosen arbitrarily small. This is in contrast to the Teukolsky approach (see, e.g. [42]) where the mapping between sequences is given by the averaged (over several orbits) GW energy-momentum fluxes and balance laws. This fact, that the mapping is given purely in terms of quantities *local* to the SCO's worldline and not by non-local balance laws, is a distinctive feature of the new kludge scheme. The implementation of this idea uses the evolution of geodesics with *varying orbital elements*; the energy, angular momentum in the spin direction, and Carter constants are then functions of time

Scheme Name	Orbital Motion	Radiation-Reaction	Waveform Generation
Peters & Mathews [38]	Keplerian Ellipses	Newtonian Order	Multipolar decomposition ($l = 2$)
Analytic Kludge [15]	Keplerian Ellipses	Low-Order PN	Multipolar decomposition ($l = 2$)
Numerical Kludge [39]	Kerr Geodesics	Calibrated Low-Order PN	Multipolar decomposition ($l \leq 3$)
EOB [14, 40, 41]	Kerr Geodesics	Calibrated, Resummed 5.5PN	Resummed 5.5PN ($l \leq 8$)
Teukolsky-based [42, 43]	Kerr Geodesics	Averaged Teukolsky	Adiabatic Teukolsky ($l \lesssim 60$)
This work	Kerr Geodesics	Local Multipolar Post-Minkowskian	Multipolar decomposition ($l \leq 4$)

TABLE I. Comparison of existent modeling schemes.

governed by the self-force.

Such an evolution scheme is a direct implementation of the *osculating orbits* method, proposed by Pound and Poisson [65] and Pound [27]. This method professes that at each point of the SCO's non-geodesic worldline there is a unique geodesic that lies tangent to it. Therefore, the worldline is simply an interpolation between these tangent geodesics. Such a scheme hinges on a fundamental assumption of EMRI modeling: *the adiabatic approximation*, which assumes the deviation vector between adjacent tangent geodesics is small, ie. the radiation-reaction time scale is much longer than all other timescales, particularly the orbital one. As Gralla and Wald [26] explained, the adiabatic approximation only holds quasi-locally around some small neighborhood of proper time at each point of the SCO's worldline. This problem can be circumvented, however, if at each point on the worldline the deviation vector is recomputed, which is exactly the basis of the method of osculating orbits [27, 65].

In the new kludge scheme, the evolution of orbital elements is prescribed by the SCO's self-acceleration, but this quantity is not known exactly (numerically or otherwise) for generic orbits around a spinning MBH. In view of this, we model the self-force via a *radiative approximation*, ie., through the time-asymmetric part of the radiation field, given by the "half-retarded minus half-advanced" Green function [66]. This can be implemented with a high-order multipolar, post-Minkowskian expansion, which assumes gravitational radiation is small relative to the gravitational field of the background, ie. an expansion in powers of Newton's gravitational constant G.

The new kludge, local self-force prescription is completed once we say how the multipole moments depend on the orbital trajectories. This can be achieved by asymptotically matching a PN and a post-Minkowskian solution [67–72]. In this paper, we use only the leading-order expressions for these multipoles, although in the future it would be trivial to including higher PN corrections. As such, we are not consistently keeping a given PN order, but instead using leading-order expressions for the multipole moments, while keeping several such moments in the expansions.

The use of the radiative, multipolar post-Minkowskian expansion is only because of the lack of a more precise self-force. Clearly, this radiative approximation neglects the conservative part of the self-force, which could be important in GW modeling [65]. Once the full self-force becomes available, however, one could easily employ it instead of its post-Minkowskian expansion. Our set-up is general and easily adaptable to other, more precise expressions for the self-force.

Once the orbital evolution has been prescribed, one can construct the GWs again through multipolar, post-Minkowskian expressions in terms of a sum over multipole moments. Since the mapping between Boyer-Lindquist and harmonic coordinates is known, there are no coordinate issues to relate the trajectories obtained from the orbital evolution to the trajectories that enter the definition of the multipole moments. We here employ an expansion to second-order in the multipole moments, including both the mass hexadecapole and the current octopole, thus keeping contributions one order higher than traditional kludge waveforms.

Let us emphasize that the new kludge waveforms are only *approximate* gravitational wave solutions, meant to be used for qualitative descoping studies and investigations of resonant behavior. That is, the waveforms constructed could be used to determine the accuracy to which parameters could be extracted given a detection with new space-based gravitational wave observatories as a function of the detector. Moreover, one could also study how the resonances found by Flanagan and Hinderer [73] affect such parameter estimation and detection. Having said that, improvements would have to be implemented before our kludge waveforms can be used as realistic templates in data analysis. As we will see, the new kludge scheme is amenable to such improvements, which will be the focus of future work.

C. Comparison to Standard Kludge Waveforms

The main advantage of the new kludge scheme is the fact that the radiation-reaction effects are described in terms of a *local* self-force. This means that the inspiral description does not need to average certain gravitational-wave fluxes over a number of periods/orbits like is traditionally done in kludge implementations. Instead, the self-force is prescribed through a multipolar, post-Minkowskian expansion (e.g. the quantity $\mathcal{A}_{\rm RR}$ mentioned above) that contains time-derivatives of the system multipole moments in a non-averaged form.

When implementing such a non-averaged and local scheme, it is critical to use an exact mapping between Boyer-Lindquist coordinates, used in the integration of

the geodesic equations of motion, and harmonic coordinates, employed in the calculation of the multipolar, post-Minkowskian self-force. This eliminates gauge issues that plague kludge waveforms due to the neglect of such a mapping (ie. kludge schemes simply use Boyer-Lindquist like Cartesian coordinates in the multipolar decomposition of the GWs).

The use of a local self-force provides the freedom to choose how often to apply radiation reaction effects in the numerical implementation of the dynamics (trajectory and waveform construction) of the new kludge scheme. The two extremes are: (i) We can apply the self-force at every single time step, which corresponds to the case of a continuous local self-force, or (ii) we can store the information about the self-force and apply it after a certain period of time, mimicking the averaging procedure of other schemes.

These two *extreme* ways of using the new kludge scheme are in correspondence with two very relevant potential applications. Whereas the type of application (ii) can be used to try to generate efficiently EMRI gravitational wave templates for parameter estimation and data analysis development purposes, the type of application (i) seems to be very well fitted for studying local phenomena in the dynamics of EMRIs. In this sense, an important application of our scheme would be to study the transient resonances that Flanagan and Hinderer [73] have recently reported in generic EMRI orbits (eccentric and inclined) when the fundamental orbital frequencies become commensurate. The new kludge scheme can be in principle used to study such behavior and shed some light on the relevance that it may have for future EMRI detection with LISA-like detectors.

Let us clearly state, however, that the new kludges presented here are not intended to model comparable mass systems, for which the effective-one-body framework has proven the most successful [48]. Instead, we here focus on EMRIs only and we are interested in studying local phenomena that no other kludge scheme can currently handle. Perhaps in the future, one could also use effective-one-body tools for such studies, but this would require a tested framework capable of handling completely generic orbits. Work along this lines is currently underway [14, 40, 41].

D. Executive Summary of Main Results

In this paper we present the new kludge scheme, introducing one by one each of its ingredients, from the form of the equations of motion for the inspiral to the GW construction, including the details of the approximations that we use to construct the local self-force that drives the inspiral. From a technical point of view, one of the main challenges of the numerical implementation of our scheme is the computation of high-order time derivatives (of the mass and current multipole moments), which are crucial for the estimation of the radiation reaction effects (the multipolar post-Minkowskian self-force involves up to eight-order time derivatives of the trajectory in harmonic coordinates) and the GW construction (since we are using up to the mass hexadecapole and current octopole multipoles in the calculation, we require up to fourth-order time derivates of the trajectory in harmonic coordinates). The computation of these time derivatives is very challenging, forcing us to implement numerical techniques adapted to the properties of EMRIs dynamics. The key point is to use the fact that geodesic orbits have, in the generic case of eccentric and inclined trajectories, three fundamental frequencies. This then allows us to fit any quantity that needs differentiating to a multiple Fourier series, using a standard least-squares technique. Numerical derivatives of such quantities can then be obtained simply by analytically differentiating the Fourier expansion. Numerical experimentation has shown that this technique works remarkably well, even for the highest-order time derivatives that the new kludge requires.

To illustrate the capabilities of our scheme we show in this paper results from evolutions for different types of orbits: circular equatorial, eccentric equatorial, circular inclined, and the generic eccentric inclined orbits. Using these evolutions we study different aspects of the new kludge scheme. First, we consider the impact of harmonic coordinates in the trajectories and waveform observables in comparison with using other coordinate systems. We find that not properly accounting for this transformation can lead to huge errors in the amplitude and phase of the waveform, eg. up to errors of order a factor of 2 in the total accumulated cycles after a one year evolution. Second, we study the impact of the different radiation reaction potentials in the resulting waveforms. Although these corrections have a smaller impact than the proper use of coordinates, they are still large for strong-field EMRIs. For example, including higher-order terms to the Burke-Thorne potential leads to corrections of order 10^4 radians in a two month evolution. Third, we investigate the use of a quadrupole waveform prescription versus a more accurate hexadecapole-octopole prescription. We find no change in the resulting waveform phases, but an amplitude correction of less than 5%. Fourth, we consider the time-evolution of different orbital parameters when we apply radiation-reaction effects locally in time through our multipolar, post-Minkowskian self-force. Although there are some orbital parameters whose time evolution is not affected, other parameters like the inclination angle can acquire small oscillations with period equal to the orbital period. Such small oscillations are not captured if the self-force is orbit-averaged.

Finally, we perform some tests and comparisons with results in the literature to validate the new kludge numerical implementation. In particular we test the prediction that the inclination angle remains almost constant during the evolution, a test that our scheme successfully passes.

E. Notation and Organization of the Paper

Throughout this paper we use the metric signature $(-,+,+,+)$ and geometric units in which $G = c = 1$. The MBH geometry, whose metric we denote by $\mathrm{g}^{\mathrm{K}}_{\alpha\beta}$, is determined by its mass $M_\bullet$ and (magnitude of the) spin angular momentum $S_\bullet = M_\bullet a$, with dimensionless, Kerr spin parameter $a/M_\bullet$ ($-1 \leq a/M_\bullet \leq 1$). The SCO is parameterized only in terms of its mass $m_\star$ since we neglect its spin and other internal properties. The binary system's parameters are the mass ratio $q \equiv m_\star/M_\bullet$ and the total mass $M_{\rm Tot} = m_\star + M_\bullet$. The reduced mass of the system is therefore $\mu \equiv m_\star M_\bullet/M_{\rm Tot}$, while the symmetric mass ratio is $\eta \equiv \mu/M_{\rm Tot} = q/(1+q)^2$.

The SCO orbit can be parameterized in terms of the constants of geodesic motion $\mathcal{I}^A = (E, L_z, Q/C)$, which stand for the SCO's energy normalized with respect to $m_\star$, the z-component of the angular momentum normalized to $m_\star^2$, and the Carter constant also normalized to $m_\star^2$ (C and Q stand for two definitions of the Carter constant that we use in this paper). Alternatively, we will also parameterize the SCO orbit in terms of the orbital elements $\mathcal{O}^A = (e, p, \iota/\theta_{\rm inc})$, which are also constants of the geodesic motion, where e is the orbit eccentricity, p is the semi-latus rectum, and ι and $\theta_{\rm inc}$ are two measures of the orbit inclination. We present the mappings between $\mathcal{I}^A$ and $\mathcal{O}^A$ in Appendix E. The SCO spacetime trajectory is denoted via $z^\mu(\tau)$, where τ is proper time and thus, its four-velocity is the unit timelike vector $u^\mu \equiv dz^\mu/d\tau$.

Post-Newtonian orders always refer to a *relative* ordering scheme (instead of an absolute one), such that the N-th PN order term refers to one of the form $A = A_{\rm Newtonian}[1 + \ldots + \mathcal{O}(v^{2N}/c^{2N})]$, where $A_{\rm Newtonian}$ is the leading order contribution. We shall commonly drop the factor of $1/c$ when referring to PN expansions.

Greek letters in index lists are used to denote indices on the 4-dimensional spacetime, while Latin letters in the middle of the alphabet $i, j, k, \ldots$ denote spatial indices only. Covariant differentiation is denoted using the symbol ∇_μ, while partial derivatives with respect to the coordinate x^μ are denoted as $\partial_\mu B_\nu$ or $B_{\nu,\mu}$. We denote symmetrization and antisymmetrization with parenthesis and square brackets around the indices respectively, such as $A_{(\mu\nu)} \equiv [A_{\mu\nu} + A_{\nu\mu}]/2$ and $A_{[\mu\nu]} \equiv [A_{\mu\nu} - A_{\nu\mu}]/2$.

We use two main sets of coordinate systems: Boyer-Lindquist coordinates $x^\mu_{\rm BL}$ and harmonic coordinates $x^\mu_{\rm H}$. Other systems of coordinates that we also consider are asymptotic-Cartesian mass-centered (ACMC) coordinates, $x^\mu_{\rm ACMC}$, and approximate harmonic coordinates, $x^\mu_{\rm AH}$. Retarded time is denoted in harmonic coordinates via $t_r \equiv t_{\rm H} - r_{\rm H}$, where $r_{\rm H} \equiv (x^2_{\rm H} + y^2_{\rm H} + z^2_{\rm H})^{1/2}$. When we refer to the Kerr metric, we sometimes use the label K, e.g. $\mathrm{g}^{\rm K}_{\alpha\beta}$ and $\mathrm{g}^{\alpha\beta}_{\rm K}$. In some situations, it is crucial to specify in which coordinate system the metric has to be written in a certain equation, like in a coordinate transformation. In those situations, we also incorporate in the metric (or related objects) a label associated with the coordinate system, e.g. $\mathrm{g}^{\rm K,H}_{\alpha\beta}$ or $\mathrm{g}^{\rm K,BL}_{\alpha\beta}$. As for angular coordinates, we shall find it convenient to sometimes perform multipolar decompositions as in [47], with spin-weighted spherical harmonics ${}_{-2}Y^{\ell m}$ and symmetric and trace-free spherical harmonic tensors $\mathcal{Y}^{\ell m}_L$, where $L = (i_1, i_2, \ldots, i_n)$ is a multi-index (see [47] for details on the multi-index notation).

The organization of this paper is as follows. Section II introduces the self-force approach to EMRI modeling and some basic details of the method of osculating orbits. Section III describes in detail the new kludge scheme, including the MBH geometry and the properties of the geodesic orbits, the application to them of the method of osculating orbits, the multipolar post-Minkowskian approximation to the self-force we use and the radiation-reaction potentials from which it can be obtained, the mapping between Boyer-Lindquist and harmonic coordinates, and the multipolar post-Minkowskian waveform generation formalism that we use in our scheme. Section IV explains the numerical implementation of the new kludge approach and the main numerical techniques that we use. This includes the algorithms for the integration of the ODEs governing the local geodesic motion and the accurate estimation of time derivatives of several orders of the multipole moments. Section V summarizes the different ways in which our scheme can be used and presents several numerical results that illustrate its main features, using from circular equatorial orbits to eccentric inclined orbits. Section VI concludes and discusses several avenues for future research applying the new kludge scheme.

We have attempted to present the main ingredients of our approach in the main body of the paper, relegating some details to the Appendices. Appendix A gives explicit expressions of the different pieces of the multipolar post-Minkowskian self-force in terms of the radiation-reaction and local potentials. It also gives formulae to simplify the computation of the different spatial derivatives of the Kerr local potentials. Appendix B provides complementary formulae related to the mapping between Boyer-Lindquist and harmonic coordinates. In particular, we give expressions for the components of the Jacobian and Hessian, and for the components of the covariant and contravariant Kerr metric tensor in harmonic coordinates. Appendix C constructs a system of asymptotically, mass-centered coordinates and a system of approximate harmonic coordinates that we compare with the exact harmonic coordinates of Sec. III D. Appendix D performs a far-field expansion of the Kerr metric coefficients in the approximate harmonic coordinates of Appendix C. Appendix E describes in detail how to implement the one-to-one mapping between the orbital elements $\mathcal{O}^A = (e, p, \iota/\theta_{\rm inc})$ and the constants of motion $\mathcal{I}^A = (E, L_z, C/Q)$. Appendix F summarizes the main formulae for the computation of the fundamental frequencies and periods with respect to the Boyer-Lindquist coordinate time. Finally, Appendix G provides expressions for the coefficients that determine the evolution of

the radius and Carter constants of an inspiral through circular non-equatorial geodesics.

II. THE SELF-FORCE APPROACH TO EMRIS

In this section we review some of the basic and well-established concepts related to the self-force as they are related to the new kludge approach (see the review papers [30, 31, 74] for details).

The foundations for the first-order perturbative description of EMRIs were laid down in the papers by Mino, Tanaka, and Sasaki [24] and Quinn and Wald [25]. The main result of these papers was the equation of motion of a massive point-like object (describing the SCO) in the geometry of a MBH. The stress-energy tensor of the SCO is then given by

$$T^{\alpha\beta} = m_* \int \frac{d\tau}{\sqrt{-\mathrm{g}}}\, \delta^4\left[x^\mu - z^\mu(\tau)\right] \frac{dz^\alpha}{d\tau}\frac{dz^\beta}{d\tau}\,, \qquad (1)$$

where g denotes the determinant of $\mathrm{g}_{\alpha\beta}$. Then, the SCO generates metric perturbations, $h_{\alpha\beta}$, around the MBH background geometry that in the Lorenz gauge,

$$\nabla_\mu \tilde{h}^{\mu\nu} = 0\,, \quad \tilde{h}^{\alpha\beta} \equiv h^{\alpha\beta} - \frac{1}{2}\mathrm{g}^{\alpha\beta}h\,, \quad h \equiv \mathrm{g}^{\mu\nu}h_{\mu\nu}\,, \quad (2)$$

satisfy the linearized Einstein equations

$$\Box\, \tilde{h}^{\alpha\beta} + 2\, R^{\alpha}{}_{\mu}{}^{\beta}{}_{\nu}\, \tilde{h}^{\mu\nu} = -16\,\pi\, m_\star\, T^{\alpha\beta}\,, \qquad (3)$$

where $\bar{R}^{\mu}{}_{\alpha\nu\beta}$ is the Riemann tensor of the MBH background geometry. However, according to this equation, the metric perturbations diverge at the particle location. Then, the gravitational *backreaction* on the particle motion, the self-force, is provided by the regularized part of the perturbations, say $h^{\mathrm{R}}_{\alpha\beta}$, according to a Hadamard prescription given in [24]. Then, the equation of motion for an EMRI, the MiSaTaQuWa equation, is

$$\frac{d^2 z^\alpha}{d\tau^2} + \Gamma^\alpha_{\mu\nu} u^\mu u^\nu = F^\alpha_{\mathrm{SF}}\,, \qquad (4)$$

where the self-force, F^α_{SF}, is given by

$$F^\alpha_{\mathrm{SF}} = -\frac{1}{2} m_\star \left(\mathrm{g}^{\alpha\lambda} + u^\alpha u^\lambda\right) u^\mu u^\nu \left(2\nabla_\mu h^{\mathrm{R}}_{\nu\lambda} - \nabla_\lambda h^{\mathrm{R}}_{\mu\nu}\right)\,. \qquad (5)$$

Therefore, the dynamics of EMRIs is determined by the coupled system of Eqs. (4),(5), and (2) with a practical regularization scheme (like the *mode sum scheme* [75]). A remarkable point is that Eqs. (4) and (5) can be rewritten as geodesic equations of motion for a point particle in a perturbed geometry that only take into account the regularized part of the metric perturbations, ie. geodesic in the geometry $\mathrm{g}_{\alpha\beta} + h^{\mathrm{R}}_{\alpha\beta}$ [76].

But how do we evolve the trajectory of the SCO accounting for the self-force in a self-consistent way? As it was proposed in [65] (see also [77] and [78] for a recent use of this technique), one can use a relativistic extension of the well-known method of *osculating orbits*. The idea is to take the trajectory to be always tangent to a geodesic orbit, such that the motion transitions smoothly from one geodesic to the next. Such smooth transition is facilitated in EMRI by the fact that EMRI trajectories are very close to a (local) geodesic for a long time. This is because of the clean separation in EMRI time scales: the radiation reaction time scale is much larger than the orbital (geodesic) one, except for the tiny fraction corresponding to the merger-plunge phase.

The way to carry out this transition is to properly account for the time-evolution of the set of *orbital elements* that completely characterize a geodesic orbits. Following [65], it is important to distinguish between two sets of orbital elements: *principal* orbital elements, in our case either $\mathcal{I}^A = (E, L_z, Q/C)$ or $\mathcal{O}^A = (e, p, \iota/\theta_{\mathrm{inc}})$; and *positional* orbital elements that determine the initial position in the geodesic as well as the geodesic initial spatial orientation. The radiation reaction changes in the principal elements are due to the dissipative part of the self-force, while radiation reaction changes in the positional elements are due to the conservative part of the self-force. In this work we only consider dissipative effects and hence we are only concerned with changes in the principal orbital elements.

The implementation of the method of osculating orbits consists in the translation of the fact that at any time there will be a geodesic trajectory, z^μ_{G}, with orbital elements whose position and velocity at that time will coincide with those of the accelerated trajectory. This can be written in the following way:

$$z^\alpha(\tau) = z^\alpha_{\mathrm{G}}\left(\tau; \mathcal{P}^A(\tau); \mathcal{I}^A(\tau)\right)\,, \qquad (6)$$

$$\frac{dz^\alpha}{d\tau}(\tau) = \frac{\partial z^\alpha_{\mathrm{G}}}{\partial \tau}\left(\tau; \mathcal{P}^A(\tau); \mathcal{I}^A(\tau)\right)\,, \qquad (7)$$

where $\mathcal{P}^{\mathcal{A}}$ denote the positional orbital elements. Although we have used here the constants of motion as principal orbital elements, we could also have used $\mathcal{O}^A$. Combining these osculation conditions with the equations of motion (4), we can arrive at the following equations [65]:

$$\frac{\partial z^\alpha_{\mathrm{G}}}{\partial \mathcal{P}^{\mathcal{A}}}\,\frac{d\mathcal{P}^{\mathcal{A}}}{d\tau} + \frac{\partial z^\alpha_{\mathrm{G}}}{\partial \mathcal{I}^{\mathcal{A}}}\,\frac{d\mathcal{I}^{\mathcal{A}}}{d\tau} = 0\,, \qquad (8)$$

$$\frac{\partial}{\partial \mathcal{P}^{\mathcal{A}}}\left(\frac{\partial z^\alpha_{\mathrm{G}}}{\partial \tau}\right)\frac{d\mathcal{P}^{\mathcal{A}}}{d\tau} + \frac{\partial}{\partial \mathcal{I}^{\mathcal{A}}}\left(\frac{\partial z^\alpha_{\mathrm{G}}}{\partial \tau}\right)\frac{d\mathcal{I}^{\mathcal{A}}}{d\tau} = a^\alpha_{\mathrm{SF}}\,, \qquad (9)$$

where a^α_{SF} is the SCO self-acceleration, which is related to the self-force of Eq. (5) by $a^\alpha_{\mathrm{SF}} = m_\star^{-1} F^\alpha_{\mathrm{SF}}$. This is due to the fact that $\mathcal{I}^A$ has been defined as the SCO constants of motion per unit mass. From the inversion of these equations we can obtain the evolution of the different orbital elements. In this paper, we will focus exclusively on the dissipative effects of the self-force which only affect to the principal orbital elements (either $\mathcal{I}^A$ or $\mathcal{O}^A$), ie. $d\mathcal{P}^A/d\tau = 0$ and we ignore the first term in Eqs. (8) and (9). We will refer to the principal orbital elements simply as orbital elements.

III. THE NEW KLUDGE SCHEME

In this section we present all the details of the new kludge scheme. As explained in the previous sections, we separate the problem into two parts: that of constructing the SCO's trajectory and that of building the waveform from these trajectories. We begin then with a description of the background MBH geometry and its associated geodesics. We then show how to enhance the geodesic equation system to allow for the variation of the constants of the motion. The latter require knowledge of the self-acceleration, which we calculate in a multipolar, post-Minkowskian expansion. Finally, we present an explicit transformation between Boyer-Lindquist coordinates (used to evolve the modified geodesic system) and harmonic coordinates, needed to generate waveforms in a multipolar decomposition.

A. MBH Geometry and Geodesic Motion

The geometry of the MBH is modeled by the Kerr metric [79], a vacuum stationary and axisymmetric spacetime that describes the final state of gravitational collapse, according to the BH *no-hair* conjecture [80] and uniqueness theorems (see, e.g. [81]). In Boyer-Lindquist coordinates [82], $(x^\mu_{\rm BL}) = (t, r, \theta, \phi)$, the line element corresponding to the Kerr metric, $\mathrm{g}^{\rm K}_{\alpha\beta}$, is given by

$$ds^2 = -dt^2 + \frac{\rho^2}{\Delta} dr^2 + \rho^2 d\theta^2 + (r^2 + a^2)\sin^2\theta\, d\phi^2 + \frac{2M_\bullet r}{\rho^2}(dt - a\sin^2\theta\, d\phi)^2\,, \tag{10}$$

where $\rho^2 \equiv r^2 + a^2\cos^2\theta$ and $\Delta \equiv r^2 - 2M_\bullet r + a^2 = r^2 f + a^2$, with $f \equiv 1 - 2M_\bullet/r$. For convenience, we also define the quantity $\Sigma^2 \equiv (r^2+a^2)^2 - a^2\Delta\sin^2\theta$. The function Δ has two roots:

$$r_\pm \equiv M_\bullet \pm \sqrt{M_\bullet^2 - a^2}\,. \tag{11}$$

The root r_+ ($\geq r_-$) coincides with the location of the event horizon.

The Kerr geometry is stationary, as described by the timelike Killing vector field $\zeta^\alpha_{(t)} = \delta^\alpha_t$, and axisymmetric, as described by a spacelike Killing vector field $\zeta^\alpha_{(\phi)} = \delta^\alpha_\phi$. It also well-known that the Kerr geometry has an additional symmetry described by a 2-rank Killing tensor, $\xi_{\alpha\beta}$, given by

$$\xi_{\alpha\beta} = \Delta\, k_{(\alpha} l_{\beta)} + r^2\, \mathrm{g}^{\rm K}_{\alpha\beta}\,, \tag{12}$$

where k^α and l^α are the two null principal directions of the Kerr geometry

$$k^\alpha = \left[\frac{r^2+a^2}{\Delta}, -1, 0, \frac{a}{\Delta}\right], \quad l^\alpha = \left[\frac{r^2+a^2}{\Delta}, 1, 0, \frac{a}{\Delta}\right]. \tag{13}$$

When the effect of the self-force is neglected (or equivalently, in the limit of zero mass for the SCO), the SCO follows geodesics orbits of the MBH geometry. The Boyer-Lindquist coordinates of a timelike geodesic can be parameterized in terms of proper time as $z^\mu(\tau) = (t(\tau), r(\tau), \theta(\tau), \phi(\tau))$. For a given geodesic, we can construct three geodesic constants of motion, corresponding to each of the three symmetries of the Kerr spacetime. Stationarity leads to a conserved energy, $\mathcal{E}$, or equivalently an energy per unit mass

$$E \equiv \mathcal{E}/m_\star \equiv -\zeta^{(t)}_\alpha u^\alpha\,. \tag{14}$$

Axial symmetry leads to a conserved component of the angular momentum vector (the one along the spin axis, which we choose to be the z axis)

$$L_z \equiv \mathcal{L}_z/m_\star \equiv \zeta^{(\phi)}_\alpha u^\alpha\,. \tag{15}$$

The Killing tensor symmetry (12) leads to a conserved Carter constant, which can be defined as follows

$$Q \equiv \mathcal{Q}/m_\star^2 \equiv \xi_{\alpha\beta} u^\alpha u^\beta\,, \tag{16}$$

but also we will use the alternative definition

$$C \equiv Q - (L_z - aE)^2\,. \tag{17}$$

The existence of these three symmetries makes the geodesic equations for $z^\mu(\tau)$ integrable and completely separable [83]. The separation can be carried out using the definitions of these constants of motion and also the normalization condition of the four-velocity, $\mathrm{g}^{\rm K}_{\mu\nu} u^\mu u^\nu = -1$. The separated equations of motion for the components of $z^\mu(\tau)$ obey the following set of ordinary differential equations (see [84] for a detailed analysis of the physical properties of the solutions of these equations):

$$\rho^2 \frac{dt}{d\tau} = \frac{1}{\Delta}\left(\Sigma^2 E - 2M_\bullet a r L_z\right), \tag{18}$$

$$\rho^4 \left(\frac{dr}{d\tau}\right)^2 = \left[\left(r^2+a^2\right)E - aL_z\right]^2 - \left(Q + r^2\right)\Delta\,, \tag{19}$$

$$\rho^4 \left(\frac{d\theta}{d\tau}\right)^2 = C - \cot^2\theta L_z^2 - a^2\cos^2\theta\left(1 - E^2\right), \tag{20}$$

$$\rho^2 \frac{d\phi}{d\tau} = \frac{1}{\Delta}\left[2M_\bullet\, a\, r E + \frac{L_z}{\sin^2\theta}\left(\Delta - a^2\sin^2\theta\right)\right]. \tag{21}$$

We are interested here in timelike bound and stable geodesics, what we call *orbits*. These orbits, apart from being characterized by the three constants of motion $\mathcal{I}^A$, can also be characterized by the orbital elements $\mathcal{O}^A$, which can be defined in terms of the turning points of the radial and polar motion (see Appendix E for more details). The turning points for the radial motion are just the minimum and maximum of r, also known as

pericenter and apocenter, $r_{\rm peri}$ and $r_{\rm apo}$, which can be used to introduce the concepts of semi-latus rectum and eccentricity

$$r_{\rm peri} = \frac{pM_\bullet}{1+e}\,, \qquad r_{\rm apo} = \frac{pM_\bullet}{1-e}\,, \tag{22}$$

or equivalently

$$p = \frac{2\,r_{\rm peri}\,r_{\rm apo}}{M_\bullet(r_{\rm peri}+r_{\rm apo})}\,, \qquad e = \frac{r_{\rm apo}-r_{\rm peri}}{r_{\rm peri}+r_{\rm apo}}\,. \tag{23}$$

The turning point for the polar motion is just the minimum of θ, $\theta_{\rm min} \in [0,\pi/2]$, which determines the interval in which θ oscillates, ie. $(\theta_{\rm min}, \pi-\theta_{\rm min})$ and it can be used to introduce the concept of inclination angle, $\theta_{\rm inc} \in [-\pi/2,\pi/2]$, as

$$\theta_{\rm inc} = {\rm sign}(L_z)\left[\frac{\pi}{2}-\theta_{\rm min}\right]\,. \tag{24}$$

Another common definition of orbital inclination angle uses the constants of motion $\mathcal{I}^A$

$$\cos\iota = \frac{L_z}{\sqrt{L_z^2+C}}\,. \tag{25}$$

Alternatively, the orbits can also be characterized in terms of three *fundamental* frequencies (see e.g. [85–87]) with respect to the Boyer-Lindquist coordinate time (they can be also constructed using proper time or any other time): Ω_r, associated with the radial motion (from periapsis to apoapsis and back); Ω_θ, associated with polar motion; and Ω_ϕ, associated with azimuthal motion. These frequencies are important because precessional orbital effects are due to mismatches between them and because they can be used to decompose, among other things, the GW in a Fourier expansion [86].

Expressions for these frequencies in terms of quadratures have been obtained for Kerr in [85], and recently also in [86, 87]. Appendix F provides explicit formulae for the fundamental frequencies and periods used in this paper.

A final consideration regarding geodesic motion that is going to be important in this paper is the $3+1$ splitting of the four-velocity into spatial and time components. This splitting is associated with the time variable used to evolve the geodesic equations, in this paper Boyer-Lindquist time t. The four-velocity of the SCO, $u^\alpha = dz^\mu/d\tau$, choosing the Boyer-Lindquist time parameterization $z^\mu(t) = (t, z^i(t))$, can then be decomposed as

$$u^\mu = \left(\frac{dt}{d\tau}, \frac{dz^i}{d\tau}\right) \equiv \Gamma\,(1, v^i)\,, \tag{26}$$

where Γ and v^i are given by

$$\Gamma = u^t = \frac{dt}{d\tau}\,, \qquad v^i = \Gamma^{-1}u^i = \frac{dz^i}{dt}\,. \tag{27}$$

Using the normalization condition ${\rm g}^{\rm K}_{\mu\nu}u^\mu u^\nu = -1$, the factor Γ, the GR generalization of the special-relativistic Lorentz factor, can be written in terms of the metric and the components of the velocity v^i as follows:

$$\Gamma = \left(-{\rm g}^{\rm K}_{tt} - 2{\rm g}^{\rm K}_{ti}v^i - {\rm g}^{\rm K}_{ij}v^iv^j\right)^{-1/2}\,. \tag{28}$$

B. New kludge Osculating Trajectories

In this work we consider a version of our scheme in which we only include the dissipative effects of the self-force, ie. those that only affect to principal orbital elements. In Sec. VI we discuss how to introduce conservative pieces of the self-force in the new kludge scheme. The time scale of change of $\mathcal{I}^A(\tau)/\mathcal{O}^A(\tau)$, the radiation reaction time scale $T_{\rm RR}$, is much bigger than the orbital time scales $T_{\rm Orbital}$, such that the ratio of these time scales satisfies: $T_{\rm Orbital}/T_{\rm RR} \sim q$.

Following the method of osculating orbits described in Sec. II, we can describe the orbital evolution as given locally in time by the geodesic equations (18)-(21), where the constants of motion are promoted to time-dependent quantities:

$$\mathcal{I}^A \;\longrightarrow\; \mathcal{I}^A(\tau)\,, \qquad \mathcal{O}^A \;\longrightarrow\; \mathcal{O}^A(\tau)\,. \tag{29}$$

Although here we parameterize the time dependence of these quantities in terms of proper time, in practice we will use coordinate time, that corresponds to time associated with distant observers. For our discussion, we denote the solution of the evolution equations (18)-(21) with the modifications of Eq. (29) by $z^\mu(\tau) = [t(\tau), r(\tau), \theta(\tau), \phi(\tau)]$, but it is clear that it would no longer be a solution of the original geodesic equations. We do not decompose this solution, which takes into account self-force effects, into a background geodesic plus a deviation [26], as the deviations grow secularly in time and after a certain number of cycles it cannot be considered a *small* deviation of the background geodesic orbit. Instead, in the spirit of the osculating orbits method, we treat z^μ as a new, self-consistent trajectory that is *continuously* corrected away from geodesic motion during evolution. In this sense, we are constructing an orbit that is made out of geodesic patches corresponding to different constants of motion. The transition from one patch to another is given by the (multipolar, post-Minkowskian) self-force, lacking a more accurate prescription. The length (duration) of the geodesic patches, or equivalently, the frequency at which the constants of motion are updated, is a free parameter that we can choose in the new kludge numerical implementation.

The evolution equations for $\mathcal{I}^A(\tau)/\mathcal{O}^A(\tau)$ can be obtained from the equations of osculating orbits, Eqs. (8) and (9). In our case, the inversion of these equations to find $d\mathcal{I}^A(\tau)/d\tau$ can be done easily by using the symmetries of the Kerr geometry. By applying ${\rm g}^{\rm K}_{\alpha\beta}\zeta^\beta_{(t)}$, ${\rm g}^{\rm K}_{\alpha\beta}\zeta^\beta_{(\phi)}$, and $\xi_{\alpha\beta}u^\beta$ to Eq. (9) in combination with Eqs. (14)-(17) we obtain the evolution equations for E, L_z, and C/Q

respectively.

$$\frac{dE}{d\tau} = -\zeta^{(t)}_{\alpha} a^{\alpha}_{\rm SF}\,, \tag{30}$$

$$\frac{dL_z}{d\tau} = \zeta^{(\phi)}_{\alpha} a^{\alpha}_{\rm SF}\,, \tag{31}$$

$$\frac{dQ}{d\tau} = 2\,\xi_{\alpha\beta} u^{\alpha} a^{\beta}_{\rm SF}\,, \tag{32}$$

$$\frac{dC}{d\tau} = \frac{dQ}{d\tau} + 2\,(aE - L_z)\left(\frac{dL_z}{d\tau} - a\frac{dE}{d\tau}\right)\,. \tag{33}$$

The evolution of these quantities with respect to coordinate time t introduces a factor Γ^{-1} in the above equations, due to the relation: $d/dt = \Gamma^{-1} d/d\tau$. The most important quantity here is the self-acceleration $a^{\alpha}_{\rm SF}$, which as we shall see scales $\sim \Gamma^2$ [see Eq. (57)] and is given by the metric perturbations $h^{\rm R}_{\alpha\beta}$. This is probably the main ingredient of self-force descriptions of EMRIs, which is described in more detail in the next section.

For certain special orbits, the rate of change of the orbital elements satisfies special relations due to the symmetries. One of these are equatorial orbits, ie. orbits with $\theta(t) = \pi/2$. We can see that from Eq. (20) this implies $C = 0$. Therefore, equatorial orbits are characterized by $\theta(t) = \pi/2$ and $C = 0$. Equation (33) allows us to write $dC/d\tau = 2\mathcal{C}_{\alpha} a^{\alpha}_{\rm SF}$, where

$$\mathcal{C}_{\alpha} = (\delta^{\beta}_{\alpha} + u_{\alpha}u^{\beta})\left[\xi_{\beta\lambda}u^{\lambda} + (aE - Lz)\left(\zeta^{(\phi)}_{\beta} + a\zeta^{(t)}_{\beta}\right)\right]\,. \tag{34}$$

The vector $\mathcal{C}_{\alpha}$ vanishes for equatorial geodesics, which implies that the Carter constant $C(t)$ is always zero and $Q(t)$ can be obtained directly from a combination of dE/dt and dLz/dt. The self-force then maps equatorial geodesics to equatorial geodesics, ie. the equatorial character of geodesics is preserved upon self-force evolution.

Another type of orbits with extra symmetries are equatorial and circular orbits. These orbits have a helical symmetry described by an approximate Killing vector (which is exact on the geodesic intervals). This symmetry can be derived from the fact that for these special orbits $d\phi/dt = \Omega_{\phi} = $ const. [see Eq. (21)]. The angular velocity Ω_{ϕ} can be written as (see [84]):

$$\Omega_{\phi} = \pm \frac{v_o^3}{M_{\bullet}\left(1 \pm \frac{a}{M_{\bullet}} v_o^3\right)}\,, \tag{35}$$

where the upper/lower sign corresponds to prograde/retrograde circular orbits (ie. that corotate/counterrotate with the MBH spin and have $L_z > 0/L_z < 0$), $v_o \equiv \sqrt{M_{\bullet}/r_o}$, and r_o is the Boyer-Lindquist radial coordinate of the circular orbit. Then, the helical Killing vector is $\zeta^{\alpha}_{\rm Hel} = \zeta^{\alpha}_{(t)} + \Omega_{\phi}(r)\zeta^{\alpha}_{(\phi)} = \partial^{\alpha}_{t} + \Omega_{\phi}(r)\partial^{\alpha}_{\phi}$. The associated constant of motion is then $\Lambda \equiv {\rm g}^{\rm K}_{\alpha\beta}\zeta^{\alpha}_{\rm Hel}u^{\beta} = -E + \Omega_{\phi}L_z$. The evolution of Λ is $d\Lambda/d\tau = \zeta^{\rm Hel}_{\alpha} a^{\alpha}_{\rm SF}$ and it can be shown that $d\Lambda/d\tau = 0$ for locally circular equatorial orbits. Hence, the evolution of the angular momentum in the spin direction is related to the evolution of the energy by $dL_z/dt = \Omega^{-1}_{\phi} dE/dt$.

Finally, let us consider circular but non-equatorial orbits, ie. orbits with $r = r_o = $ const. but $C \neq 0$. There is no helical symmetry for these orbits due to the fact that the MBH spin is not aligned with the orbital angular momentum. Nevertheless, as shown in [88, 89] the radiation-reaction evolution of these orbits preserves their circular character (see also [42]). These orbits are then characterized by the vanishing of the right-hand side of Eq (19), $R(r_o) \equiv \left[\left(r_o^2 + a^2\right)E - aL_z\right]^2 - \left(Q + r_o^2\right)\Delta(r_o) = 0$ (the radial coordinate does not change), and its first radial derivative, $R'(r_o) \equiv (dR(r)/dr)_{r_o} = 0$ (the orbit is always at a turning point of the radial motion). In addition, the condition $R''(r_o) < 0$ has to be satisfied for the circular orbit to be stable. Following [42], the preservation of the circularity of the orbit along the inspiral translates into the following two conditions: $\dot{R} = 0$ and $\dot{R}' = 0$. From these two conditions we can express the time evolution of the radius of the orbit and the evolution of the Carter constant in terms of the evolution of the energy and angular momentum of the orbit:

$$\left(\begin{array}{c} \dot{C} \\ \dot{r}_o \end{array}\right) = -\frac{1}{d}\left(\begin{array}{cc} c_{11} & c_{12} \\ c_{21} & c_{22} \end{array}\right)\left(\begin{array}{c} \dot{E} \\ \dot{L}_z \end{array}\right)\,, \tag{36}$$

where the coefficients c_{AB} $(A, B = 1, 2)$ and d are functions of $(M_{\bullet}, a; E, L_z, C, r_o)$ and are given in Appendix G. Therefore, the evolution of C and r_o can be obtained by evaluating dE/dt and dL_z/dt from the multipolar, post-Minkowskian self-force.

To finish this section, and as a consistency check, we take the Newtonian limit of the rate of change of the orbital elements in Eqs. (30)-(32). In this limit, we find that to leading order

$$\dot{E} = a^{t}_{\rm RR} = v_i a^{i}_{\rm RR}\,, \tag{37}$$

$$\dot{L}_z = r^2\,\sin^2\theta\, a^{\phi}_{\rm RR}\,, \tag{38}$$

$$\dot{Q} = -2\,r^2\,\sin^2\theta\, a\, a^{\phi}_{\rm RR}\,, \tag{39}$$

$$\dot{C} = -4\,M_{\bullet}\,a\,r\,\cos^2\theta\sin^2\theta\, a^{\phi}_{\rm RR}\,, \tag{40}$$

which agrees with the Newtonian expressions of [90] after transforming to Cartesian coordinates. Notice, however, that Eqs. (30)-(32) contain many more terms than in [90], due to the fact that in the latter the Γ factor is expanded in the low-speed and weak-field limit.

C. Multipolar Post-Minkowskian Self-Acceleration

Here we discuss a method to obtain an approximation for the self-force (5). The most rigorous approach would be to compute this force within the framework of BH perturbation theory, but as already argued, such a task is still under development and in computational terms would be very costly. A different approach is to extract the self-force from the PN equations of motion. Such a path was taken by Pound and Poisson [65] for

a Schwarzschild background and Gair, et al. for a Kerr background [78]. This approach, however, is built under a PN approximation, which is not ideal for EMRI modeling as the SCO can reach relativistic velocities, with significant relativistic Γ factor, as it orbits close to the MBH.

Instead of either of these approaches, we here approximate the self-force via a multipolar, post-Minkowskian expansion (see e.g. [64, 91, 92]):

$$\mathrm{g}^{\rm PM}_{00} = -1 + 2V - 2V^2 + 2V_{\rm RR} + \mathcal{O}(G^{9/2})\,, \quad (41)$$
$$\mathrm{g}^{\rm PM}_{0i} = -4V^i - 4V^i_{\rm RR} + \mathcal{O}(G^{9/2})\,, \quad (42)$$
$$\mathrm{g}^{\rm PM}_{ij} = \delta_{ij}\left[1 + 2V + 2V_{\rm RR} + \mathcal{O}(G^4)\right]\,, \quad (43)$$

where V and V^i are *time-symmetric* potentials, in the sense that they are made out of the half-sum of retarded and advanced integrals of the stress-energy tensor over the source, ie. the half-sum of the retarded and advanced Green functions associated with the perturbative equations. As a consequence, these potentials are invariant under time inversion. The quantities $V_{\rm RR}$ and $V^i_{\rm RR}$ are *time-asymmetric* radiation-reaction potentials, constructed from the half-difference of retarded and advanced waves, and hence, odd under time inversion. These potentials are given by [64, 93]

$$V_{\rm RR}(t_{\rm H}, \boldsymbol{x}_{\rm H}) = -\frac{1}{5}x^{ij}_{\rm H}M^{(5)}_{ij}(t_{\rm H}) + \frac{1}{189}x^{ijk}_{\rm H}M^{(7)}_{ijk}(t_{\rm H}) - \frac{1}{70}\boldsymbol{x}^2_{\rm H}x^{ij}_{\rm H}M^{(7)}_{ij}(t_{\rm H}) + \mathcal{O}(x^{\rm H}_{ij}M^{(9)}_{ij})\,, \quad (44)$$

$$V^i_{\rm RR}(t_{\rm H}, \boldsymbol{x}_{\rm H}) = \frac{1}{21}x^{<ijk>}_{\rm H}M^{(6)}_{jk}(t_{\rm H}) - \frac{4}{45}\epsilon_{ijk}x^{jl}_{\rm H}S^{(5)}_{kl}(t_{\rm H}) + \mathcal{O}(x^{ijk}_{\rm H}M^{(8)}_{ij})\,, \quad (45)$$

where we recall that $(x^\alpha_{\rm H}) = (t_{\rm H}, x^i_{\rm H})$ are spacetime harmonic coordinates, ϵ_{ijk} is the antisymmetric Levi-Civita symbol, and

$$\hat{x}^{<ijk>}_{\rm H} \equiv x^{ijk}_{\rm H} - \frac{3}{5}\boldsymbol{x}^2_{\rm H}\delta^{(ij}x^{k)}_{\rm H}\,. \quad (46)$$

is the symmetric trace-free (STF) projection of the multi-index quantity $x^{ijk} = x^i x^j x^k$. The first term in $V_{\rm RR}$ [Eq. (44)] corresponds to the well-known Burke-Thorne radiation reaction potential [94]:

$$V_{\rm Burke-Thorne}(t_{\rm H}, \boldsymbol{x}_{\rm H}) = -\frac{1}{5}x^{ij}_{\rm H}M^{(5)}_{ij}(t_{\rm H})\,. \quad (47)$$

The quantities $M^{(n)}_{ij}$, $M^{(n)}_{ijk}$, and $S^{(n)}_{ij}$ are the nth-time-derivative of the STF mass quadrupole, mass octopole and current quadrupole moments. Formally, the radiation-reaction potentials depend on the integral of certain derivatives of the asymmetric sum (half-difference of retarded and advanced waves) of multipole moments (see, e.g. Eqs. (2.8) in [93]). Equation (45), however, is obtained by expanding these integrals in a slow-velocity approximation, after which the arguments of the radiation-reaction potentials depend on time only. This is consistent with the fact that the radiation-reaction force is to be evaluated in the source zone of the SCO, and not in the wave zone.

Let us provide explicit expressions for these multipole moments. To lowest order, the mass moments are given by

$$M_{ij} = \eta\, m\, z_{<ij>}\,, \qquad M_{ijk} = \eta\,\delta m\, z_{<ijk>} \quad (48)$$

and the current moment is

$$S_{ij} = \eta\,\delta m\,\epsilon_{kl<i}z_{j>}{}^k\dot{z}^l\,, \quad (49)$$

where angle-brackets are STF projections. To higher order, these moments become more complicated as there are now non-linear contributions from the non-reactive potentials (ie. non-linear contributions from the background) as well as tail and memory contributions. These expressions can be found for example in Eq. (3.1)–(3.3) of [95] and Eq. (5.3)–(5.5) of [96]. In BH perturbation theory language, these higher-order terms would contribute conservative and dissipative corrections to the dissipative equations of motion. We neglect these contributions in the current version of the new kludge approach, but they can be easily incorporated in future improvements of the scheme.

The metric given in Eqs. (41)-(42) is expanded in the far-field limit, a resummation of which is necessary in order to use it for self-force calculations. All terms that are independent of the radiation-reaction potentials can be identified with MBH background geometry terms, corrected perhaps by the presence of the SCO. Neglecting the latter, we can *exactly re-sum* the metric in Eqs. (41)-(43) so that it can written as follows

$$\mathrm{g}^{\rm PM}_{tt} = \mathrm{g}^{\rm K,H}_{tt} + h^{\rm RR}_{tt} + \mathcal{O}(G^{9/2})\,, \quad (50)$$
$$\mathrm{g}^{\rm PM}_{ti} = \mathrm{g}^{\rm K,H}_{ti} + h^{\rm RR}_{ti} + \mathcal{O}(G^{9/2})\,, \quad (51)$$
$$\mathrm{g}^{\rm PM}_{ij} = \mathrm{g}^{\rm K,H}_{ij} + h^{\rm RR}_{ij} + \mathcal{O}(G^4)\,, \quad (52)$$

where $\mathrm{g}^{\rm K,H}_{\mu\nu}$ is the Kerr metric in harmonic coordinates (we shall discuss the issue of coordinates in more detail in Sec. III D) and where we have introduced the metric perturbation, $h^{\rm RR}_{\mu\nu}$, which is given by

$$h^{\rm RR}_{tt} = 2\,V_{\rm RR}\,, \quad h^{\rm RR}_{ti} = -4\,V^i_{\rm RR}\,, \quad h^{\rm RR}_{ij} = 2\,\delta_{ij}V_{\rm RR}\,. \quad (53)$$

These are the metric perturbations that are going to describe the *radiation reaction* effects in our new kludge scheme, and hence they are our approximation to the regularized metric perturbations $h^{\rm R}_{\alpha\beta}$ in Eqs. (4) and (5).

Regarding the MBH background geometry, it is useful for the purposes of this work to introduce some scalar, vector, and tensor *potentials* in harmonic coordinates, which contain information equivalent to the potentials V and V^i in Eqs. (41)-(43):

$$K \equiv K_{00} = \mathrm{g}^{\rm K,H}_{00} + 1\,, \quad Q \equiv Q^{00} = \mathrm{g}^{00}_{\rm K,H} + 1\,, \quad (54)$$

$$K_i \equiv K_{0i} = \mathrm{g}^{\rm K,H}_{0i}\,, \quad Q^i \equiv Q^{0i} = \mathrm{g}^{0i}_{\rm K,H}\,, \quad (55)$$

$$K_{ij} \equiv \mathrm{g}^{\mathrm{K,H}}_{ij} - \delta_{ij}\,, \quad Q^{ij} \equiv \mathrm{g}^{ij}_{\mathrm{K,H}} - \delta^{ij}\,, \tag{56}$$

or more compactly $K_{\mu\nu} \equiv \mathrm{g}^{\mathrm{K,H}}_{\mu\nu} - \eta_{\mu\nu}$ and $Q^{\mu\nu} \equiv \mathrm{g}^{\mu\nu}_{\mathrm{K,H}} - \eta^{\mu\nu}$. The expressions from these local potentials can be derived directly from the expressions of the components of the Kerr metric in harmonic coordinates given in Appendix B 2.

We are now in a position to compute the self-acceleration in terms of the radiation-reaction potentials of Eqs. (44) and (45) through Eq. (53) and Eq. (5). In what follows we develop the expression for the acceleration in order to describe its structure and the role of the different terms that appear on it. The first step is to use the decomposition of the SCO four-velocity given in Eqs. (26) and (27) in such a way as to rewrite Eq. (5) in the following form:

$$a^{\alpha}_{\mathrm{RR}} = -\Gamma^2 P^{\alpha\beta}\left(A^{(1)}_{\beta} + A^{(2)}_{\beta}\right)\,, \tag{57}$$

where we have factored out the dependence on the relativistic Γ factor [see Eq. (A3) for the expression of Γ in terms of the potentials $K_{\mu\nu}$ and the spatial velocity v^i] $P^{\alpha\beta}$ is the projector orthogonal to the SCO four-velocity, $P^{\alpha\beta} = \mathrm{g}^{\alpha\beta}_{\mathrm{K}} + u^{\alpha}u^{\beta}$ (in terms of the potentials $Q^{\mu\nu}$ it is given in Eq. (A2)). The two pieces of the self-acceleration in Eq. (57) contain different terms. The first piece, $A^{(1)}_{\alpha}$, only contains gradients of the radiation-reaction potentials and the spatial velocity v^i, whereas the second piece, $A^{(2)}_{\alpha\beta}$, contains explicit couplings between the MBH potentials (actually their derivatives) and the radiation reaction potentials. The form of these two terms is the following:

$$A^{(1)}_{\alpha} = \mathcal{G}^{\mathrm{RR}}_{\mu\nu\alpha}\, v^{\mu}v^{\nu}\,, \tag{58}$$

where

$$\mathcal{G}^{\mathrm{RR}}_{\mu\nu\alpha} \equiv \frac{1}{2}\left(\partial_{\mu}h^{\mathrm{RR}}_{\nu\alpha} + \partial_{\nu}h^{\mathrm{RR}}_{\mu\alpha} - \partial_{\alpha}h^{\mathrm{RR}}_{\mu\nu}\right)\,, \tag{59}$$

and

$$A^{(2)}_{\alpha} = -h^{\mathrm{RR}}_{\alpha\beta}\,\Gamma^{\beta}_{\mu\nu}\,v^{\mu}v^{\nu}\,, \tag{60}$$

where the connection is to be computed with the Kerr background metric in harmonic coordinates. Putting all these different ingredients together and separating space and time components, we arrive at the following structure for the piece $A^{(1)}_{\alpha}$:

$$A^{(1)}_{t} = \mathcal{A}^{\mathrm{RR}}\,, \qquad A^{(1)}_{i} = \mathcal{A}^{\mathrm{RR}}_{i}\,, \tag{61}$$

where the expressions for the quantities $\mathcal{A}^{\mathrm{RR}}$ and $\mathcal{A}^{\mathrm{RR}}_{i}$, which depend only on the three-velocity v^i and spacetime derivatives of the radiation reaction potentials V^{RR} and V^{RR}_{i}, are given in Eqs. (A4) and (A5) of Appendix A. The second piece of the self-acceleration, $A^{(2)}_{\alpha}$, has the following structure:

$$\begin{aligned} A^{(2)}_{t} &= \left[\mathcal{B}_{\mathrm{RR}} + \mathcal{C}_{\mathrm{RR}} + \mathcal{D}_{\mathrm{RR}}\right] V_{\mathrm{RR}} \\ &\quad + \left[\mathcal{B}^{i}_{\mathrm{RR}} + \mathcal{C}^{i}_{\mathrm{RR}} + \mathcal{D}^{i}_{\mathrm{RR}}\right] V^{\mathrm{RR}}_{i}\,, \end{aligned} \tag{62}$$

$$\begin{aligned} A^{(2)}_{i} &= -2\left[\mathcal{B}_{\mathrm{RR}} + \mathcal{C}_{\mathrm{RR}} + \mathcal{D}_{\mathrm{RR}}\right] V^{\mathrm{RR}}_{i} \\ &\quad - \frac{1}{2}\delta_{ij}\left[\mathcal{B}^{j}_{\mathrm{RR}} + \mathcal{C}^{j}_{\mathrm{RR}} + \mathcal{D}^{j}_{\mathrm{RR}}\right] V_{\mathrm{RR}}\,, \end{aligned} \tag{63}$$

where the quantities $\mathcal{B}_{\mathrm{RR}}$, $\mathcal{B}^{i}_{\mathrm{RR}}$, $\mathcal{C}_{\mathrm{RR}}$, $\mathcal{C}^{i}_{\mathrm{RR}}$, $\mathcal{D}_{\mathrm{RR}}$, and $\mathcal{D}^{i}_{\mathrm{RR}}$, which depend on the SCO three-velocity v^i and the MBH potentials (K, K_i, K_{ij}) and (Q, Q^i, Q^{ij}) and their spatial derivatives, are all given explicitly in Eqs. (A6)-(A11) of Appendix A.

One can check that in the limit $\mathrm{g}^{\mathrm{K,H}}_{\mu\nu} \to \eta_{\mu\nu}$ (or equivalently, $(K, K_i, K_{ij}) \to (2V(1-V), -4V_i, 2V\delta_{ij})$ and $|v| \ll 1$ (in units $c = 1$), the spatial components of the acceleration in Eq. (57) reduce exactly to Eq. (3.11) in [91, 92] order by order. This can be checked by realizing that the self-acceleration here, Eq. (57), is related to the self-acceleration in [91, 92], let us call it a^{i}_{IW}, via

$$a^{i}_{\mathrm{IW}} = \frac{d^2z^i}{dt^2} = \frac{dv^i}{dt} = \Gamma^{-2}\left(a^{i}_{\mathrm{RR}} - v^i a^{t}_{\mathrm{RR}}\right)\,. \tag{64}$$

D. From Boyer-Lindquist to Harmonic Coordinates

The resummed MBH background metric in Eq. (52), the background Kerr metric, must be written in harmonic coordinates in order for all terms to be in the same coordinate system and to be consistent with other ingredients of the new kludge scheme, like the waveform generation procedure described in Sec. III E. However, there are parts of this scheme that are easier to implement in Boyer-Lindquist coordinates, such as the integration of the geodesic equations. Therefore, it is crucial to determine out how to transform from Boyer-Lindquist to harmonic coordinates.

Harmonic coordinates refers to any member of the family of coordinate systems, say $\{x^{\alpha}_{\mathrm{H}}\}$, that satisfy the equation

$$\Box\, x^{\alpha}_{\mathrm{H}} = 0\,, \tag{65}$$

where $\Box$ is the D'Alembertian operator: $\Box \equiv \mathrm{g}^{\alpha\beta}\nabla_{\alpha}\nabla_{\beta}$. When we write down the D'Alembertian operator in this coordinate system, this condition is equivalent to the condition: $\mathrm{g}^{\alpha\beta}_{\mathrm{H}}\Gamma^{\mu,\mathrm{H}}_{\alpha\beta} = 0$, which in turn is equivalent to requiring $\partial_{\beta}\mathfrak{g}^{\alpha\beta}_{\mathrm{H}} = 0$, where $\mathfrak{g}^{\alpha\beta}_{\mathrm{H}} = \sqrt{-g_{\mathrm{H}}}\ \mathrm{g}^{\alpha\beta}_{\mathrm{H}}$. Notice that the harmonic coordinate condition and the harmonic gauge condition are different things. The first expresses a property of a given coordinate system in a given spacetime, whereas the second refers to the correspondence between the background and perturbed spacetimes in perturbation theory. In this sense, the gauge condition $\partial_{\mu}h^{\mu\nu} = 0$, where $h^{\mu\nu} = \mathfrak{g}^{\alpha\beta} - \eta^{\alpha\beta}$, enforces harmonic coordinates at first order in perturbations around flat spacetime. Although the Lorenz gauge condition Eq. (2) is similar to the harmonic gauge condition, these conditions are in general different, coinciding only for perturbations around Minkowski spacetime.

The most commonly employed coordinate systems in GR to describe BH geometries are Schwarzschild or

Boyer-Lindquist coordinates, neither of which is actually harmonic. Although the time and azimuthal Boyer-Lindquist coordinates, t and ϕ, satisfy Eq. (65), the radial and polar coordinates, r and θ, do not. One can further check that Eddington-Finkelstein and Kerr-Schild coordinates are also non-harmonic. Of course, if one considers a vacuum, Minkowski spacetime, then Eq. (65) becomes trivial, $\partial^\alpha \partial_\alpha x^\mu = 0$, which is generically satisfied by many coordinate systems.

Harmonic coordinates for the Kerr metric have been studied extensively in the literature. A harmonic slicing of the Kerr metric was found in [97], where the time-function T is related to Boyer-Lindquist coordinates via

$$T = t + \frac{r_+^2 + a^2}{r_+ - r_-} \ln\left|\frac{r - r_+}{r - r_-}\right| , \tag{66}$$

where $r_\pm$ are given in Eq. (11). Although the slicing is harmonic, the full set of four-dimensional coordinates is not. Ref. [98] did find a full set of harmonic coordinates for Kerr but no explicit expressions for the metric components were given. In [99], based on work by Ding (see Ref. [99] for references on this), a different transformation to harmonic coordinates was found, where the time slicing was not modified. This is very convenient for the new kludge scheme, which is why we adopted this choice in this paper.

Following [99], we can map the Kerr metric from Boyer-Lindquist coordinates (t, r, θ, ϕ) to harmonic ones $(t_{\rm H}, x_{\rm H}, y_{\rm H}, z_{\rm H})$ via the coordinate transformation

$$t_{\rm H} = t \,, \tag{67}$$

$$x_{\rm H} = \sqrt{(r - M_\bullet)^2 + a^2}\ \sin\theta \cos[\phi - \Phi(r)] \,, \tag{68}$$

$$y_{\rm H} = \sqrt{(r - M_\bullet)^2 + a^2}\ \sin\theta \sin[\phi - \Phi(r)] \,, \tag{69}$$

$$z_{\rm H} = (r - M_\bullet)\ \cos\theta \,. \tag{70}$$

while the inverse transformation is

$$t = t_{\rm H} \,, \qquad \phi = \Phi(r) + \arctan\left(\frac{y_{\rm H}}{x_{\rm H}}\right) , \tag{71}$$

$$r = M_\bullet + \frac{1}{\sqrt{2}}\left[r_{\rm H}^2 - a^2 + \sqrt{(r_{\rm H}^2 - a^2)^2 + 4a^2 z_{\rm H}^2}\right]^{1/2} , \tag{72}$$

$$\theta = \arccos\left(\frac{z_{\rm H}}{r - M_\bullet}\right) , \tag{73}$$

We have here introduced the short-hand notation

$$r_{\rm H} \equiv (x_{\rm H}^2 + y_{\rm H}^2 + z_{\rm H}^2)^{1/2} \,, \tag{74}$$

and the angle function $\Phi(r)$, which is given by

$$\Phi(r) = \frac{\pi}{2} - \arctan\left\{\frac{\frac{r - M_\bullet}{a} + \Omega(r)}{1 - \frac{r - M_\bullet}{a}\,\Omega(r)}\right\} , \tag{75}$$

with

$$\Omega(r) = \tan\left[\frac{a}{2\sqrt{M_\bullet^2 - a^2}} \ln\left(\frac{r - r_-}{r - r_+}\right)\right] . \tag{76}$$

The coordinate transformation between Boyer-Lindquist and harmonic coordinates requires expressions for $(\cos\Phi, \sin\Phi)$ and the Jacobian and Hessian of the transformation, which we provide in Appendix B.

We have checked that Eq. (65) is satisfied identically for $(x^\alpha_{\rm H}) = (t_{\rm H}, x_{\rm H}, y_{\rm H}, z_{\rm H})$ in the Kerr background. Moreover, one can see that this transformation reduces to the standard one from Schwarzschild to harmonic coordinates [100] in the $a \to 0$ limit. In this limit, the transformation (68)-(70) reduces to the Euclidean transformation from spherical to Cartesian coordinates, with $r_{\rm H}$ playing the role of the spherical coordinate, related to the radial coordinate r by $r_{\rm H} = r - M_\bullet$.

This explicit coordinate transformation allows us to compute certain ingredients of the new kludge scheme in Boyer-Lindquist coordinates and then transform the result to harmonic coordinates when needed. For instance, the Kerr metric in harmonic coordinate is then simply

$$\mathrm{g}^{\rm K,H}_{\mu\nu} = \mathrm{g}^{\rm K,BL}_{\rho\sigma}\, \frac{\partial x^\rho_{\rm BL}}{\partial x^\mu_{\rm H}} \frac{\partial x^\sigma_{\rm BL}}{\partial x^\nu_{\rm H}} \tag{77}$$

where the Jacobian $\partial x^\rho_{\rm BL}/\partial x^\mu_{\rm H}$ is given in Appendix B 1 and the transformation is shown explicitly in Appendix B 2.

In particular, in the current implementation of the new kludge scheme, we choose to perform the quasi-geodesic evolution using variables associated with Boyer-Lindquist coordinates (see Sec. IV). Then, from the information of the trajectory in Boyer-Lindquist coordinates we can compute the velocity and accelerations in harmonic coordinates using the following relations

$$\dot{\boldsymbol{r}}_{\rm H} = \frac{\partial \boldsymbol{r}_{\rm H}}{\partial x^i_{\rm BL}}\, \dot{x}^i_{\rm BL} = \frac{\partial \boldsymbol{r}_{\rm H}}{\partial r}\, \dot{r} + \frac{\partial \boldsymbol{r}_{\rm H}}{\partial \theta}\, \dot{\theta} + \frac{\partial \boldsymbol{r}_{\rm H}}{\partial \phi}\, \dot{\phi} \,, \tag{78}$$

$$\begin{aligned}\ddot{\boldsymbol{r}}_{\rm H} &= \frac{\partial \boldsymbol{r}_{\rm H}}{\partial x^i_{\rm BL}}\, \ddot{x}^i_{\rm BL} + \frac{\partial^2 \boldsymbol{r}_{\rm H}}{\partial x^i_{\rm BL}\, \partial x^j_{\rm BL}}\, \dot{x}^i_{\rm BL}\, \dot{x}^j_{\rm BL} \\ &= \frac{\partial \boldsymbol{r}_{\rm H}}{\partial r}\, \ddot{r} + \frac{\partial \boldsymbol{r}_{\rm H}}{\partial \theta}\, \ddot{\theta} + \frac{\partial \boldsymbol{r}_{\rm H}}{\partial \phi}\, \ddot{\phi} \\ &+ \frac{\partial^2 \boldsymbol{r}_{\rm H}}{\partial^2 r}\, \dot{r}^2 + \frac{\partial^2 \boldsymbol{r}_{\rm H}}{\partial^2 \theta}\, \dot{\theta}^2 + \frac{\partial^2 \boldsymbol{r}_{\rm H}}{\partial^2 \phi}\, \dot{\phi}^2 \\ &+ 2\left(\frac{\partial^2 \boldsymbol{r}_{\rm H}}{\partial r\, \partial \theta}\, \dot{r}\, \dot{\theta} + \frac{\partial^2 \boldsymbol{r}_{\rm H}}{\partial r\, \partial \phi}\, \dot{r}\, \dot{\phi} + \frac{\partial^2 \boldsymbol{r}_{\rm H}}{\partial \theta\, \partial \phi}\, \dot{\theta}\, \dot{\phi}\right) .\end{aligned} \tag{79}$$

where the Hessian $\partial^2 \boldsymbol{r}_{\rm H}/\partial x^i_{\rm BL}\, \partial x^j_{\rm BL}$ is given in Appendix B 3. Notice that we only need the spatial components of the self-acceleration in Eqs. (30)-(32). With

this acceleration, we can then compute the change in the constants of the motion as we osculate from one geodesic to the next.

On the other hand, thinking about extending the new kludge scheme to systems in which the central object, the MBH in our case, is not described by the Kerr metric but by a different metric tensor (either because the central object corresponds to an exotic distribution of mass or because it is governed by an alternative theory of gravity, or perhaps both), it may happen that transforming to harmonic coordinates may be a very difficult task, even when given an explicit coordinate transformation as the one above is known (although in this case one may resort to numerical computations). Fortunately, one does not need a full coordinate transformation to read off the multipole moments of the background. Thorne [47] has shown that it suffices to work with so-called *asymptotically Cartesian and mass centered coordinates of order N* (ACMC-N). These coordinates are defined such that the background metric is time-independent and has a certain spherical harmonic structure (see, e.g. Eq.(11.1a) in [47]). Thorne has further shown that harmonic coordinates are ACMC-∞, and found an explicit map between Boyer-Lindquist and ACMC-2 coordinates [47]. In Appendix C we construct an ACMC-4 coordinate system and compare it to the exact harmonic coordinates described in this section. The difference between a standard ACMC-4 and its harmonic generalization appears only near the horizon, and in particular, it should affect results when PN corrections to the multipole moments are taken into account. We work here directly in harmonic coordinates as given by Eqs. (67)-(70) and explained in detail in Appendix B.

E. Waveform Generation

Once the orbital evolution, including self-force backreaction, has been computed, one can construct the resulting GWs. Expressions for these as a function of the trajectories can be obtained by solving Eq. (3) either numerically or analytically, via some approximation scheme. Here we use the solution for the waveforms that comes from the combination of post-Minkowskian and PN expansions and which gives rise to standard multipolar expressions (see e.g. [101] for a review). In this way we can write the plus- and cross-polarized solution to Eq. (3) as an infinite series expansion in terms of derivatives of mass and current multipole moments [47, 102]:

$$h_+ - i\,h_\times = \frac{1}{\sqrt{2}}\sum_{\ell,m}\left[U^{\ell m}(t_r) - iV^{\ell m}(t_r)\right]{}_{-2}Y^{\ell m}, \quad (80)$$

where t_r denotes retarded time and $U^{\ell m}$ and $V^{\ell m}$ are *radiative* mass and current multipole moments:

$$U^{\ell m} \equiv \frac{16\pi}{(2\ell+1)!!}\sqrt{\frac{(\ell+1)(\ell+2)}{2\ell(\ell-1)}}\,\mathcal{U}_L\,\mathcal{Y}^{\ell m *}_L\,, \quad (81)$$

$$V^{\ell m} \equiv \frac{-32\pi\ell}{(2\ell+1)!!}\sqrt{\frac{(\ell+2)}{2\ell(\ell+1)(\ell-1)}}\,\mathcal{V}_L\,\mathcal{Y}^{\ell m *}_L\,, \quad (82)$$

where $(\mathcal{U}_L, \mathcal{V}_L)$ are symmetric, trace-free, mass-type and current-type multipole moment tensors (see, e.g. Eq.(15) in [102]). Even for the case of comparable-mass BH mergers, such an expansion taken only up to quadrupole order ($l = 2$) has been shown to be sufficient to recover the waveform to excellent accuracy [103].

This prescription is then complete, once expressions for the radiative moments are given in terms of derivatives of the orbital trajectories. Such identification, however, is difficult, as these moments are defined in the *far-zone* (many gravitational wavelengths away from the center of mass of the binary), and have no knowledge of the *source* multipole moments, defined in the *near zone* (less than a gravitational wavelength from the center of mass). Asymptotic matching can be used to relate the radiative to the source multipole moments [101], yielding explicit expressions that depend only on derivatives of the orbital trajectories in the near-zone. Here, in this initial version of the new kludge scheme, we only consider just the leading order contributions to the multipoles moments, ie. we identify the source and radiative moments: $\mathcal{U}_L = M_L$ and $\mathcal{V}_L = S_L$, ignoring in this way subleading corrections that correspond to tail and memory effects.

In a transverse-traceless gauge, one can rewrite the harmonically decomposed metric perturbation in the following simpler form:

$$h^{\rm TT}_{ij} = \sum_{\ell=2}^{\infty}\left[\frac{4}{\ell!}\frac{1}{r}M^{(\ell)}_{L-2}(t_r)N_{L-2} + \frac{8\ell}{(\ell+1)!}\frac{1}{r}\epsilon_{kl(i}S_{j)kL-1}(t_r)n_l N_{L-2}\right]^{\rm STF}, \quad (83)$$

which, when we consider only multipoles up to the mass hexadecapole and the current octopole, reduces to

$$h^{\rm TT}_{ij} = \frac{2}{r}\ddot{M}^{\rm STF}_{ij} + \frac{2}{3r}\left[\dddot{M}_{ijk}n^k + 4\epsilon^{kl}{}_{(i}\ddot{S}_{j)k}n_l\right]^{\rm STF} + \frac{1}{6r}\left[\ddddot{M}_{ijkl}n^k n^l + 6\epsilon^{kl}{}_{(i}\dddot{S}_{j)km}n^l n^m\right]^{\rm STF}. \quad (84)$$

The expressions for these multipole moments have been given in Eqs. (48) and (49), except for the mass hexadecapole and current octopole multipoles, which are given respectively by

$$M_{ijkl} = \eta\, m\, z_{<ijkl>}\,, \quad (85)$$

$$S_{ijk} = \eta\, m\, \epsilon_{lm<i}z_{jk>}{}^{l}\,\dot{z}^m\,. \quad (86)$$

Again, these moments contain higher order corrections that can also be easily included in subsequent improvements of the new kludge scheme. The plus and cross-polarized projections can then be constructed via

$$h_{+,\times} = e^{ij}_{+,\times} h^{\rm TT}_{ij} \,, \tag{87}$$

where $e^{ij}_{+,\times}$ is the plus- and cross-polarization tensors.

Finally, the observables that one wishes to compute are the GW response functions, which are given by a projection of the plus- and cross-polarized waveform with the beam pattern functions of the detectors. For a detector like LISA there are two such functions, $F_{+,I/II}$ and $F_{\times,I/II}$ (see, e.g. [15, 104] for expressions of these functions) and the response is thus

$$h \equiv \frac{\sqrt{3}}{2\,D_{_L}} \sum_{A=I,II} \left(F_{+,A}\, h_+ + F_{\times,A} h_\times \right) \,, \tag{88}$$

where $D_{_L}$ is the luminosity distance from the source to the observer and the prefactor of $\sqrt{3}/2$ is due to the triangular arrangement of the LISA detector.

F. Summary of the New Kludge Approach

The physical quantity one is interested in is the response function, which is given by Eq. (88) in terms of the beam-pattern functions (see, e.g. [15]) and the plus- and cross-polarized waveform. The latter is given in Eq. (87) in terms of the transverse-traceless metric perturbation. The first approximation we make is to expand $h^{\rm TT}_{ij}$ in post-Minkowskian multipole moments M_{ij}, M_{ijk} and S_{ij} through Eq. (84), where we neglect tail and memory corrections. The second approximation we make is to treat these moments in a Newtonian-like fashion through Eq. (48) and (49) in terms of the trajectory of the bodies, neglecting post-Newtonian corrections due to non-linearities. These two approximations provide the response function as a function of the trajectory of the bodies in harmonic coordinates.

The orbital trajectories are obtained by solving the geodesic equations enhanced by time-varying orbital elements in Boyer-Lindquist coordinates. The time variation of the orbital elements is prescribed by the radiation-reaction acceleration in Eqs. (61), (62) and (63) in harmonic coordinates and in terms of quantities that depend on the harmonic Kerr background [with the map given in Eqs. (C5)-(C8)] and reactive potentials, in turn given in Eq. (45). To evolve osculating orbits, one must therefore map the Boyer-Lindquist acceleration and velocity to harmonic coordinates via Eqs. (78)-(79), so as to compute the rates of change of the orbital elements, which then in turn allows us to map between osculating geodesics. Once the SCO's world-line has been completely obtained, we can use it in harmonic coordinates in the waveform prescription.

The kludge nature of the approach then becomes clear. We employ a combination of approximation schemes that include a multipolar, post-Minkowskian expansion (for the far-zone metric perturbation and for the local prescription of the self-force) a post-Newtonian expansion (for the multipole moments in terms of the trajectories) and a BH perturbation theory expansion (when treating the trajectories as self-adjusting geodesics). All of this is tied together via a non-trivial numerical implementation that is described next.

IV. NUMERICAL IMPLEMENTATION OF THE NEW KLUDGE SCHEME

In this section we provide details of how we have implemented each of the ingredients of the new kludge scheme described in the previous section. The numerical code that we have developed is written in C language [105] and uses different parts of the GNU scientific library [106] as we describe below.

A. Integration of the Equations of Motion

We need to integrate numerically the set of ODEs consisting of Eqs. (18)-(21), and at the same time we need to update the value of the *constants* of motion $(E, L_z, C/Q)$. The separation of the geodesic equations has produced equations for the radial and polar Boyer-Lindquist coordinates, Eqs. (19) and (20) respectively, that have turning points (at pericenter and apocenter in the case of the radial coordinate, and at the location of the orbital inclination angle in the case of the polar coordinate), and at these points we have $\dot{r} = 0$ and $\dot{\theta} = 0$. This means that these are not the best variables for the numerical integration, as ODE solvers present convergence problems at turning points.

To avoid this problem, we introduce new variables in the place of the radial and polar Boyer-Lindquist coordinates, r and θ. These new coordinates are angle variables defined by the following expressions:

$$r = \frac{p M_\bullet}{1 + e\cos\psi} \,, \qquad \cos^2\theta = \cos^2\theta_{\rm min}\cos^2\chi \,. \tag{89}$$

We can write the equations for r and θ in terms of their turning points and other extrema (points at which the time derivatives vanish but are not accessible to the motion). In the case of the radial motion, we can write the right-hand side of Eq. (19) as

$$(1-E^2)(r_{_{\rm apo}} - r)(r - r_{_{\rm peri}})(r - r_3)(r - r_4) \,, \tag{90}$$

where r_3 and r_4 satisfy $r_{_{\rm apo}} > r_{_{\rm peri}} > r_3 > r_4$. In the same way, we can write the right-hand side of the equation for the polar motion [Eq. (20)] in the following form

$$\frac{a^2(1-E^2)}{1-z}\left(z_+ - z\right)\left(z - z_-\right) \,, \tag{91}$$

where

$$z = \cos^2\theta\,, \qquad z_- = \cos^2\theta_{\rm min}\,, \tag{92}$$

and $z_+ > z_-$. We describe in Appendix E the relations between these extrema, ie. $(r_{\rm apo}, r_{\rm peri}, r_3, r_4)$ and (z_-, z_+), and how to find them.

For convenience, we parametrize the trajectory in terms of the Boyer-Lindquist coordinate time t, which is also a time harmonic coordinate, instead of the proper time τ. This is done using Eq. (18) to rewrite the evolution equations with respect to t. In this way, the resulting equations for $(\psi(t), \chi(t), \phi(t))$ are (see also, e.g. [86]):

$$\frac{d\psi}{dt} = \frac{M_\bullet\sqrt{1-E^2}\sqrt{[p(1-e)-p_3(1+e\cos\psi)]\,[p(1+e)-p_4(1+e\cos\psi)]}}{(1-e^2)\,[\Psi(\psi)+a^2E\,z(\chi)]}\,, \tag{93}$$

$$\frac{d\chi}{dt} = \frac{\sqrt{a^2(1-E^2)\left(z_+ - z_-\cos^2\chi\right)}}{\Psi(\psi)+a^2E\,z(\chi)}\,, \tag{94}$$

$$\frac{d\phi}{dt} = \frac{1}{\Psi(\psi)+a^2E\,z(\chi)}\left\{\frac{2M_\bullet a r(\psi)E}{\Delta(r(\psi))} + \left(\frac{1}{1-z(\chi)} - \frac{a^2}{\Delta(r(\psi))}\right)L_z\right\}\,, \tag{95}$$

where we have introduced the following definitions: $p_3 \equiv r_3(1-e)/M_\bullet$, $p_4 \equiv r_4(1+e)/M_\bullet$,

$$\Psi(\psi) \equiv \left[\frac{(r^2(\psi)+a^2)^2}{\Delta(r(\psi))} - a^2\right]E - \frac{2M_\bullet a r(\psi)L_z}{\Delta(r(\psi))}\,, \tag{96}$$

and $r(\psi)$ and $z(\chi)$ are given through Eq. (89). Therefore, the actual outcome of the numerical integration of the ODEs of Eqs. (93)-(95) is a time series of the three angles $(\psi(t), \chi(t), \phi(t))$, which grows monotonically in time. The numerical method we use to integrate these ODEs is the Bulirsch-Stoer extrapolation method ([107]) as described by [108] (see also [109]).

B. Estimation of Time Derivatives

Probably the main challenge in the numerical implementation of the new kludge scheme is the evaluation of the time derivatives of the different quantities involved. To understand the nature of this problem let us focus on the computation of our multipolar, post-Minkowskian self-force. If we look at the expression for the radiation reaction potentials $V_{\rm RR}$ and $V^i_{\rm RR}$, Eqs. (44) and (45), we realize that we need to compute up to the seventh time derivative of the mass quadrupole and octopole moments and up to the fifth time derivative of the current quadrupole moment. But since we also need to compute time derivatives of these potentials [see Eqs. (57) and (61) and also Eqs. (A4) and (A5)] we also need the eighth time derivative of the mass quadrupole and octopole moments and the sixth time derivative of the current quadrupole moment.

In principle, one could think about computing these derivatives analytically by using the equations of motion, Eqs. (18)-(21). The problem is that we need the time derivatives of the trajectory in harmonic coordinates, and to pass from the ODE angles $(\psi(t), \chi(t), \phi(t))$ to harmonic coordinates we need to first use Eq. (89) to go from these angles to Boyer-Lindquist coordinates, and then Eqs. (67)-(70) to go from Boyer-Lindquist to harmonic coordinates. Therefore, we would need to obtain analytically higher time-derivatives of the ODE angles (up to eighth order), which involves using the Christoffel symbols of the Kerr metric and several of their derivatives, and also to differentiate several times Eqs. (89) and (67)-(70). In practice, this makes the analytical computations unfeasible, even using modern computer algebra systems, and even if they weren't, one would worry about the reliability of the numerical evaluation of the huge expressions that one would result.

For these reasons, we resort to a numerical evaluation of these derivatives. The starting point is the fact that we can compute the trajectory, the velocity, and the acceleration almost directly from the integration of the ODE equations (18)-(21) and with a high accuracy. From there, and using purely analytical expressions, we can directly obtain the second time derivatives of the mass quadrupole and octopole moments and the first time derivative of the current quadrupole moment. Thus, we just need to compute up to the six additional time derivative for the mass moments (ie., starting from their second time derivative) and up to the five additional time derivative for the current quadrupole moment (ie., starting from its first time derivative).

Computing numerical derivatives, in contrast to numerical integration, is a subtle task (see, e.g. [109]). For instance, if we consider finite difference formulae for the different derivatives, the computation requires the particular combinations of the function we want to differentiate at points close to the evaluation point, and these combi-

nations are divided by a power of the offset between the different evaluation points. If one chooses the offset to be too small, high-order cancelations in the combinations of the function evaluations can occur beyond machine precision, yielding a meaningless final result. If instead one chooses the offset to be too big, the function might be evaluated at points where its behavior is very different from the one near the evaluation points, which in turn can also lead to large errors in the numerical derivatives. In many situations one can find an interval of offset values in which the high-order derivatives are sufficiently accurate, but such an interval depends on the orbit characteristics and it is not easy to predict. Although we tried many different finite difference rules (from rules involving a few points to rules involving more than 20 evaluation points), as well as other generic numerical differentiation techniques (such as numerical interpolation or Chebyshev differentiation), a large amount of fine-tuning that was difficult to predict seemed essential in all cases.

The key point to improve the differentiation algorithm is to realize that the methods we have just discussed are more general than needed for the EMRI problem. In the latter, one is always dealing with functions with certain properties that can be exploited to construct a better numerical differentiation method. The key feature is that multipole moments are functionals of the trajectories, which are are piecewise timelike bounded Kerr geodesics, and in turn can be characterized by three fundamental frequencies (in the generic case, see the discussion in Sec. III A). Following [86], we know that a general functional of Kerr orbits, let us call it $f[\psi,\chi,\phi](t)$, can be expanded in a multiple Fourier series of these frequencies, that is

$$f[\psi,\chi,\phi](t) = \sum_{k,m,n} f_{k,m,n} e^{-i\,(k\Omega_r + m\Omega_\theta + n\Omega_\phi)\,t}\,, \quad (97)$$

where (k,m,n) are integers running from $-\infty$ to $+\infty$ and $f_{k,m,n}$ are complex coefficients such that $f_{-k,-m,-n} = \bar{f}_{k,m,n}$. There are three special cases in which this expansion is simplified: (i) Circular equatorial orbits; (ii) Equatorial non-circular orbits; (iii) Circular non-equatorial orbits. In case (i), the Fourier series contains only a single frequency, the azimuthal one Ω_ϕ. In case (ii), there are two independent frequencies, Ω_r and Ω_ϕ. In case (iii), there are also two independent frequencies, but they are Ω_θ and Ω_ϕ.

Our procedure to estimate time derivatives is then to first fit an expansion like that of Eq. (97) to the multipole moments that are required using a standard least-square fitting algorithm, and then then to estimate time derivatives via

$$f^{(N)}[\psi,\chi,\phi](t) = \sum_{k,m,n} f^N_{k,m,n} e^{-i\,(k\Omega_r + m\Omega_\theta + n\Omega_\phi)\,t}\,, \quad (98)$$

where

$$f^N_{k,m,n} = (-i)^N (k\Omega_r + m\Omega_\theta + n\Omega_\phi)^N\, f_{k,m,n}\,. \quad (99)$$

The Fourier fits to the multipole moments, therefore, play a crucial role in the accuracy of the high-order derivatives. We carry these fits out by evaluating the function to be fitted on a certain number of points along a geodesic piece of the orbit. As we have already mention, we can compute analytically the first time derivatives of the multipoles, so the time-dependent functions that we actually fit are: $M^{(2)}_{ij}(t)$, $M^{(2)}_{ijk}(t)$, and $S^{(1)}_{ij}(t)$ for the radiation reaction potentials, and also $M_{ijkl}(t)$ and $S_{ijk}(t)$ for the waveforms. The parameters that we need to choose for the least-squares fit are: (i) the size in time of the interval where we fit the function; (ii) the number of points in this interval where the function is going to be evaluated (ie. the number of points to be fitted); and (iii) the number of harmonics/frequencies that we include in the finite expansion of Eq. (97). For choice (i), we take a fixed fraction of the shortest orbital period (ie. of the minimum of $T_r = 2\pi/\Omega_r$, $T_\theta = 2\pi/\Omega_\theta$, and $T_\phi = 2\pi/\Omega_\phi$; see Appendix F). For choice (ii), we use between $50 - 500$ points, depending on the case we are dealing with (generic or very particular) and the precision we want to achieve. For choice (iii), we use between 2 and 5 harmonics of the fundamental frequencies. Adding more harmonics would increase the accuracy of the derivatives, but we have empirically found that 5 harmonics is usually sufficient.

For the practical implementation of the least-squares fit we use the GNU Scientific Library [106]. We have performed a number of experiments for different types of functions (and also for multipole moments of the orbital trajectory) and we have found that this technique is very robust and provides very high accuracy even for the highest derivatives. For instance, for the sixth time derivative we find typical accuracies of one part in 10^5. Taking into account that the magnitude of the time derivatives of the multipole moments decreases significantly with the order of the derivative, this accuracy is more than enough for our purposes. Another important feature of this technique is that is has appeared to be quite robust with respect to the three choices of parameters we have discussed above.

V. NUMERICAL RESULTS

In this section, and in order to illustrate the new kludge scheme, we present some numerical results from a numerical code that we have developed to implement new kludges, as well as some comparison with other results in the literature. The examples of new kludge evolutions shown here are all for prograde orbits but there are no obstacle to produce similar results for retrograde orbits.

Let us first consider our proper use of harmonic coordinates, an ingredient of new kludges that is very different from traditional kludge implementations. In the latter, (see, e.g. [39]) harmonic coordinates are approximated via (Euclidean) Cartesian Boyer-Lindquist coordinates, ie. $(x_{\rm BL}, y_{\rm BL}, z_{\rm BL}) = (r\sin\theta\cos\phi\,, r\sin\theta\sin\phi, r\cos\theta)$.

Such coordinates will differ from true harmonic coordinates greatly in the strong-field regime. In turn, this will modify the resulting trajectories and waveforms, as the proper choice of coordinates is crucial in the calculation of multipole moments, both in radiation reaction computations and in waveform production.

Let us then compare how much error is introduced by the use of the wrong coordinate system in EMRI waveform construction. For this, we employ circular equatorial orbits as they are simpler when comparing the waveform phase. Figure 1 shows a circular-equatorial inspiral orbit for a system with: $a/M_\bullet = 0.1$, $q = 1/10$ and $p_o = 10$, where p_o is the initial value of the semi-latus rectum. That is, both orbits have the same initial semi-latus rectum, and hence the same initial energy and orbital frequency Ω_ϕ. We have chosen such a large mass ratio in this case, so that one could see the trajectory tracks in the figure. The orbit on the left panel has been built and represented using the harmonic coordinates $x^\alpha_{\rm H}$ whereas the orbit on the right has been built and represented using the Cartesian Boyer-Lindquist coordinates $x_{\rm BL}$ (these coordinates are used both for the integration of the geodesic equations of motion and for the estimation of the self-force).

The trajectories in this figure are stopped at the radius of the last stable circular equatorial orbit (LSO), given by [84]:

$$r_{\rm LSO} = M_\bullet \left\{ 3 + Z_2 \mp \sqrt{(3 - Z_1)\,(3 + Z_1 + 2Z_2)} \right\} , \tag{100}$$

where the upper (lower) sign is for prograde (retrograde) orbits, and

$$Z_1 = 1 + \left(1 - \frac{a^2}{M_\bullet^2}\right)^{\frac{1}{3}} \left[\left(1 + \frac{a}{M_\bullet}\right)^{\frac{1}{3}} + \left(1 - \frac{a}{M_\bullet}\right)^{\frac{1}{3}} \right] ,$$

$$Z_2 = \sqrt{3\frac{a^2}{M_\bullet^2} + Z_1^2} .$$

For the evolutions shown in Fig. 1, the LSO $r \approx 5.67 M_\bullet$ and $r_{\rm H} \approx 4.67 M_\bullet$, consistent with $r_{\rm H} \sim r - M_\bullet$.

One must be careful when comparing trajectory tracks, since these are completely coordinate dependent (by definition). Instead, we can compare the number of GW cycles, which are directly observable. The number of orbital cycles in the case of harmonic coordinates is essentially double that of the Boyer-Lindquist Cartesian coordinate case, and consequently, the same is true for the associated waveforms (not shown here). This extremely large distance is perhaps a bit of an overestimate, since we considered very strong field EMRIs and used the two different systems of coordinates in both the waveform generation and the calculation of the multipolar, post-Minkowskian self-force. This last point is important because in many kludge schemes the coordinates only enter in the trajectory and in the waveform construction, whereas the radiation-reaction part is based on PN results or on BH perturbation theory. In any case, this example shows that the proper and consistent choice of coordinates can play a major role in the final waveforms produced.

Let us now consider how other choices in the new kludge scheme modify the final waveforms produced. One approximation one can make to simplify new kludges is to ignore the local potentials $K_{\mu\nu}$ and $Q^{\mu\nu}$ introduced in Eqs. (54)-(56), ie. to pick $K_{\mu\nu} = Q^{\mu\nu} = 0$, or in the case that we use the approximate harmonic coordinates of Appendix C we can use the expansions of Appendix D for these potentials to any order. Obviously this can make a big difference and in our simulations we have always used the Kerr local potentials in exact harmonic coordinates [Eqs. (54)-(56)].

Another approximation one can make is to use just the radiation reaction potential of Burke and Thorne [Eq. (47)] (with $V^i_{\rm RR} = 0$), instead of the full potentials of Eqs. (44) and (45) (see [91, 92]). In order to illustrate the waveform difference in this case we have studied the inspiral of a system with $M_\bullet = 4.5 \times 10^6 M_\odot$, $a/M_\bullet = 0.98$ and $q = 10^{-5}$. In Figure 2 we show the evolution of the semi-latus rectum for two cases, one with $p(t = t_o) \equiv p_o = 3$ (the plot on the left), being t_o the evolution initial time, and the other one with $p_o = 8$. As we can see from the figure, the higher-derivative corrections to the Burke-Thorne radiation-reaction potential [Eqs. (44) and (45)] increase the radiation-reaction effects, in the sense that p and the other orbital elements change more rapidly when these corrections are included. Moreover, these corrections are more significant in the strong field region, near the last stable orbit, and less so as the distance to the MBH increases.

We can assess quantitatively the difference due to introducing corrections to the Burke-Thorne potential by looking at the GWs emitted. To that end, we introduce the following definition:

$$h_+ - i h_\times = \mathcal{A}_{\rm GW}\, e^{i\Phi_{\rm GW}} , \tag{101}$$

where $\mathcal{A}_{\rm GW} = \sqrt{h_+^2 + h_\times^2}$ is the GW amplitude and $\Phi_{\rm GW} = \arctan\left(h_\times/h_+\right)$ is the accumulated GW phase. The GW phase difference induced by the presence of the corrections to the Burke-Thorne potential is shown in Fig. 3 for the evolution with $p_o = 8$ that corresponds to the right panel of Fig. 2. Observe that the GW phase difference increases with time to accumulate up to 4.54 rad for a total evolution time of 0.2 yr. This means we can expect a dephasing of more than 3 cycles for a 1 yr evolution, ie. the radiation reaction corrections to the Burke-Thorne potential are of relevance for precise and long EMRI evolutions. The situation is even more dramatic for the strong field evolution that starts with $p_o = 3$ (left panel of Fig. 2), where the evolution with only the Burke-Thorne potentials takes 55.2 days while the one with the full radiation-reaction potentials takes 42.8 days before reaching an unstable orbit, which translates in a difference of 2862.5 GW cycles.

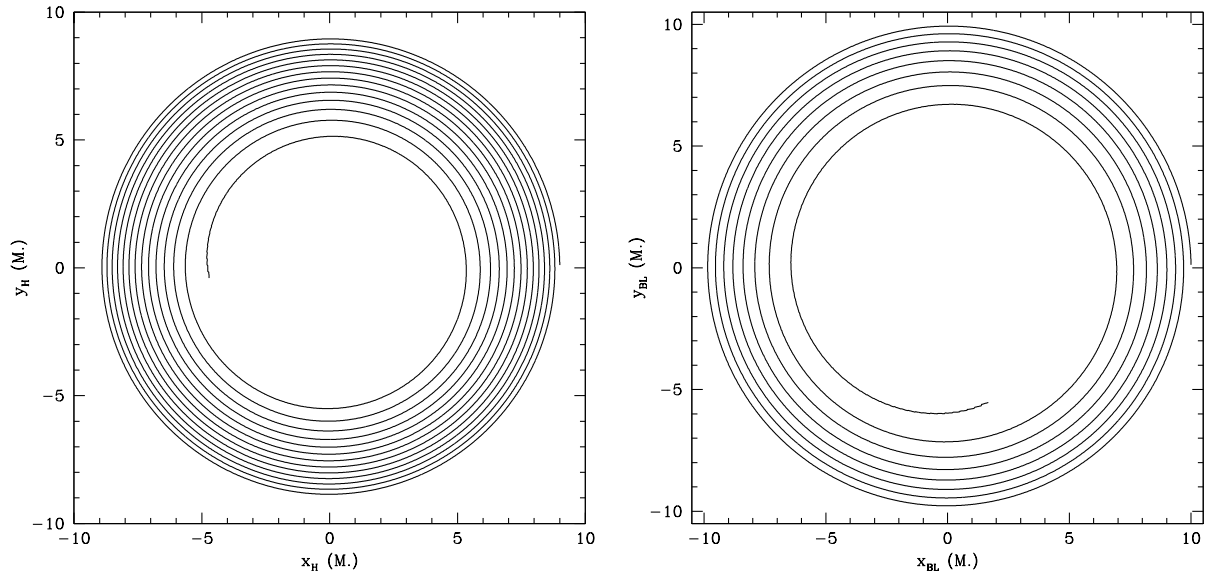

FIG. 1. Circular and equatorial inspiral of a binary system characterized by $a/M_\bullet = 0.1$ and $q = 1/10$. The inspiral starts at $(x, y) = (10, 0)M_\bullet$. The figure on the left shows the inspiral using harmonic coordinates and the figure on the right using Cartesian Boyer-Lindquist coordinates.

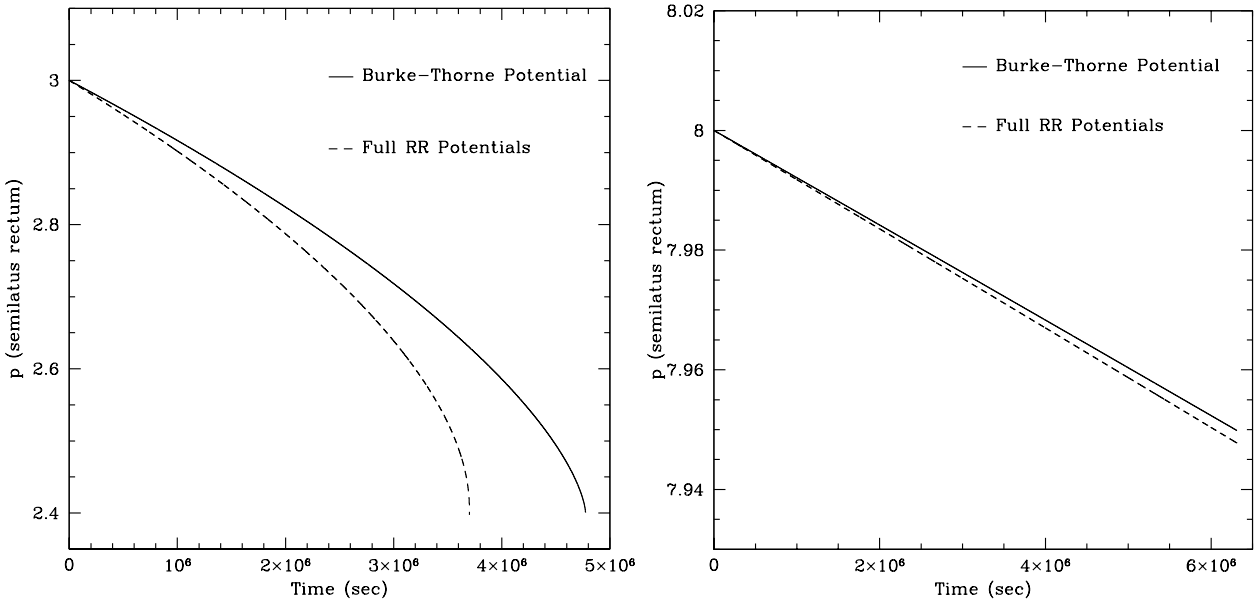

FIG. 2. Evolution of the semi-latus rectum in circular and equatorial inspirals of a binary system characterized by: $M_\bullet = 4.5 \times 10^6 M_\odot$, $a/M_\bullet = 0.98$, and $q = 10^{-5}$. The figure on the left shows an inspiral that has started with $p_o = 3$ and the figure on the right an inspiral that has started with $p_o = 8$. While the one on the left stopped near the last stable circular orbit, the one on the right was stopped after 0.2 yr of evolution.

Finally, let us look at the choices associated with the waveform construction model. In this part of the new kludge scheme, we can choose the multipolar order of the expansion of the gravitational radiation field as described in Sec. III E. Three possibilities present themselves here: (i) *Quadrupolar waveforms*; (ii) *Octopole-Quadrupolar waveforms*; and (iii) *Hexadecapole-Octopolar waveforms*. Case (i) is the lowest-order approximation and consists of considering only the mass quadrupole term in the waveform expansion. This is equivalent to considering up to second time derivatives of the trajectory, ie. up to accelerations. Case (ii) accounts for the next order multipole,

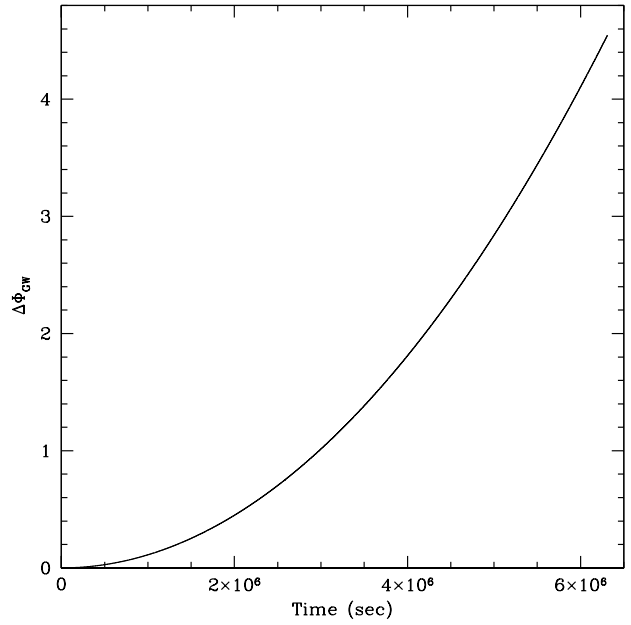

FIG. 3. Evolution of the GW phase difference between two inspirals characterized by: $M_\bullet = 4.5 \times 10^6 M_\odot$, $a/M_\bullet = 0.98$, $q = 10^{-5}$ and $p_o = 8$. The GW phase difference is computed using the formula: $\Delta\Phi_{\rm GW}(t) = \Phi_{\rm GW}^{\rm Burke-Thorne}(t) - \Phi_{\rm GW}^{\rm Full\ RR}(t)$, where $\Phi_{\rm GW}^{\rm Burke-Thorne}$ is the GW phase for an evolution that uses only the Burke-Thorne potential [Eq. (47)] and $\Phi_{\rm GW}^{\rm Full\ RR}$ is the GW phase for an evolution that uses the full radiation-reaction potentials [Eqs. (54)-(56)].

that is, the mass octopole and the current quadrupole. This is equivalent to considering up to third time derivatives of the trajectory, ie. up to the *jerk*: $j^i \equiv d^3x^i/dt^3$. Case (iii) adds one more multipole, that is, the mass hexadecapole and the current octopole. This is equivalent to considering up to the fourth time derivatives of the trajectory, ie. up to the *snap*: $s^i \equiv d^4x^i/dt^4$.

In general, adding more multipoles does not affect the GW phase but it introduces amplitude corrections that depend on the inspiral character. For instance, comparing the quadrupole waveforms with the hexadecapole-octopole waveforms for the evolutions corresponding to Fig. 2, we find no difference in the GW phase, but a 3.3% (for the case with $p_o = 8$) and 4.8% (for the case with $p_o = 3$) difference in the averaged GW amplitude. In this comparison we have used the full radiation-reaction potentials for all evolutions.

Let us now present some results for orbits more generic than circular equatorial, since our kludges can easily handle these as well. Consider first circular non-equatorial orbits, since these are the simplest kind of orbits that allow us to study the evolution of the orbital inclination, either as described by $\theta_{\rm inc}$ [see Eq. (E1)] or by ι [see Eq. (25)]. In this sense, it is interesting to test the conclusions of [42] (see also [110]) that inclination remains almost constant for most such EMRIs and also to compare some quantitative results in order to assess the present new kludge implementation.

The approximation $d\iota/dt = 0$ has been considered by different authors in order to obtain an evolution equation for the Carter constant:

$$\frac{d\iota}{dt} = 0 \quad \Rightarrow \quad \dot{C} = \frac{2C}{L_z}\dot{L}_z\,. \tag{102}$$

Given that it is not simple to estimate the evolution of C within the framework of perturbation theory (see [58, 111]), this approximation provides a clear path to the construction of generic EMRI waveforms. The PN leading-order prediction for the evolution of the inclination given by Ryan [112] predicts a grow in the inclination. Although this prediction is known to overestimate the inclination growth (see [110] for a discussion), it agrees with BH perturbation computations valid in the strong field.

Table II presents some results of the evolution of the radius r_o and Carter constant C for circular non-equatorial orbits characterized by:

(i) $a/M_\bullet = 0.05$, $r_o/M_\bullet = 100$, and $\iota = 60.0$ deg;

(ii) $a/M_\bullet = 0.95$, $r_o/M_\bullet = 100$, and $\iota = 60.05$ deg;

(iii) $a/M_\bullet = 0.05$, $r_o/M_\bullet = 7$, and $\iota = 60.17$ deg;

(iv) $a/M_\bullet = 0.95$, $r_o/M_\bullet = 7$, and $\iota = 60.43$ deg.

These evolutions use Eq. (36) and the formulae of Appendix G. Observe from the table that the new kludge results are in very good agreement with Teukolsky like evolutions, even though the former has not really been refined or optimized.

The local nature of new kludges can also be appreciated in the local, non-uniform temporal changes of the inclination angle, ie. $d\iota/dt$ is not constant in time but oscillates with the orbital period T_θ (see Table III for the value of the fundamental frequencies Ω_θ and Ω_ϕ for the cases of Table II). In contrast, we find that dr_o/dt is approximately constant within orbital time scales. We illustrate these facts in Fig. 4 where we compare the evolution of both quantities for a total time of $\Delta t = 800\, M_\bullet$ and for the third case of Table II, characterized by $a/M_\bullet = 0.05$, $r_o/M_\bullet = 7$, and $\iota = 60.17$ deg. The results of Table II can be obtained via a simple linear regression of the evolution of ι over a number of orbital periods (we quote the slope as the value of $d\iota/dt$ in Table II).

Let us comment further on the results of Table II, classifying them into weak field calculations [cases (i) and (ii)] and strong field ones [cases (iii) and (iv)]. First, as it was already discussed, the new kludge results in the weak field do not differ much using the Burke-Thorne or the full radiation-reaction potentials, whereas in the strong field the differences are significative. Second, considering the absolute value of the numbers quoted in the table, new kludges tend to always underestimate the rate of decay of the radius of the circular orbit, r_o, with respect to the Teukolsky results of [43]. This is in contrast

$a/M_\bullet$	$r_o/M_\bullet$	ι (deg)	Quantity	PN (Ref. [89])	Teukolsky (Ref. [43])	New Kludge Burke-Thorne	New Kludge Full RR
0.05	100	60.00	$q^{-1}\,(dr_o/dt)$	-1.2797×10^{-5}	-1.2676×10^{-5}	-1.1700×10^{-5}	-1.1708×10^{-5}
			$(M_\bullet/q)\,(d\iota/dt)$	7.0439×10^{-12}	6.6936×10^{-12}	6.1597×10^{-12}	6.5089×10^{-12}
0.95	100	60.05	$q^{-1}\,(dr_o/dt)$	-1.2733×10^{-5}	-1.2610×10^{-5}	-1.1622×10^{-5}	-1.1634×10^{-5}
			$(M_\bullet/q)\,(d\iota/dt)$	1.3389×10^{-10}	1.2040×10^{-10}	1.1628×10^{-10}	1.2273×10^{-10}
0.05	7	60.17	$q^{-1}\,(dr_o/dt)$	-3.6762×10^{-2}	-1.0964×10^{-1}	-8.3338×10^{-2}	-8.9633×10^{-2}
			$(M_\bullet/q)\,(d\iota/dt)$	1.5867×10^{-5}	1.0875×10^{-5}	9.6088×10^{-6}	1.6233×10^{-5}
0.95	7	60.43	$q^{-1}\,(dr_o/dt)$	-2.7499×10^{-2}	-4.6574×10^{-2}	-3.4547×10^{-2}	-3.6825×10^{-2}
			$(M_\bullet/q)\,(d\iota/dt)$	3.0806×10^{-4}	1.2073×10^{-4}	1.6023×10^{-4}	2.5962×10^{-4}

TABLE II. Evolution of the radius, r_o, and inclination angle, ι, of circular non-equatorial orbits characterized by (columns 1st to 3rd from top to bottom): (i) $a/M_\bullet = 0.05$, $r_o/M_\bullet = 100$, and $\iota = 60.0$ deg; (ii) $a/M_\bullet = 0.95$, $r_o/M_\bullet = 100$, and $\iota = 60.05$ deg; (iii) $a/M_\bullet = 0.05$, $r_o/M_\bullet = 7$, and $\iota = 60.17$ deg; (iv) $a/M_\bullet = 0.95$, $r_o/M_\bullet = 7$, and $\iota = 60.43$ deg. Column 5th gives the value of $q^{-1}\,(dr_o/dt)$ and $(M_\bullet/q)\,(d\iota/dt)$ obtained from the PN calculations of Ryan [89]; column 6th gives the value obtained by Hughes [43] solving the Teukolsky equation; and columns 7th and 8th are the values obtained with our current new kludge implementation using the Burke-Thorne [Eq. (47)] and the full [Eqs. (44) and (45)] radiation reaction potentials respectively.

$a/M_\bullet$	$r_o/M_\bullet$	ι (deg)	$M_\bullet\Omega_\theta$	$M_\bullet\Omega_\phi$
0.05	100	60.00	9.9992×10^{-4}	1.0000×10^{-3}
0.95	100	60.05	9.9856×10^{-4}	1.0004×10^{-3}
0.05	7	60.17	5.3776×10^{-2}	5.4065×10^{-2}
0.95	7	60.43	4.9813×10^{-2}	5.4537×10^{-2}

TABLE III. Values of the fundamental frequencies Ω_θ and Ω_ϕ (see Appendix F for details) for the four cases shown in Table II. The values of the frequencies are normalized with respect to the MBH mass $M_\bullet$.

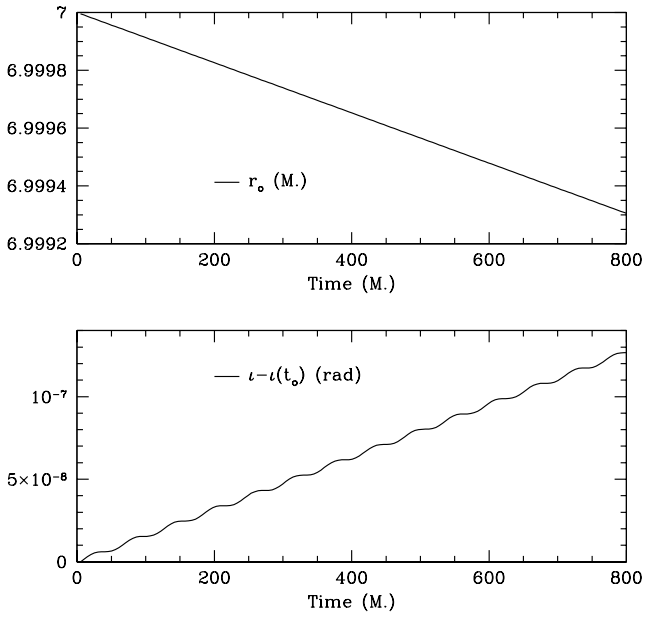

FIG. 4. Evolution of the radius r_o (upper plot) and inclination ι (lower plot) for the circular non-equatorial orbit characterized by $a/M_\bullet = 0.05$, $r_o/M_\bullet = 7$, and $\iota = 60.17$ deg. This is the third case in Table II. The total time of the evolution in units of the MBH mass is $800M_\bullet$.

with the PN results of [89], which overestimate dr_o/dt in the weak field and underestimate it in the strong field.

Regarding the evolution of the inclination angle ι the situation is a bit different, although we can still see similar differences between using the Burke-Thorne and the full radiation-reaction potentials in the strong field computations. For the weak field computations, the differences are significantly bigger for the evolution of ι than for the evolution of r_o. To put these numbers in context, the errors in the new kludge estimations of the rates of r_o and ι, as compared with the Teukolsky estimations, are: for dr_o/dt, $7.63 - 7.83\%$ for the weak field computations and $18.24 - 25.82\%$ for the strong field ones; for $d\iota/dt$, $1.93 - 7.97\%$ for the weak field computations and $11.64 - 115.04\%$ for the strong field ones. In the weak field, the new kludge computations, again assuming that the Teukolsky computations are the correct ones, in general do worse than the PN ones for dr_o/dt but they do better for $d\iota/dt$, whereas in the strong field the new kludge computations seem to be better than the PN ones in general. Of course, this assumes that the Teukolsky waveforms are exactly correct, which is not the case either. A more detailed comparison between Teukolsky and new kludge results will be carried out elsewhere.

Let us finish by considering an example of generic, eccentric and inclined orbital evolutions with the new kludge scheme. For such orbits, all the constants of motion/orbital elements change in time, plotted in Fig. 5 for a sufficiently long time, including many orbital periods. The main figure hides the changes in the orbital time scales, so we have included subplots where we can see that the evolution details scale with the orbital periods. As we have already discussed above, this is a consequence of using a local in time self-force. These effects are not present in evolutionary schemes based on flux averaging over a certain number of orbital periods (essentially all other models currently used).

As we can see in Fig. 5, the local evolution of the different quantities presents slightly different patterns. The difference in these patterns are enhanced if one chooses

a more extreme orbit (more eccentric and more strong field). We can also appreciate that looking at the global evolution (over the long time scale) all quantities decay in time except for the inclination, which grows in time. However, if one looks at the details of the evolution over the orbital periods, one can see (eg. for the eccentricity) that it can locally grow in time although the global tendency is to decay. Therefore, the new kludge scheme leads to quite reach evolutionary patterns due to its local in time character, which also makes it a very valuable tool to investigate questions like the appearance of transient resonances in EMRIs [73].

To illustrate the multipolar waveforms produced by the new kludge scheme for general orbits, Fig. 6 shows short fragments (for the sake of clarity) of the GWs associated with the last evolution of Fig. 5, ie. for the inspiral of a system with $M_\bullet = 10^6 M_\odot$, $a/M_\bullet = 0.98$, and $q = 10^{-5}$, and with initial orbital elements $(p, e, \iota) = (7, 0.6, 57.39$ deg). The waveforms polarizations shown in Fig. 6, which correspond to an observer along the spin axis, present the richness of EMRI GWs for eccentric and inclined orbits.

VI. CONCLUSIONS AND DISCUSSION

We have introduced the new kludge scheme to model the dynamics and the GW emission of EMRIs, which in principle could also be used for intermediate-mass ratio systems. This scheme combines ingredients from the multipolar, post-Minkowskian formalism and black hole perturbation theory to evolve a non-geodesic word line (with respect to the geometry of the binary's large component, assumed here to be a MBH) and construct waveforms. The orbits are built as a sequence of local geodesics whose orbital elements evolve according to a local self-force that we approximate via a multipolar, post-Minkowskian expansion. The leading order term of this self-force corresponds to the well-known Burke-Thorne radiation-reaction potential. We have seen that a crucial ingredient in this construction is the mapping from Boyer-Lindquist coordinates, in which we integrate locally in time the orbits to the harmonic coordinates required both by the multipolar, post-Minkowskian self-force and for the GW multipolar expansion. Once we have trajectories in harmonic coordinates, it is straightforward to build waveforms.

In practice, the implementation of the new kludge schemes requires a number of numerical/analytical ingredients. First, one must numerically integrate (locally in time) geodesic equations, for which we use appropriate angle variables that avoid turning points. From the integration of these equations, we can use analytical formulae to map the trajectories (and associated velocities and accelerations) to harmonic coordinates. Then, information from small fragments of the geodesic orbit (smaller than the fundamental orbital periods) is used to build the different multipole moments and compute their time derivatives. We have found this to be the most challenging point of the implementation as we need up to eight-order time derivatives of the multipoles, in particular of the mass quadrupole. Numerical differentiation is much more complicated than numerical integration, since the choice of the offset in finite difference formulae is crucial to obtain correct results. By experimenting with different numerical techniques we have concluded that general differentiation techniques (ie. valid for any differentiable function) are quite difficult to implement successfully (specially for the high-order derivatives required), since the derivatives require precise fine-tuning that depends on the fundamental frequencies of motion. The way out has been to use a numerical method that takes into account what we know analytically about local motion: the fundamental frequencies. More specifically, we find that fitting a truncated multi-period (the fundamental periods, which we also obtain numerically in terms of elliptic integrals) Fourier series to fragments of the local evolution using standard least-squares methods provides the accuracy that we require for a precise estimation of the radiation-reaction potentials and the self-force. With this, we can then evolve the constants of motion, thus mapping from the initial geodesic to new ones. Such a transition requires the mapping of the new constants of motion $(E, L_z, C/Q)$ to the new orbital elements $(e, p, \iota/\theta_{\rm inc})$, which can be done using analytic formulae. Repeating this procedure iteratively in time, we build the inspiral trajectory or worldline, from which we then finally construct the waveforms.

Apart from the exact harmonic coordinates of Ding (see Ref. [99]) that we use in our implementation, we have also provided approximate harmonic coordinates based on the construction of ACMC coordinates (see Appendices C and D). The construction of these coordinates is a useful exercise that can be used in scenarios where the big component of the binary is not described by the Kerr geometry but by something else either related with other theories of gravity or with the idea that MBH at galactic centers may be exotic matter configurations rather than black holes.

The results presented here serve as a first introduction and proof-of-principle of the new kludge scheme. Much work remains to be done to improve and to validate the method in order to obtain GWs to the level of accuracy required for LISA data analysis. One clear way of improving the scheme is to use better expressions for the different multipole moments that go beyond the present leading-order approximation. One caveat of doing this is that the PN corrections required are in general not known for generic spinning binaries. In any case, the currently known PN corrections will certainly improve the accuracy of the new kludge evolutions. Another way to improve the scheme would be to introduce conservative corrections to the background, for instance as it is done in the EOB formalism [48].

A more detailed and exhaustive validation of the new kludge scheme would include, as a first step, a compari-

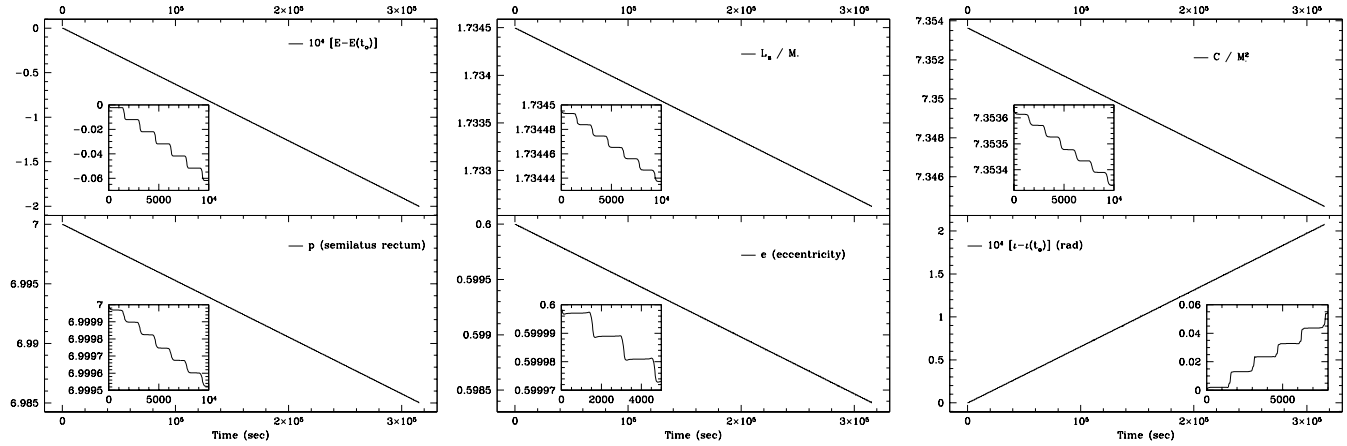

FIG. 5. Evolution (for a total time of 10^{-2} yrs) of an eccentric and inclined inspiral of a system characterized by: $M_\bullet = 10^6 M_\odot$, $a/M_\bullet = 0.98$, and $q = 10^{-5}$. The plots show the evolution of the following quantities: Energy E (top left), actually $10^4[E - E(t_o)]$, where $E(t_o) = 0.9575513$; angular momentum along the spin axis, L_z (top centre); Carter constant C (top right); semi-latus rectum, p (bottom left), with $p(t_o) = 7$; eccentricity, e (bottom centre), with $e(t_o) = 0.6$; and inclination angle ι (bottom right), actually $10^4[\iota - \iota(t_o)]$, where $\iota(t_o) = 57.39$ deg. All plots contain subplots where the detailed evolution during a few orbital periods is shown.

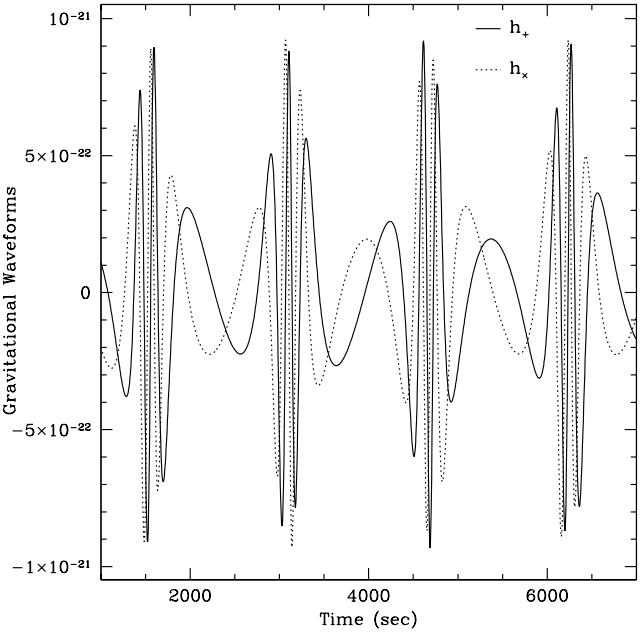

FIG. 6. Fragments of the GWs emitted from an eccentric and inclined system [with initial orbital elements $(p, e, \iota)(t_o) = (7, 0.6, 57.39 \text{ deg})$] characterized by: $M_\bullet = 10^6 M_\odot$, $a/M_\bullet = 0.98$, and $q = 10^{-5}$. The evolution of the constants of motion and orbital elements of this system are shown in Figure 5. The solid line represents the + polarization, $h_+(t)$, and the dotted line represents the × polarization, $h_\times(t)$, as seen by an observer located along the spin axis.

son of the evolution of the constants of motion with the fluxes associated with them that are calculated by solving the Teukolsky equation [42, 43]. As we have already mentioned above, one has to be careful in doing this comparison given that the latter employs averages over several cycles, while the new kludge fluxes are computed locally at the SCO's location. Once the fluxes have been validated, one should compare the waveforms themselves. An overlap study would determine the level of agreement between them.

Another interesting aspect that we can test is whether the new kludge scheme can be used for IMRIs and even for systems with moderate mass ratios. Recently, comparisons between self-force, PN, and numerical relativity computations have arrived to the conclusion that by replacing the mass ratio q by the symmetric mass ratio η, the self-force predictions compare quite well with numerical relativity and PN predictions in the comparable-mass range [33, 35]. These results may allow for a simpler description of IMRIs, which otherwise would require either long full numerical computations or higher-order perturbative computations, or a combination of both. In the new kludge scheme, $q \to \eta$ is actually mostly built in already, since the mass ratio information enters through the definition of the multipole moments [see Eqs. (48), (49), (85), and (86)]. For these, we already use general binary expressions, instead of effective one-body ones with mass $qM_\bullet$. Therefore, it would be interesting to see whether future improvements of the new kludge scheme can produce reasonably good results for systems other than EMRIs.

The ability to compute approximate local quantities at the location of the SCO, in particular the multipolar, post-Minkowskian self-force, makes the new kludge scheme an interesting tool to study certain local behavior believed to exist in EMRIs. For example, Flanagan and Hinderer [73] have recently reported that certain rapid changes in orbital elements can arise for generic EMRIs when the orbital frequencies become commensurate.

During these rapid changes, it has been postulated that the EMRI waveforms might suffer a "glitch," not unlike those observed in pulsar astronomy. Questions remain though as to the exact nature of this effect. One could compare the effect of these glitches in waveforms as computed from an averaged-scheme (such as the Teukolsky one) and a local one (such as the new kludge approach). These, and other studies, would provide one more piece to the EMRI puzzle.

ACKNOWLEDGMENTS

We would like to thank Leor Barack, Jon Gair and Frans Pretorius for useful comments and suggestions. We also thank the anonymous referee for criticisms and suggestions that have improved the paper. CFS acknowledges support from the Ramón y Cajal Programme of the Ministry of Education and Science of Spain, by a Marie Curie International Reintegration Grant (MIRG-CT-2007-205005/PHY) within the 7th European Community Framework Programme, and from the contract ESP2007-61712 of the Spanish Ministry of Education and Science. CFS also acknowledges the hospitality of Princeton University and M.I.T. where part of this work was completed. NY acknowledges support from NSF grant PHY-0745779 and PHY-1114374, as well as support provided by the National Aeronautics and Space Administration through Einstein Postdoctoral Fellowship Award Number PF0-110080, issued by the Chandra X-ray Observatory Center, which is operated by the Smithsonian Astrophysical Observatory for and on behalf of the National Aeronautics Space Administration under contract NAS8-03060. NY also acknowledges support from NASA grant NNX11AI49G, under sub-award 00001944, and the hospitality of the Institut de Ciències de l'Espai (CSIC-IEEC) where part of this work was completed. We also acknowledge the Centro de Supercomputación de Galicia (CESGA) project no ICTS-CESGA-200.

Appendix A: Useful Formulae for the Computation of the Self-Acceleration

In this appendix we define the quantities relevant to the multipolar, post-Minkowskian radiation-reaction acceleration of Eq. (57), where the pieces $A^{(1)}_\alpha$ and $A^{(2)}_\alpha$ are given in Eqs. (58) and (60) respectively. We also need the expression of the projector orthogonal to the SCO four-velocity. This quantity can be written in terms of the potentials $K_{\mu\nu}$ and $Q^{\mu\nu}$ as follows:

$$P^{\alpha\beta} = \eta^{\alpha\beta} + Q^{\alpha\beta} + \Gamma^2 v^\alpha v^\beta \,, \tag{A1}$$

$$P_{\alpha\beta} = \eta_{\alpha\beta} + K_{\alpha\beta} + \Gamma^2 v_\alpha v_\beta \,. \tag{A2}$$

where the Γ factor was already given in Eq. (28), but it can also be rewritten, in terms of the $K_{\mu\nu}$ potentials, as

$$\Gamma = \frac{1}{\sqrt{1 - v^2 - K - 2K_i v^i - K_{ij} v^{ij}}} \,, \tag{A3}$$

where we can see how the relativistic Γ factor is modified, with respect to the Special Relativity form $\Gamma = (1 - v^2)^{-1/2}$, due to Kerr *local* potentials.

The first piece of the self-acceleration, $A^{(1)}_\alpha$, is determined by the object $\mathcal{G}^{\rm RR}_{\mu\nu\alpha}$ [Eq. (59)]. The time and spatial components of $A^{(1)}_\alpha$ [see (61)] are given by

$$\mathcal{A}^{\rm RR} = \left(1 - v^2\right) \partial_t V_{\rm RR} + 2 v^i \partial_i V_{\rm RR} - 4 v^{ij} \partial_i V^{\rm RR}_j \,, \tag{A4}$$

$$\mathcal{A}^{\rm RR}_i = -\left(1 + v^2\right) \partial_i V_{\rm RR} + 2 v_i \partial_t V_{\rm RR} + 2 v_i v^j \partial_j V^{\rm RR} - 8 v^j \partial_{[j} V^{\rm RR}_{i]} - 4 \partial_t V^{\rm RR}_i \,. \tag{A5}$$

The second piece of the self-acceleration, $A^{(2)}_\alpha$, is linear in the radiation-reaction potentials $V_{\rm RR}$ and $V^{\rm RR}_i$ [see Eq. (60)]. The coefficients of the linear combinations of these potentials in the time and spatial components of $A^{(2)}_\alpha$ [Eqs. (62) and (63) respectively] have the following form:

$$\mathcal{B}_{\rm RR} = Q^i \partial_i K \,, \tag{A6}$$

$$\mathcal{C}_{\rm RR} = 2 \left(1 - Q\right) v^i \partial_i K + 4 Q^i v^j \partial_{[i} K_{j]} \,, \tag{A7}$$

$$\mathcal{D}_{\rm RR} = 2 \left(1 - Q\right) v^{ij} \partial_i K_j - Q^i v^{jk} \left(2 \partial_{(j} K_{k)i} - \partial_i K_{jk}\right) \,, \tag{A8}$$

$$\mathcal{B}^i_{\rm RR} = -2 \left(\delta^{ij} + Q^{ij}\right) \partial_j K \,, \tag{A9}$$

$$\mathcal{C}^i_{\rm RR} = 4 Q^i v^j \partial_j K + 8 \left(\delta^{ik} + Q^{ik}\right) v^j \partial_{[j} K_{k]} \,, \tag{A10}$$

$$\mathcal{D}^i_{\rm RR} = 4 Q^i v^{jk} \partial_j K_k + 2 \left(\delta^{il} + Q^{il}\right) v^{jk} \left(2 \partial_{(j} K_{k)l} - \partial_l K_{jk}\right) \,. \tag{A11}$$

All contractions in these expressions are to be performed with the Kronecker delta, $\delta_{ij} = \delta^{ij} = {\rm diag}(1, 1, 1)$, and we recall that Latin indices in the middle of the alphabet stand for spatial coordinates only (thus, all tensors are purely spatial).

For the purposes of the new kludge scheme we need to compute these local potentials associated with the Kerr metric ($K_{\rm H}$, $K^{\rm H}_i$, and $K^{\rm H}_{ij}$) and its inverse ($Q_{\rm H}$, $Q^i_{\rm H}$, and $Q^{ij}_{\rm H}$) in harmonic coordinates. They are need for the orthogonal projector [Eqs. (A1) and (A2)], for the Γ factor [Eq. (28)], and for the coefficients of the second piece of the acceleration, $A^{(2)}_\alpha$ [Eqs. (A6)-(A11)]. Moreover, for these coefficients we also need to compute the first spatial derivatives of the metric potentials ($\partial_k K_{\rm H}$, $\partial_k K^{\rm H}_i$, and $\partial_k K^{\rm H}_{ij}$). This can be done in an efficient way by using the following relations:

$$\partial_k K_{\rm H} = {\rm g}^{\rm K,BL}_{t\mu} \, {}^{\rm BL}\Gamma^\mu_{ti} \, \frac{\partial x^i_{\rm BL}}{\partial x^k_{\rm H}} \,, \tag{A12}$$

$$\partial_k K^{\rm H}_i = {\rm g}^{\rm K,BL}_{\mu(t}\,{}^{\rm BL}\Gamma^{\mu}_{m)n}\,\frac{\partial x^n_{\rm BL}}{\partial x^k_{\rm H}}\,\frac{\partial x^m_{\rm BL}}{\partial x^i_{\rm H}} + 2\,{\rm g}^{\rm K,BL}_{tm}\,\frac{\partial^2 x^m_{\rm BL}}{\partial x^i_{\rm H}\partial x^k_{\rm H}}\,, \tag{A13}$$

$$\partial_k K^{\rm H}_{ij} = \left\{ {\rm g}^{\rm K,BL}_{\mu(\ell}\,{}^{\rm BL}\Gamma^{\mu}_{m)n}\,\frac{\partial x^n_{\rm BL}}{\partial x^k_{\rm H}}\,\frac{\partial x^m_{\rm BL}}{\partial x^i_{\rm H}} + 2\,{\rm g}^{\rm K,BL}_{\ell m}\,\frac{\partial^2 x^m_{\rm BL}}{\partial x^i_{\rm H}\partial x^k_{\rm H}} \right\}\frac{\partial x^\ell_{\rm BL}}{\partial x^i_{\rm H}}\,. \tag{A14}$$

The advantage of these expressions is that they only involve the Jacobian and Hessian of the coordinate transformation between Boyer-Lindquist and harmonic coordinates, and the Christoffel symbols in Boyer-Lindquist coordinates. The latter are relatively simple functions and have to be computed anyway for other purposes (e.g. to compute the accelerations of Boyer-Lindquist coordinates).

Appendix B: Harmonic Coordinates for Rotating Black Holes

In this appendix we describe more properties of the set of harmonic coordinates for rotating BHs employed in this paper. Eqs. (67)-(70) and Eqs. (71)-(73) provide the explicit expressions for the transformation from Boyer-Lindquist to harmonic coordinates and the inverse transformation. From these transformations, we find that the relation between the Boyer-Lindquist radial coordinate r and the spatial harmonic coordinates $(x_{\rm H}, y_{\rm H}, z_{\rm H})$ is:

$$\frac{x^2_{\rm H}+y^2_{\rm H}}{(r-M_\bullet)^2+a^2}+\frac{z^2_{\rm H}}{(r-M_\bullet)^2}=1\,, \tag{B1}$$

which resembles the relation between r and the spatial Kerr-Schild Cartesian coordinates (see, e.g. [113]). This relation allows us to write r as a function of $r_{\rm H}$ as given in Eq. (72), which we find convenient to rewrite as $r \equiv M_\bullet + \varrho$, where

$$\varrho = \sqrt{\frac{1}{2}\left[r^2_{\rm H}-a^2+\sqrt{(r^2_{\rm H}-a^2)^2+4(\boldsymbol{s}\cdot\boldsymbol{r}_{\rm H})^2}\right]}\,. \tag{B2}$$

and where the dot here denotes the flat-space three-dimensional scalar product. Moreover, we have here introduced the following notation in the spirit of the usual three-dimensional flat space vector algebra: a *position* vector $\boldsymbol{r}_{\rm H} = (x_{\rm H}, y_{\rm H}, z_{\rm H})$, whose spatial norm (under the flat three-dimensional metric) was defined in Eq. (74), and the reduced spin vector $\boldsymbol{s}$ which, for consistency with the choices made in the paper we take it to be aligned with the z-axis: $\boldsymbol{s} = (0, 0, a)$. Nevertheless, one does not need to assume this specific form for $\boldsymbol{s}$, as the expressions we present in this Appendix are invariant under the action of the rotation group. We can then use the above expressions for arbitrary directions of the spin angular momentum of the BH. Note from Eq. (B2) that we always have $r^2_{\rm H} \geq \varrho^2 \geq r^2_{\rm H} - a^2$, and clearly the equality holds for the Schwarzschild case ($a = 0$). These inequalities translate in the following inequalities for r:

$$r_{\rm H} + M_\bullet \geq r \geq \sqrt{r^2_{\rm H}-a^2} + M_\bullet\,. \tag{B3}$$

An important ingredient of the construction of the harmonic coordinates is the angle function $\Phi(r)$, which was already given in Eq. (75). However, its proper definition is actually [99]

$$\Phi(r) \equiv -\int_r^\infty dr' \frac{aM^2_\bullet}{\Delta(r')[\Delta(r')+M^2_\bullet]}\,, \tag{B4}$$

where we recall that $\Delta(r) \equiv r^2 - 2M_\bullet r + a^2$. An alternative expression for $\Phi(r)$ can be obtained by simplifying Eq. (75) into

$$\Phi(r) = \frac{\pi}{2} - \arctan\left(\frac{r-M_\bullet}{a}\right) - \frac{a}{2\sqrt{M^2_\bullet - a^2}}\ln\left(\frac{r-r_-}{r-r_+}\right)\,. \tag{B5}$$

Two important relations to evaluate the coordinate transformation of Eqs. (67)-(70) are:

$$\cos\Phi = \frac{\frac{r-M_\bullet}{a}+\Omega(r)}{\sqrt{[1+\Omega^2(r)]\left\{1+\left(\frac{r-M_\bullet}{a}\right)^2\right\}}}\,, \tag{B6}$$

$$\sin\Phi = \frac{1-\frac{r-M_\bullet}{a}\,\Omega(r)}{\sqrt{[1+\Omega^2(r)]\left\{1+\left(\frac{r-M_\bullet}{a}\right)^2\right\}}}\,. \tag{B7}$$

where $\Omega(r)$ is given in Eq. (76). The explicit form of the components of the Kerr metric and its inverse in harmonic coordinates is given in Appendix A of [99]. These expressions are quite lengthy and, in that form, not very efficient for numerical computations. In what follows, we present an alternative method to compute the components of the transformed metric in an efficient way. At the same time, we introduce expressions that are invariant under the rotation group, in the sense that they do no longer assume the BH spin axis is aligned with the $\hat{z}_{\rm H}$-axis.

1. Jacobian

We start by presenting the expressions of the components of the Jacobian associated with the coordinate transformation between Boyer-Lindquist and harmonic coordinates. In other words, we compute the matrices $\mathbf{J}^{\rm BL}_{\rm H} = D(t, r, \theta, \phi)/D(t_{\rm H}, x_{\rm H}, y_{\rm H}, z_{\rm H})$ and $\mathbf{J}^{\rm H}_{\rm BL} = D(t_{\rm H}, x_{\rm H}, y_{\rm H}, z_{\rm H})/D(t, r, \theta, \phi)$, which obviously are inverses of each other: $\mathbf{J}^{\rm H}_{\rm BL}\cdot\mathbf{J}^{\rm BL}_{\rm H} = \mathbf{J}^{\rm BL}_{\rm H}\cdot\mathbf{J}^{\rm H}_{\rm BL} = \mathbf{Id}_3$, where

$\mathbf{Id}_3$ is the identity matrix in three-dimensions. The components of the Jacobian $\mathbf{J}^{\rm BL}_{\rm H}$ are

$$\frac{\partial t}{\partial t_{\rm H}} = 1\,, \qquad \frac{\partial t}{\partial \boldsymbol{r}_{\rm H}} = \mathbf{0}\,, \tag{B8}$$

$$\frac{\partial r}{\partial t_{\rm H}} = \frac{\partial \theta}{\partial t_{\rm H}} = \frac{\partial \phi}{\partial t_{\rm H}} = 0\,, \tag{B9}$$

$$\frac{\partial r}{\partial \boldsymbol{r}_{\rm H}} = \frac{\varrho\left\{\varrho^2 \boldsymbol{r}_{\rm H} - (\boldsymbol{s}\cdot\boldsymbol{r}_{\rm H})\boldsymbol{s}\right\}}{\sqrt{r_{\rm H}^2 - \varrho^2}\,[\varrho^4 + (\boldsymbol{s}\cdot\boldsymbol{r}_{\rm H})^2]}\,, \tag{B10}$$

$$\frac{\partial \theta}{\partial \boldsymbol{r}_{\rm H}} = \frac{\varrho\left\{(\boldsymbol{s}\cdot\boldsymbol{r}_{\rm H})\boldsymbol{r}_{\rm H} - \varrho^2 \boldsymbol{s}\right\}}{\sqrt{r_{\rm H}^2 - \varrho^2}\,[\varrho^4 + (\boldsymbol{s}\cdot\boldsymbol{r}_{\rm H})^2]}\,, \tag{B11}$$

$$\frac{\partial \phi}{\partial \boldsymbol{r}_{\rm H}} = -\frac{a}{(r_{\rm H}^2 - \varrho^2)(\varrho^2 + a^2)}\boldsymbol{s}\times\boldsymbol{r}_{\rm H} + \frac{a M_\bullet^2 \varrho\left\{\varrho^2 \boldsymbol{r}_{\rm H} - (\boldsymbol{s}\cdot\boldsymbol{r}_{\rm H})\boldsymbol{s}\right\}}{(\varrho^2 + a^2)(\varrho^2 + a^2 - M_\bullet^2)\,[\varrho^4 + (\boldsymbol{s}\cdot\boldsymbol{r}_{\rm H})^2]}\,, \tag{B12}$$

where the $\times$ denotes the usual flat-space three-dimensional vector product. The components of the inverse Jacobian, ie. $\mathbf{J}^{\rm H}_{\rm BL}$, are

$$\frac{\partial t_{\rm H}}{\partial t} = 1\,, \qquad \frac{\partial t_{\rm H}}{\partial r} = \frac{\partial t_{\rm H}}{\partial \theta} = \frac{\partial t_{\rm H}}{\partial \phi} = 0\,, \tag{B13}$$

$$\frac{\partial \boldsymbol{r}_{\rm H}}{\partial r} = \frac{\varrho^2 \boldsymbol{r}_{\rm H} - (\boldsymbol{s}\cdot\boldsymbol{r}_{\rm H})\boldsymbol{s}}{\varrho(\varrho^2 + a^2)} - \frac{M_\bullet^2}{(\varrho^2 + a^2)(\varrho^2 + a^2 - M_\bullet^2)}\boldsymbol{s}\times\boldsymbol{r}_{\rm H}\,, \tag{B14}$$

$$\frac{\partial \boldsymbol{r}_{\rm H}}{\partial \theta} = \frac{\boldsymbol{s}\cdot\boldsymbol{r}_{\rm H}}{\varrho\sqrt{r_{\rm H}^2 - \varrho^2}}\boldsymbol{r}_{\rm H} - \frac{\varrho\,(\varrho^2 + a^2)}{a^2\sqrt{r_{\rm H}^2 - \varrho^2}}\boldsymbol{s}\,, \tag{B15}$$

$$\frac{\partial \boldsymbol{r}_{\rm H}}{\partial \phi} = \frac{1}{a}\boldsymbol{s}\times\boldsymbol{r}_{\rm H}\,. \tag{B16}$$

2. Kerr Metric in Harmonic Coordinates

The expressions above can be used to compute the transformed Kerr metric and its inverse in harmonic coordinates systematically and efficiently. The covariant components of the metric in harmonic coordinates are

$$\mathrm{g}^{\rm K,H}_{tt} = \mathrm{g}^{\rm K,BL}_{tt}\,, \qquad \mathrm{g}^{\rm K,H}_{t\boldsymbol{r}} = \mathrm{g}^{\rm K,BL}_{t\phi}\frac{\partial \phi}{\partial \boldsymbol{r}_{\rm H}}\,, \tag{B17}$$

$$\mathrm{g}^{\rm K,H}_{\boldsymbol{r}\boldsymbol{r}} = \mathrm{g}^{\rm K,BL}_{rr}\frac{\partial r}{\partial \boldsymbol{r}_{\rm H}}\frac{\partial r}{\partial \boldsymbol{r}_{\rm H}} + \mathrm{g}^{\rm K,BL}_{\theta\theta}\frac{\partial \theta}{\partial \boldsymbol{r}_{\rm H}}\frac{\partial \theta}{\partial \boldsymbol{r}_{\rm H}} + \mathrm{g}^{\rm K,BL}_{\phi\phi}\frac{\partial \phi}{\partial \boldsymbol{r}_{\rm H}}\frac{\partial \phi}{\partial \boldsymbol{r}_{\rm H}}\,, \tag{B18}$$

where unlabeled coordinates on the right-hand sides stand for Boyer-Lindquist coordinates as usual. Similarly, the contravariant components of the metric in harmonic coordinates are

$$\mathrm{g}^{tt}_{\rm K,H} = \mathrm{g}^{tt}_{\rm K,BL}\,, \qquad \mathrm{g}^{t\boldsymbol{r}}_{\rm K,H} = \mathrm{g}^{t\phi}_{\rm K,BL}\frac{\partial \boldsymbol{r}_{\rm H}}{\partial \phi}\,, \tag{B19}$$

$$\mathrm{g}^{\boldsymbol{r}\boldsymbol{r}}_{\rm K,H} = \mathrm{g}^{rr}_{\rm K,BL}\frac{\partial \boldsymbol{r}_{\rm H}}{\partial r}\frac{\partial \boldsymbol{r}_{\rm H}}{\partial r} + \mathrm{g}^{\theta\theta}_{\rm K,BL}\frac{\partial \boldsymbol{r}_{\rm H}}{\partial \theta}\frac{\partial \boldsymbol{r}_{\rm H}}{\partial \theta} + \mathrm{g}^{\phi\phi}_{\rm K,BL}\frac{\partial \boldsymbol{r}_{\rm H}}{\partial \phi}\frac{\partial \boldsymbol{r}_{\rm H}}{\partial \phi}\,. \tag{B20}$$

It is easy to see that, under transformation of the three-dimensional rotation group, the covariant and contravariant $(t_{\rm H}, t_{\rm H})$ components transform as scalars, the covariant and contravariant $(t_{\rm H}, r^i_{\rm H})$ components transform as vectors, and the covariant and contravariant $(r^i_{\rm H}, r^j_{\rm H})$ components transform as 2-rank tensors. The expressions of all these components are invariant.

The computation of the components of the Kerr metric and its inverse in harmonic coordinates requires expressions for the Boyer-Lindquist components of the Kerr metric in harmonic coordinates. The covariant components are

$$\mathrm{g}^{\rm K,BL}_{tt} = -\frac{\varrho^2(\varrho^2 - M_\bullet^2) + (\boldsymbol{s}\cdot\boldsymbol{r}_{\rm H})^2}{\varrho^2(\varrho + M_\bullet)^2 + (\boldsymbol{s}\cdot\boldsymbol{r}_{\rm H})^2}\,, \tag{B21}$$

$$\mathrm{g}^{\rm K,BL}_{t\phi} = -\frac{2M_\bullet}{a}\frac{\varrho^2(\varrho + M_\bullet)^2(r_{\rm H}^2 - \varrho^2)}{\varrho^2(\varrho + M_\bullet)^2 + (\boldsymbol{s}\cdot\boldsymbol{r}_{\rm H})^2}\,, \tag{B22}$$

$$\mathrm{g}^{\rm K,BL}_{rr} = \frac{\varrho^2(\varrho + M_\bullet)^2 + (\boldsymbol{s}\cdot\boldsymbol{r}_{\rm H})^2}{\varrho^2(\varrho^2 + a^2 - M_\bullet^2)}\,, \tag{B23}$$

$$\mathrm{g}^{\rm K,BL}_{\theta\theta} = \frac{\varrho^2(\varrho + M_\bullet)^2 + (\boldsymbol{s}\cdot\boldsymbol{r}_{\rm H})^2}{\varrho^2}\,, \tag{B24}$$

$$\mathrm{g}^{\rm K,BL}_{\phi\phi} = \frac{r_{\rm H}^2 - \varrho^2}{a^2}\left[(\varrho + M_\bullet)^2 + a^2 + \frac{2M_\bullet\varrho^2(\varrho + M_\bullet)(r_{\rm H}^2 - \varrho^2)}{\varrho^2(\varrho + M_\bullet)^2 + (\boldsymbol{s}\cdot\boldsymbol{r}_{\rm H})^2}\right]\,, \tag{B25}$$

while the contravariant components are

$$\mathrm{g}^{tt}_{\mathrm{K,BL}} = -\varrho^2 \frac{\left[(\varrho+M_\bullet)^2+a^2\right]^2 - (\varrho^2+a^2-M_\bullet^2)(r_{\mathrm{H}}^2-\varrho^2)}{[\varrho^2(\varrho+M_\bullet)^2+(\boldsymbol{s}\cdot\boldsymbol{r}_{\mathrm{H}})^2]\,(\varrho^2+a^2-M_\bullet^2)}\,, \tag{B26}$$

$$\mathrm{g}^{t\phi}_{\mathrm{K,BL}} = -\frac{2M_\bullet a\varrho^2(\varrho+M_\bullet)}{[\varrho^2(\varrho+M_\bullet)^2+(\boldsymbol{s}\cdot\boldsymbol{r}_{\mathrm{H}})^2]\,(\varrho^2+a^2-M_\bullet^2)}\,, \tag{B27}$$

$$\mathrm{g}^{rr}_{\mathrm{K,BL}} = \frac{\varrho^2(\varrho^2+a^2-M_\bullet^2)}{\varrho^2(\varrho+M_\bullet)^2+(\boldsymbol{s}\cdot\boldsymbol{r}_{\mathrm{H}})^2}\,, \tag{B28}$$

$$\mathrm{g}^{\theta\theta}_{\mathrm{K,BL}} = \frac{\varrho^2}{\varrho^2(\varrho+M_\bullet)^2+(\boldsymbol{s}\cdot\boldsymbol{r}_{\mathrm{H}})^2}\,, \tag{B29}$$

$$\mathrm{g}^{\phi\phi}_{\mathrm{K,BL}} = \frac{a^2\left[\varrho^2(\varrho^2-M_\bullet^2)+(\boldsymbol{s}\cdot\boldsymbol{r}_{\mathrm{H}})^2\right]}{[\varrho^2(\varrho+M_\bullet)^2+(\boldsymbol{s}\cdot\boldsymbol{r}_{\mathrm{H}})^2]\,(\varrho^2+a^2-M_\bullet^2)(r_{\mathrm{H}}^2-\varrho^2)}\,. \tag{B30}$$

3. Hessian

Let us now present explicit expressions for the Hessian of the transformation between harmonic and Boyer-Lindquist coordinates, needed for the computation of the accelerations in harmonic coordinates. Also, for the computation of the derivatives of the metric in harmonic coordinates we need the Hessians of the Boyer-Lindquist coordinates with respect to the harmonic ones. More specifically, for the computation of the coefficients of the second piece of the acceleration, $A^{(2)}_\alpha$ [Eqs. (A6)-(A11)]. We give here these expressions using the three-dimensional vector notation introduced above. The expressions for the Hessian matrix $\partial^2 \boldsymbol{r}^k_{\mathrm{H}}/(\partial x^i_{\mathrm{BL}}\,\partial x^j_{\mathrm{BL}})$ are:

$$\frac{\partial^2 \boldsymbol{r}_{\mathrm{H}}}{\partial r^2} = -\frac{1}{(\varrho^2+a^2)^2}\left[1-\frac{M_\bullet^4}{(\varrho^2+a^2-M_\bullet^2)^2}\right]\boldsymbol{s}\times\boldsymbol{s}\times\boldsymbol{r}_{\mathrm{H}} + \frac{2M_\bullet^2\,\varrho}{(\varrho^2+a^2)(\varrho^2+a^2-M_\bullet^2)^2}\boldsymbol{s}\times\boldsymbol{r}_{\mathrm{H}}\,, \tag{B31}$$

$$\frac{\partial^2 \boldsymbol{r}_{\mathrm{H}}}{\partial r\,\partial\theta} = \frac{1}{(\varrho^2+a^2)\sqrt{r_{\mathrm{H}}^2-\varrho^2}}\left\{\boldsymbol{s}\times\boldsymbol{r}_{\mathrm{H}}\times\boldsymbol{r}_{\mathrm{H}} - \frac{M_\bullet^2(\boldsymbol{s}\cdot\boldsymbol{r}_{\mathrm{H}})}{\varrho(\varrho^2+a^2-M_\bullet^2)}\boldsymbol{s}\times\boldsymbol{r}_{\mathrm{H}}\right\}\,, \tag{B32}$$

$$\frac{\partial^2 \boldsymbol{r}_{\mathrm{H}}}{\partial r\,\partial\phi} = \frac{1}{a(\varrho^2+a^2)}\left\{\varrho(\boldsymbol{s}\times\boldsymbol{r}_{\mathrm{H}}) - \frac{M_\bullet^2}{\varrho^2+a^2-M_\bullet^2}\boldsymbol{s}\times\boldsymbol{s}\times\boldsymbol{r}_{\mathrm{H}}\right\}\,, \tag{B33}$$

$$\frac{\partial^2 \boldsymbol{r}_{\mathrm{H}}}{\partial\theta^2} = -\boldsymbol{r}_{\mathrm{H}}\,, \qquad \frac{\partial^2 \boldsymbol{r}_{\mathrm{H}}}{\partial\theta\,\partial\phi} = \frac{(\boldsymbol{s}\cdot\boldsymbol{r}_{\mathrm{H}})}{a\varrho\sqrt{r_{\mathrm{H}}^2-\varrho^2}}\boldsymbol{s}\times\boldsymbol{r}_{\mathrm{H}}\,, \qquad \frac{\partial^2 \boldsymbol{r}_{\mathrm{H}}}{\partial\phi^2} = \frac{1}{a^2}\boldsymbol{s}\times\boldsymbol{s}\times\boldsymbol{r}_{\mathrm{H}}\,. \tag{B34}$$

and the expressions for its inverse $\partial^2 x^k_{\mathrm{BL}}/(\partial \boldsymbol{r}^i_{\mathrm{H}}\,\partial \boldsymbol{r}^j_{\mathrm{H}})$ are:

$$\begin{aligned}\frac{\partial^2 r}{\partial \boldsymbol{r}_{\mathrm{H}}\partial \boldsymbol{r}_{\mathrm{H}}} = \frac{\varrho}{\varrho^4+(\boldsymbol{s}\cdot\boldsymbol{r}_{\mathrm{H}})^2}\Bigg\{&\boldsymbol{I}\boldsymbol{d}_3 + \boldsymbol{s}\odot\boldsymbol{s} + \frac{2}{\varrho^4+(\boldsymbol{s}\cdot\boldsymbol{r}_{\mathrm{H}})^2}\left[\varrho^2\boldsymbol{r}_{\mathrm{H}}-(\boldsymbol{s}\cdot\boldsymbol{r}_{\mathrm{H}})\boldsymbol{s}\right]\odot\left[\varrho^2\boldsymbol{r}_{\mathrm{H}}+(\boldsymbol{s}\cdot\boldsymbol{r}_{\mathrm{H}})\boldsymbol{s}\right]\\ &+\frac{(\boldsymbol{s}\cdot\boldsymbol{r}_{\mathrm{H}})^2-3\varrho^4}{\left[\varrho^4+(\boldsymbol{s}\cdot\boldsymbol{r}_{\mathrm{H}})^2\right]^2}\left[\varrho^2\boldsymbol{r}_{\mathrm{H}}+(\boldsymbol{s}\cdot\boldsymbol{r}_{\mathrm{H}})\boldsymbol{s}\right]\odot\left[\varrho^2\boldsymbol{r}_{\mathrm{H}}+(\boldsymbol{s}\cdot\boldsymbol{r}_{\mathrm{H}})\boldsymbol{s}\right]\Bigg\}\,,\end{aligned} \tag{B35}$$

$$\begin{aligned}\frac{\partial^2\theta}{\partial \boldsymbol{r}_{\mathrm{H}}\partial \boldsymbol{r}_{\mathrm{H}}} = \frac{1}{\sqrt{r_{\mathrm{H}}^2-\varrho^2}\,[\varrho^4+(\boldsymbol{s}\cdot\boldsymbol{r}_{\mathrm{H}})^2]}\Bigg\{&\left[\left(\frac{r_{\mathrm{H}}^2}{r_{\mathrm{H}}^2-\varrho^2}-\frac{4\,\varrho^4}{\varrho^4+(\boldsymbol{s}\cdot\boldsymbol{r}_{\mathrm{H}})^2}\right)\frac{\partial r}{\partial \boldsymbol{r}_{\mathrm{H}}}-\frac{\varrho}{r_{\mathrm{H}}^2-\varrho^2}\,\boldsymbol{r}_{\mathrm{H}}\right]\odot\left[(\boldsymbol{s}\cdot\boldsymbol{r}_{\mathrm{H}})\boldsymbol{r}_{\mathrm{H}}-\varrho^2\boldsymbol{s}\right]\\ &+\varrho(\boldsymbol{s}\cdot\boldsymbol{r}_{\mathrm{H}})\left[\boldsymbol{I}\boldsymbol{d}_3-\boldsymbol{s}\odot\boldsymbol{r}_{\mathrm{H}}\right]\Bigg\}\,,\end{aligned} \tag{B36}$$

$$\frac{\partial^2\phi}{\partial \boldsymbol{r}_{\mathrm{H}}\partial \boldsymbol{r}_{\mathrm{H}}} = \boldsymbol{\phi}^1_{\boldsymbol{r}_{\mathrm{H}}\boldsymbol{r}_{\mathrm{H}}} + \frac{\partial^2\Phi}{\partial \boldsymbol{r}_{\mathrm{H}}\partial \boldsymbol{r}_{\mathrm{H}}} = \boldsymbol{\phi}^1_{\boldsymbol{r}_{\mathrm{H}}\boldsymbol{r}_{\mathrm{H}}} + \Phi''\frac{\partial r}{\partial \boldsymbol{r}_{\mathrm{H}}}\odot\frac{\partial r}{\partial \boldsymbol{r}_{\mathrm{H}}} + \Phi'\frac{\partial^2 r}{\partial \boldsymbol{r}_{\mathrm{H}}\partial \boldsymbol{r}_{\mathrm{H}}}\,, \tag{B37}$$

where $\boldsymbol{\phi}^1_{\boldsymbol{r}_{\mathrm{H}}\boldsymbol{r}_{\mathrm{H}}}$ is the following symmetric matrix

$$\boldsymbol{\phi}^1_{\boldsymbol{r}_{\mathrm{H}}\boldsymbol{r}_{\mathrm{H}}} = \begin{pmatrix} \frac{2x_{\mathrm{H}}y_{\mathrm{H}}}{(x_{\mathrm{H}}^2+y_{\mathrm{H}}^2)^2} & \frac{y_{\mathrm{H}}^2-x_{\mathrm{H}}^2}{(x_{\mathrm{H}}^2+y_{\mathrm{H}}^2)^2} & 0 \\ * & -\frac{2x_{\mathrm{H}}y_{\mathrm{H}}}{(x_{\mathrm{H}}^2+y_{\mathrm{H}}^2)^2} & 0 \\ * & * & 0 \end{pmatrix}\,, \tag{B38}$$

and where $\odot$ denotes symmetric tensor product: $\boldsymbol{a}\odot\boldsymbol{b} = (\boldsymbol{a}\otimes\boldsymbol{b}+\boldsymbol{b}\otimes\boldsymbol{a})/2$.

Appendix C: ACMC and approximate Harmonic Coordinate Systems

In this Appendix, we construct an ACMC-6 coordinate system and a system of approximate harmonic coordinates associated with these ACMC-6 coordinates that we compare with the exact harmonic coordinates presented in Sec. III D. Thorne [47] constructed an explicit map between Boyer-Lindquist coordinates $(x^\alpha_{\rm BL}) = (t, r, \theta, \phi)$ and ACMC-2 for a Kerr BH with mass $M_\bullet$ and Kerr spin parameter a. The extension of this map from Boyer-Lindquist coordinates to ACMC-6 coordinates, $(x^\alpha_{\rm ACMC}) = (T, X, Y, Z)$, is given below for the first time:

$$t = T\,, \tag{C1}$$

$$r = R + \frac{a^2}{2R}\cos^2\bar\theta - \frac{5a^4}{8R^3}\cos^4\bar\theta + \frac{21a^6}{16R^5}\cos^6\bar\theta\,, \tag{C2}$$

$$\theta = \bar\theta - \frac{a^2}{4R^2}\sin(2\bar\theta)\left\{1 - \frac{3a^2}{2R^2}\cos^2\bar\theta + \frac{10a^4}{3R^4}\cos^4\bar\theta\right\}\,, \tag{C3}$$

$$\phi = \arctan\left(\frac{Y}{X}\right)\,, \tag{C4}$$

where we have introduced the shorthands $R = (X^2 + Y^2 + Z^2)^{1/2}$, and $\bar\theta = \arccos(Z/R)$.

Harmonic coordinates are guaranteed to be ACMC-∞ (see [47]), but the converse is not necessarily true: ACMC coordinates of order N are not necessarily harmonic. Nonetheless, one can enhance the ACMC-6 coordinate transformations of Eqs. (C1)-(C4) to construct a map from Boyer-Lindquist coordinates to approximate harmonic (AH) coordinates $(x^\alpha_{\rm AH}) = (t_{\rm AH}, x_{\rm AH}, y_{\rm AH}, z_{\rm AH})$:

$$t = t_{\rm AH}\,, \tag{C5}$$

$$r = r_{\rm AH} + M_\bullet - \frac{a^2[1-(\hat{\boldsymbol{s}}\cdot\boldsymbol{n}_{\rm AH})^2]}{2\,r_{\rm AH}} - \frac{5a^4(\hat{\boldsymbol{s}}\cdot\boldsymbol{n}_{\rm AH})^4}{8\,r^3_{\rm AH}} + \frac{21a^6(\hat{\boldsymbol{s}}\cdot\boldsymbol{n}_{\rm AH})^6}{16\,r^5_{\rm AH}}\,, \tag{C6}$$

$$\theta = \theta_{\rm AH} - \frac{a^2(\hat{\boldsymbol{s}}\cdot\boldsymbol{n}_{\rm AH})\sqrt{1-(\hat{\boldsymbol{s}}\cdot\boldsymbol{n}_{\rm AH})^2}}{2\,r^2_{\rm AH}}\left\{1 - \frac{3a^2(\hat{\boldsymbol{s}}\cdot\boldsymbol{n}_{\rm AH})^2}{2\,r^2_{\rm AH}} + \frac{10a^4(\hat{\boldsymbol{s}}\cdot\boldsymbol{n}_{\rm AH})^4}{3\,r^4_{\rm AH}}\right\}\,, \tag{C7}$$

$$\phi = \arctan\left(\frac{\hat{\boldsymbol{y}}_{\rm AH}\cdot\boldsymbol{n}_{\rm AH}}{\hat{\boldsymbol{x}}_{\rm AH}\cdot\boldsymbol{n}_{\rm AH}}\right)\,, \tag{C8}$$

where $\hat{\boldsymbol{s}}$ is a unit vector (in the Euclidean sense) along the MBH spin axis which, according to the conventions of this paper, has components $\boldsymbol{s} = (0, 0, 1)$. Moreover we have introduced the following notation in the Euclidean vector calculus style: $\boldsymbol{r}_{\rm AH} = r^i_{\rm AH} = (x_{\rm AH}, y_{\rm AH}, z_{\rm AH})$, $r_{\rm AH} = (x^2_{\rm AH} + y^2_{\rm AH} + z^2_{\rm AH})^{1/2}$, $\boldsymbol{n}_{\rm AH} = n^i_{\rm AH} = bmr_{\rm AH}/r_{\rm AH}$, $\theta_{\rm AH} = \arccos(\hat{\boldsymbol{s}}\cdot\boldsymbol{n}_{\rm AH})$, $\hat{\boldsymbol{y}}_{\rm AH}$ and $\hat{\boldsymbol{x}}_{\rm AH}$ are three-dimensional (spatial), orthogonal vectors in the plane orthogonal to the spin axis.

These approximate harmonic coordinates are not only ACMC-6 but also harmonic up to terms of order $\mathcal{O}(M^6_\bullet/r^6_{\rm AH})$, as one can check by verifying that $\partial^{\rm AH}_\beta(\sqrt{-{\rm g}_{\rm K,AH}}\,{\rm g}^{\alpha\beta}_{\rm K,AH}) = 0$, where ${\rm g}^{\rm K,AH}_{\alpha\beta}$ is the transformed Kerr metric [1] and $\partial^{\rm AH}_\alpha$ denotes partial differentiation with respect to these coordinates.

One should note that this coordinates are only *pseudo*-harmonic, in that they do not respect the harmonic coordinate condition to all orders in $M_\bullet/r_{\rm AH}$. Therefore, these coordinates differ somewhat from the transformation in Eqs. (67)-(70). We can show this by expanding Eqs. (71)-(73) in $M_\bullet/r_{\rm H} \ll 1$ and $a/r_{\rm H} \ll 1$:

$$t = t_{\rm H}\,, \tag{C9}$$

$$\begin{aligned} r = r_{\rm H} &+ M_\bullet - \frac{a^2}{2\,r_{\rm H}}[1-(\hat{\boldsymbol{s}}\cdot\boldsymbol{n}_{\rm H})^2] \\ &- \frac{a^4}{8\,r^3_{\rm H}}\left[1 - 6(\hat{\boldsymbol{s}}\cdot\boldsymbol{n}_{\rm H})^2 + 5(\hat{\boldsymbol{s}}\cdot\boldsymbol{n}_{\rm H})^4\right] \\ &- \frac{a^6}{16\,r^5_{\rm H}}\left[1 - 15(\hat{\boldsymbol{s}}\cdot\boldsymbol{n}_{\rm H})^2 + 35(\hat{\boldsymbol{s}}\cdot\boldsymbol{n}_{\rm H})^4 - 21(\hat{\boldsymbol{s}}\cdot\boldsymbol{n}_{\rm H})^6\right]\,, \end{aligned} \tag{C10}$$

$$\begin{aligned} \theta = \theta_{\rm H} &- \frac{a^2(\hat{\boldsymbol{s}}\cdot\boldsymbol{n}_{\rm H})\sqrt{1-(\hat{\boldsymbol{s}}\cdot\boldsymbol{n}_{\rm H})^2}}{2\,r^2_{\rm H}}\{1 \\ &+ \frac{3a^2}{4r^2_{\rm H}}\left[1 - 2(\hat{\boldsymbol{s}}\cdot\boldsymbol{n}_{\rm H})^2\right] \\ &+ \frac{5a^4}{24r^4_{\rm H}}\left[1 - 4(\hat{\boldsymbol{s}}\cdot\boldsymbol{n}_{\rm H})^2\right]\left[3 - 4(\hat{\boldsymbol{s}}\cdot\boldsymbol{n}_{\rm H})^2\right]\Big\}\,, \end{aligned} \tag{C11}$$

$$\begin{aligned} \phi = \phi_{\rm H} &- \frac{aM^2_\bullet}{3\,r^3_{\rm H}} \\ &- \frac{aM^2_\bullet}{10\,r^5_{\rm H}}\left[a^2 - 5a^2(\hat{\boldsymbol{s}}\cdot\boldsymbol{n}_{\rm H})^2 + 2M^2_\bullet\right]\,, \end{aligned} \tag{C12}$$

where we have used a similar vector notation as in Eqs. (C5)-(C8) with $\theta_{\rm H} = \arccos(\hat{\boldsymbol{s}}\cdot\boldsymbol{n}_{\rm H})$ and $\phi_{\rm H} = \arctan(\hat{\boldsymbol{y}}_{\rm H}\cdot\boldsymbol{n}_{\rm H}/\hat{\boldsymbol{x}}_{\rm H}\cdot\boldsymbol{n}_{\rm H})$. As we can see, disagreements arise in the radial transformation at order $\mathcal{O}(a^4)$, but this difference is proportional to a monopole (without angular dependence) and a quadrupole term (quadratic in angular dependence), which do not modify the ACMC

[1] This transformation is slightly different from that found in [114], for zero integration constants. One can show by direct evaluation, however, that both transformations lead to harmonic coordinates that are also ACMC.

condition at octopole order. Similar disagreements arise also in the angular sector of the transformation.

We have thus shown that the ACMC coordinate map we found in Eqs. (C5)-(C8) reproduces the main ingredients of the full harmonic coordinate transformation. In fact, since we have shown that Eqs. (C5)-(C8) lead to a metric that satisfies the harmonic coordinate condition, we can infer that the difference between this equation and Eqs. (71)-(73) must amount to a refinement of the coordinate system.

Appendix D: Far-Field Expansion of the Kerr Metric in Approximate Harmonic Coordinates

In this appendix we expand the Kerr metric in the far-field using the approximate harmonic coordinates $x^{\alpha}_{\rm AH}$ of Appendix C [the coordinate transformations from Boyer-Lindquist coordinates are given in Eqs. (C5)-(C8)]. Then, in transforming the Kerr metric from Boyer-Lindquist coordinates to these approximate harmonic coordinates we assume $M_\bullet/r_{\rm AH} \ll 1$ and $a/r_{\rm AH} \ll 1$. We give the expressions of the Kerr metric and its inverse in terms of the *local* potentials $K_{\alpha\beta}$ and $Q^{\alpha\beta}$. The far-field expansions of the $K_{\mu\nu}$ potentials in the approximate harmonic coordinates of Eqs. (C5)-(C8), $K^{\rm AH}_{\alpha\beta}$, is given by

$$K^{\rm AH} = K^{\rm AH}_{00} = \frac{2M_\bullet}{r_{\rm AH}}\left\{1 - \frac{M_\bullet}{r_{\rm AH}} + \frac{1}{2\,r^2_{\rm AH}}\left[2M_\bullet^2 + a^2\left(1-3(\hat{\boldsymbol{s}}\cdot\boldsymbol{n}_{\rm AH})^2\right)\right] - \frac{M_\bullet}{r^3_{\rm AH}}\left[M_\bullet^2 + a^2\left(1-4(\hat{\boldsymbol{s}}\cdot\boldsymbol{n}_{\rm AH})^2\right)\right]\right\}, \quad \text{(D1)}$$

$$K^{\rm AH}_i = K^{\rm AH}_{0i} = -\frac{2M_\bullet}{r^2_{\rm AH}}\left\{1 - \frac{M_\bullet}{r_{\rm AH}} + \frac{1}{2\,r^2_{\rm AH}}\left[2M_\bullet^2 + a^2\left(1-5(\hat{\boldsymbol{s}}\cdot\boldsymbol{n}_{\rm AH})^2\right)\right]\right\}(\hat{\boldsymbol{s}}\times\boldsymbol{n}_{\rm AH})_i\,, \quad \text{(D2)}$$

$$\begin{aligned} K^{\rm AH}_{ij} = {}& \frac{2M_\bullet}{r_{\rm AH}}\left\{\delta_{ij} + \frac{M_\bullet}{2\,r_{\rm AH}}\left(\delta_{ij} + n^{\rm AH}_i n^{\rm AH}_j\right)\right. \\ & + \frac{1}{2\,r^2_{\rm AH}}\left[2M_\bullet^2 n^{\rm AH}_i n^{\rm AH}_j + a^2\left(1-3(\hat{\boldsymbol{s}}\cdot\boldsymbol{n}_{\rm AH})^2\right)\delta_{ij}\right] \\ & + \frac{1}{2M_\bullet r^3_{\rm AH}}\left[2M_\bullet^4 n^{\rm AH}_i n^{\rm AH}_j + M_\bullet^2 a^2\left\{\left((\hat{\boldsymbol{s}}\cdot\boldsymbol{n}_{\rm AH})^2-2\right)\delta_{ij}\right.\right. \\ & + 3\left(1-(\hat{\boldsymbol{s}}\cdot\boldsymbol{n}_{\rm AH})^2\right)n^{\rm AH}_i n^{\rm AH}_j\Big\} + \frac{a^4}{4}\Big\{\left(1-3(\hat{\boldsymbol{s}}\cdot\boldsymbol{n}_{\rm AH})^2\right)\delta_{ij} \\ & - 2\left(2-9(\hat{\boldsymbol{s}}\cdot\boldsymbol{n}_{\rm AH})^2\right)n^{\rm AH}_i n^{\rm AH}_j\Big\} \\ & - \frac{a^2\left(8M_\bullet^2 - a^2\right)}{4}(\hat{\boldsymbol{s}}\cdot\boldsymbol{n}_{\rm AH})\left(n^{\rm AH}_i\hat{s}_j + n^{\rm AH}_j\hat{s}_i\right) \\ & \left. + \frac{3a^2\left(4M_\bullet^2 - a^2\right)}{4}\hat{s}_i\hat{s}_j\right]\Bigg\}\,. \end{aligned} \quad \text{(D3)}$$

The far-field expansions of the $Q^{\mu\nu}$ potentials in the approximate harmonic coordinates, of Eqs. (C5)-(C8), $Q^{\alpha\beta}_{\rm AH}$, is given by

$$Q_{\rm AH} = Q^{00}_{\rm AH} = -\frac{2M_\bullet}{r_{\rm AH}}\left\{1 + \frac{M_\bullet}{r_{\rm AH}} + \frac{1}{2\,r^2_{\rm AH}}\left[2M_\bullet^2 + a^2\left(1-3(\hat{\boldsymbol{s}}\cdot\boldsymbol{n}_{\rm AH})^2\right)\right] + \frac{M_\bullet}{r^3_{\rm AH}}\left(M_\bullet^2 - a^2\right)\right\}, \quad \text{(D4)}$$

$$Q^i_{\rm H} = Q^{0i}_{\rm H} = -\frac{2M_\bullet}{r^2_{\rm AH}}\left\{1 - \frac{M_\bullet}{r_{\rm AH}} + \frac{1}{2\,r^2_{\rm AH}}\left[4M_\bullet^2 + a^2\left(1-5(\hat{\boldsymbol{s}}\cdot\boldsymbol{n}_{\rm AH})^2\right)\right]\right\}(\hat{\boldsymbol{s}}\times\boldsymbol{n}_{\rm AH})^i\,, \quad \text{(D5)}$$

$$\begin{aligned} Q^{ij}_{\rm AH} = {}& -\frac{2M_\bullet}{r_{\rm AH}}\left\{\delta^{ij} - \frac{M_\bullet}{2\,r_{\rm AH}}\left(3\delta^{ij} - n^i_{\rm AH}n^j_{\rm AH}\right)\right. \\ & - \frac{1}{2\,r^2_{\rm AH}}\left[2M_\bullet^2 n^i_{\rm AH}n^j_{\rm AH} - \left(4M_\bullet^2 + a^2\left(1-3(\hat{\boldsymbol{s}}\cdot\boldsymbol{n}_{\rm AH})^2\right)\right)\delta^{ij}\right] \\ & + \frac{1}{2M_\bullet r^3_{\rm AH}}\left[3M_\bullet^4 n^i_{\rm AH}n^j_{\rm AH} - M_\bullet^2\left\{a^2\left(1+3(\hat{\boldsymbol{s}}\cdot\boldsymbol{n}_{\rm AH})^2\right)n^i_{\rm AH}n^j_{\rm AH}\right.\right. \\ & \left.\left. + \left(5M_\bullet^2 + a^2\left(2-9(\hat{\boldsymbol{s}}\cdot\boldsymbol{n}_{\rm AH})^2\right)\right)\delta^{ij}\right\} \\ & + \frac{a^4}{4}\left\{\left(1-3(\hat{\boldsymbol{s}}\cdot\boldsymbol{n}_{\rm AH})^2\right)\delta^{ij} - 2\left(2-9(\hat{\boldsymbol{s}}\cdot\boldsymbol{n}_{\rm AH})^2\right)n^i_{\rm AH}n^j_{\rm AH}\right\} \\ & + \frac{a^2\left(8M_\bullet^2 + 3a^2\right)}{4}(\hat{\boldsymbol{s}}\cdot\boldsymbol{n}_{\rm AH})\left(n^i_{\rm AH}\hat{s}^j + n^j_{\rm AH}\hat{s}^i\right) \\ & \left. - \frac{a^2\left(4M_\bullet^2 + 3a^2\right)}{4}\hat{s}^i\hat{s}^j\right]\Bigg\}\,. \end{aligned} \quad \text{(D6)}$$

where we recall that the symbol $\times$ refers to the Euclidean vector product and the dot product to the Euclidean scalar product. Moreover, $n^i_{\rm AH} \equiv x^i_{\rm AH}/r_{\rm AH}$ and indices are raised and lowered with the flat metric. We have checked that the above metric satisfies the differential harmonic coordinate condition to the order of approximation. That is, we have checked that $\partial^{\rm AH}_\beta(\sqrt{-{\rm g}_{\rm K,AH}}\,{\rm g}^{\alpha\beta}_{\rm K,AH}) = 0$, where here ${\rm g}^{\rm K,AH}_{\alpha\beta}$ is the expanded Kerr metric in the approximate harmonic coordinates as determined by the expansions of the potentials above, and $\partial^{\rm AH}_\alpha$ denotes partial differentiation with respect to the approximate harmonic coordinates $(x^\alpha_{\rm AH})$.

Appendix E: Relations between different orbital parameterizations

Geodesic orbits in Kerr spacetime are fully determined by the three constants of motion $\mathcal{I}^A = (E, L_z, C \text{ or } {\rm Q})$. In this work, we restrict our attention to bounded motion ($E^2 < 1$, see [115]). Then, it is also very useful to characterize the orbit in terms of the orbital parameters $\mathcal{O}^A = (p, e, \iota \text{ or } \theta_{\rm inc})$, which provide more transparent geometrical information about the properties of the orbit. Both sets of parameters are important, the set $\mathcal{I}^A$ is more adapted to the separation of the geodesic

equations and to the radiation reaction computations, whereas the set $\mathcal{O}^A$ is better in terms of orbit characterization. Therefore, it is important to know the relation between these two sets of constants of motion and how to map them. This is specially important when radiation reaction changes these parameters and we need to know the new values of $\mathcal{O}^A$ once the new values of $\mathcal{I}^A$ have been computed using Eqs. (30)-(33). The relations we present below follow from developments in [85–87].

Let us first consider the case in which the set $(p, e, \theta_{\rm inc})$ is known, ie. we parametrize the orbit in terms of these parameters and we need to find the parameters $\mathcal{I}^A$ for evolving the equations of motion. We mainly use $\theta_{\rm inc}$ instead of ι for convenience, but we shall also present formulae related to the inclination angle ι. The goal is to find the mapping from $(p, e, \theta_{\rm inc})$ to $(E, L_z, C$ or Q). First of all, given $\theta_{\rm inc}$, the minimum value that θ can take, $\theta_{\rm min}$, is [see Eq. (24)]

$$\theta_{\rm min} = \frac{\pi}{2} - {\rm sign}(L_z)\,\theta_{\rm inc}\,, \tag{E1}$$

where the sign of L_z determines whether the orbit is prograde (positive) or retrograde (negative). The sign of L_z is encoded in $\theta_{\rm inc}$ as follows: If $0 < \theta_{\rm inc} < \pi/2$, then ${\rm sign}(L_z) = 1$; if $-\pi/2 < \theta_{\rm inc} < 0$, then ${\rm sign}(L_z) = -1$. The particular case $\theta_{\rm inc} = 0$ is singular in the sense that both signs are possible for L_z.

Since $\theta = \theta_{\rm min}$ is a minimum, we have $\dot\theta(\theta_{\rm min}) = 0$, which means that the right-hand side of Eq. (20) has to vanish at $\theta_{\rm min}$, from which we obtain an expression for C

$$C = z_- \left[\frac{L_z^2}{1-z_-} + a^2(1-E^2)\right]. \tag{E2}$$

where z_- is given in Eq. (92). Now that we have an expression for C in terms of E and L_z, let us find expressions for (E, L_z) in terms of p and e. This can be done from the analysis of the radial motion, and using the expressions of the apocenter and pericenter radii, $r_{\rm apo}$ and $r_{\rm peri}$ [Eq. (22)], in terms of (p, e). These values of r are extrema and hence, the right-hand side of Eq. (19) vanishes at $r = r_{\rm apo}$ and at $r = r_{\rm peri}$, leading to two equations for the three unknowns (E, L_z, C). The Carter constant, however, is given in terms of (E, L_z) in Eq. (E2), which then leads to two equations for two unknowns, (E, L_z). These equations take the following polynomial structure

$$\alpha_I E^2 + 2\beta_I E L_z + \gamma_I L_z^2 + \lambda_I = 0\,, \tag{E3}$$

where the sub-index I stands for apocenter or pericenter and where the coefficients α_I, β_I, γ_I, and λ_I, in the case of non-circular orbits ($r_{\rm peri} \neq r_{\rm apo}$), are given by

$$\alpha_I = \left(r_I^2 + a^2\right)\left(r_I^2 + a^2 z_-\right) + 2M_\bullet r_I a^2\left(1 - z_-\right) \tag{E4}$$

$$\beta_I = -2M_\bullet r_I a\,, \tag{E5}$$

$$\gamma_I = -\frac{1}{1-z_-}\left[r_I^2 + a^2 z_- - 2M_\bullet r_I\right], \tag{E6}$$

$$\begin{aligned}\lambda_I &= -\left(r_I^2 + a^2 z_-\right)\Delta(r_I)\\ &= -\left(r_I^2 + a^2 z_-\right)\left(r_I^2 - 2M_\bullet r_I + a^2\right).\end{aligned} \tag{E7}$$

In the case of circular orbits these two relations are exactly the same and we need an extra equation. This equation comes from the fact that in the circular case $dr/d\tau$ must always vanish and hence also the radial derivative of Eq. (19) must vanish. Then, the first equation in the circular case is given by Eqs. (E4)-(E7) with $r_I = r_o = const.$, and the coefficients of the second one are given by:

$$\alpha_2 = 2r_o\left(r_o^2 + a^2\right) - a^2\left(r_o - M_\bullet\right)\left(1 - z_-\right), \tag{E8}$$

$$\beta_2 = -aM_\bullet\,, \tag{E9}$$

$$\gamma_2 = -\frac{r_o - M_\bullet}{1 - z_-}\,, \tag{E10}$$

$$\lambda_2 = -r_o\Delta(r_o) - \left(r_o - M_\bullet\right)\left(r_o^2 + a^2 z_-\right), \tag{E11}$$

One can then combine the two expressions in Eq. (E3) to eliminate one of the two unknowns. For instance, we can eliminate L_z and obtain an equation for E, which can be written in the following form:

$$\begin{aligned}&\left([\alpha,\gamma]^2 + 4[\alpha,\beta][\gamma,\beta]\right)E^4\\ &+ 2\left([\alpha,\gamma][\lambda,\gamma] + 2[\gamma,\beta][\lambda,\beta]\right)E^2 + [\lambda,\gamma]^2 = 0,\end{aligned} \tag{E12}$$

where the notation $[*,*]$ denotes the following antisymmetric product:

$$[\Pi, \Omega] \equiv \Pi_{\rm apo}\Omega_{\rm peri} - \Pi_{\rm peri}\Omega_{\rm apo}\,, \tag{E13}$$

and the subscripts denote at which radii we have to evaluate the quantity (e.g., $\Pi_{\rm apo} = \Pi(r_{\rm apo})$). Eq. (E12) is bi-quadratic in E, which means that there are two solutions for E^2 and from each of these, there are two values of E, one positive and one negative, that are related by time-inversion. From the two solutions for E^2, the larger one corresponds to retrograde orbits, while the smaller one corresponds to prograde ones. Given E^2, we can then find L_z through

$$L_z^2 = \frac{1}{[\beta,\gamma]}\left([\alpha,\beta]E^2 + [\lambda,\beta]\right), \tag{E14}$$

where the positive solution correspond to prograde orbits and the negative one for retrograde orbits. Finally, the Carter constant C is given by Eq. (E2) and Q from Eq. (17). Once we know the constants of motion (E, L_z, C) we can also find the inclination angle ι from Eq. (25).

The next point is the computation of the extrema of the radial and polar motions. For the radial motion there are four extrema [see Eq. (90)]: $r_{\rm apo} > r_{\rm peri} > r_3 > r_4$. From Eqs. (19) and (90) we know that these extrema must satisfy the following relations:

$$r_{\rm apo} + r_{\rm peri} + r_3 + r_4 = \frac{2M_\bullet}{1-E^2}\,, \tag{E15}$$

$$\begin{aligned}&r_{\rm apo}r_{\rm peri} + r_3 r_4 + (r_{\rm apo} + r_{\rm peri})(r_3 + r_4)\\ &= \frac{a^2(1-E^2) + L_z^2 + C}{1-E^2}\,,\end{aligned} \tag{E16}$$

$$(r_{\rm apo} + r_{\rm peri})r_3 r_4 + (r_3 + r_4)r_{\rm apo}r_{\rm peri} = \frac{2M_\bullet Q}{1-E^2}\,, \tag{E17}$$

$$r_{\rm apo}r_{\rm peri}r_3 r_4 = \frac{a^2 C}{1-E^2}\,. \tag{E18}$$

From these relations we can find (r_3, r_4) using, for instance, Eqs. (E15) and (E18), to get

$$r_{3,4} = \mathcal{A} \pm \sqrt{\mathcal{A}^2 - \mathcal{B}}\,, \tag{E19}$$

where the plus sign corresponds to r_3, and $\mathcal{A}$ and $\mathcal{B}$ are given by

$$\mathcal{A} = \frac{M_\bullet}{1-E^2} - \frac{r_{\rm apo} + r_{\rm peri}}{2}\,, \tag{E20}$$

$$\mathcal{B} = \frac{a^2 C}{1-E^2}\frac{1}{r_{\rm apo} r_{\rm peri}}\,. \tag{E21}$$

For the polar motion, and using the variable $z = \cos^2\theta$, there are two extrema [see Eq. (91)]: z_+ and z_-, with $z_+ > z_-$. From Eqs. (20) and (91), these extrema satisfy

$$z_- + z_+ = \frac{a^2(1-E^2) + L_z^2 + C}{a^2(1-E^2)}\,, \tag{E22}$$

$$z_- z_+ = \frac{C}{a^2(1-E^2)}\,. \tag{E23}$$

Given z_-, from Eq. (E1), we can find z_+ from any of these two.

Let us now consider the inverse case in which we know the set $(E, L_z, C/Q)$ and we want to find the orbital parameters $(p, e, \theta_{\rm inc})$ and other important quantities. We can start from the equations for the extrema for the radial and polar motions. In the first case, any extrema $r_\star$ will satisfy the following quartic [from Eqs. (19) and (90)]:

$$r_\star^4 + a_3 r_\star^3 + a_2 r_\star^2 + a_1 r_\star + a_0 = 0\,, \tag{E24}$$

where the coefficients are given by:

$$a_3 = -\frac{2M_\bullet}{1-E^2}\,, \quad a_2 = \frac{a^2(1-E^2) + L_z^2 + C}{1-E^2}\,, \tag{E25}$$

$$a_1 = -\frac{2M_\bullet Q}{1-E^2}\,, \quad a_0 = \frac{a^2 C}{1-E^2}\,. \tag{E26}$$

We can solve this quartic equation by steps (see, e.g. [116]). First, let us consider the following cubic equation:

$$y^3 + b_2 y^2 + b_1 y + b_0 = 0\,, \tag{E27}$$

where the coefficients are given by

$$b_2 = \frac{5}{2}\delta\,, \quad b_1 = 2\delta^2 - \epsilon\,, \tag{E28}$$

$$b_0 = \frac{1}{2}\delta^3 - \frac{1}{2}\delta\epsilon - \frac{1}{8}\tau^2\,, \tag{E29}$$

and where δ, τ, and ϵ are the coefficients of the *depressed* quartic $u^4 + \delta u^2 + \tau u + \epsilon = 0$. This equation is associated with the initial quartic via the change of variable: $r_\star = u - a_3/4$. Then, the relations between the coefficients of the depressed quartic and those of the initial quartic are:

$$\delta = -\frac{3}{8}a_3^2 + a_2\,, \quad \tau = \frac{1}{8}a_3^3 - \frac{1}{2}a_2 a_3 + a_1\,, \tag{E30}$$

$$\epsilon = -\frac{3}{256}a_3^4 + \frac{1}{16}a_2 a_3^2 - \frac{1}{4}a_1 a_3 + a_0\,. \tag{E31}$$

Now, let us consider a real solution to the cubic equation above, namely y_1 (a cubic equation with real coefficients always has at least one real root). Then, the four solutions of the initial quartic can be written as follows:

$$r_\star = -\frac{1}{4}a_3 + \frac{1}{2}\left\{ s_1\sqrt{\delta + 2y_1} + s_2\sqrt{-\left(3\delta + 2y_1 + s_1\frac{2\tau}{\sqrt{\delta+2y_1}}\right)}\right\}\,, \tag{E32}$$

where s_1 and s_2 are two independent signs, which lead to the four solutions. We can then immediately identify the extrema $r_{\rm apo} > r_{\rm peri} > r_3 > r_4$ and from Eq. (22) we find e and p.

In the case of the polar motion, things are a bit easier. We need to find the roots of the following quadratic equation for $z_\star = \cos^2\theta$ [from Eqs. (20) and (91)]:

$$z_\star^2 + c_1 z_\star + c_0 = 0\,, \tag{E33}$$

where the two coefficients are given by

$$c_1 = -\frac{a^2(1-E^2) + L_z^2 + C}{a^2(1-E^2)}\,, \tag{E34}$$

$$c_0 = \frac{C}{a^2(1-E^2)}\,. \tag{E35}$$

Then, the two extrema of polar motion are given by

$$z_\pm = -\frac{c_1}{2c_0} \pm \sqrt{\left(\frac{c_1}{2c_0}\right)^2 - c_0}\,, \tag{E36}$$

and from Eqs. (92) and (24) we find the inclination angle $\theta_{\rm inc}$. The inclination angle ι follows from Eq. (25) as before.

Appendix F: Formulae for the Fundamental Frequencies and Periods

In order to give formulae for the fundamental frequencies and periods with respect to the Boyer-Lindquist coordinate time, it is very convenient to start first considering the frequencies and periods with respect to a new time (see [66]): $d/d\lambda \equiv \rho^2 d/d\tau$, which separates the radial and polar dependence in the sense that it terms of λ the equations for r and θ become:

$$\left(\frac{dr}{d\lambda}\right)^2 = R(r)\,, \qquad \left(\frac{d\theta}{d\lambda}\right)^2 = \Theta(\theta)\,, \tag{F1}$$

where $R(r)$ and $\Theta(\theta)$ denote the right-hand sides of Eqs. (19) and (20) respectively. The fundamental frequencies of the radial and polar motions associated with the λ time are $\Upsilon_r = 2\pi/\Lambda_r$ and $\Upsilon_\theta = 2\pi/\Lambda_\theta$, where the periods, denoted by Λ_r and Λ_θ, are given by

$$\Lambda_r = 2\int_{r_{\rm peri}}^{r_{\rm apo}} \frac{dr}{\sqrt{R}}\,, \quad \Lambda_\theta = 2\int_{\theta_{\rm min}}^{\pi-\theta_{\rm min}} \frac{d\theta}{\sqrt{\Theta}}\,. \tag{F2}$$

Then, following [87], the radial and polar frequencies with respect to the λ time can be written as

$$\Upsilon_r = \frac{\pi\sqrt{(1-E^2)(r_{\rm apo}-r_3)(r_{\rm peri}-r_4)}}{2\,\mathcal{K}(k_r)}\,, \tag{F3}$$

$$\Lambda_\theta = \frac{\pi\, a\sqrt{(1-E^2)z_+}}{2\,\mathcal{K}(k_\theta)}\,, \tag{F4}$$

where

$$k_r = \sqrt{\frac{(r_{\rm apo}-r_{\rm peri})(r_3-r_4)}{(r_{\rm apo}-r_3)(r_{\rm peri}-r_4)}}\,,\quad k_\theta = \sqrt{\frac{z_-}{z_+}}\,, \tag{F5}$$

and $\mathcal{K}$ denotes the complete elliptic integral of the first kind (we adopt the definitions of [116] for the elliptic functions).

The right-hand side of the equations for t and ϕ, Eqs. (18) and (21), have the following structure in terms of the λ time

$$\frac{dt}{d\lambda} = T_r(r) + T_\theta(\theta) + aL_z\,, \tag{F6}$$

$$\frac{d\phi}{d\lambda} = \Phi_r(r) + \Phi_\theta(\theta) - aE\,, \tag{F7}$$

and from here we can compute the azimuthal frequency with respect to the λ time,r Υ_ϕ, and also the rate of change of the time t with respect to the time λ, Υ_t, as follows (see [87], but note that there is a typo in the first expression in equation 21, our Eq. (F9), there is a closing square bracket that is located in the wrong place, the one that has $E/2$ as coefficient):

$$\begin{aligned}\Upsilon_\phi = {}& \frac{2a\,\Upsilon_r}{\pi(r_+-r_-)\sqrt{(1-E^2)(r_{\rm apo}-r_3)(r_{\rm peri}-r_4)}}\left\{\frac{2M_\bullet E\, r_+ - aL_z}{r_3-r_+}\left[\mathcal{K}(k_r) - \frac{r_{\rm peri}-r_3}{r_{\rm peri}-r_+}\Pi(-h_+,k_r)\right]\right.\\ & \left. -\ (+\ \longleftrightarrow\ -)\right\} + \frac{2L_z}{\pi a\,\sqrt{(1-E^2)z_+}}\Upsilon_\theta\,,\end{aligned} \tag{F8}$$

$$\begin{aligned}\Upsilon_t = {}& 4M_\bullet^2 E + \frac{2a\,E\sqrt{z_+}}{\pi\sqrt{1-E^2}}\left[\mathcal{K}(k_\theta) - \mathcal{E}(k_\theta)\right]\Upsilon_\theta\\ & + \frac{2\Upsilon_r}{\pi\sqrt{(1-E^2)(r_{\rm apo}-r_3)(r_{\rm peri}-r_4)}}\left\{\frac{E}{2}\left[\left(r_3(r_{\rm apo}+r_{\rm peri}+r_3) - r_{\rm apo}r_{\rm peri}\right)\mathcal{K}(k_r)\right.\right.\\ & \left. + (r_{\rm peri}-r_3)(r_{\rm apo}+r_{\rm peri}+r_3+r_4)\Pi(-h_r,k_r) + (r_{\rm apo}-r_3)(r_{\rm peri}-r_4)\mathcal{E}(k_r)\right]\\ & + 2M_\bullet E\left[r_3\mathcal{K}(k_r) + (r_{\rm peri}-r_3)\Pi(-h_r,k_r)\right]\\ & \left. + \frac{2M_\bullet}{r_+-r_-}\left[\frac{(4M_\bullet^2E - aL_z)r_+ - 2M_\bullet a^2E}{r_3-r_+}\left(\mathcal{K}(k_r) - \frac{r_{\rm peri}-r_3}{r_{\rm peri}-r_+}\Pi(-h_+,k_r)\right)\ -\ (+\ \longleftrightarrow\ -)\right]\right\}\,,\end{aligned} \tag{F9}$$

where $\mathcal{E}$ and Π denote the complete elliptic integrals of the second and third kinds respectively, and

$$h_r = \frac{r_{\rm apo}-r_{\rm peri}}{r_{\rm apo}-r_3}\,, \tag{F10}$$

$$h_\pm = \frac{(r_{\rm apo}-r_{\rm peri})(r_3-r_\pm)}{(r_{\rm apo}-r_3)(r_2-r_\pm)}\,. \tag{F11}$$

From these expressions for the fundamental frequencies and periods with respect to the λ time we can compute the corresponding ones for the Boyer-Lindquist coordinate time t by using the following simple expressions:

$$\Omega_r = \frac{\Upsilon_r}{\Upsilon_t}\,,\quad \Omega_\theta = \frac{\Upsilon_\theta}{\Upsilon_t}\,,\quad \Omega_\phi = \frac{\Upsilon_\phi}{\Upsilon_t}\,, \tag{F12}$$

and

$$T_r = \frac{2\pi}{\Omega_r}\,,\quad T_\theta = \frac{2\pi}{\Omega_\theta}\,,\quad T_\phi = \frac{2\pi}{\Omega_\phi}\,. \tag{F13}$$

Appendix G: Formulae for the Evolution of Circular non-Equatorial Orbits

Here we provide the expressions of the components of the matrix that determines the evolution of the Carter constant and radius of circular non-equatorial orbits in terms of the evolution of the energy and angular momentum component along the spin axis [see Eq. (36)]. The expressions of the c_{AB} $(A,B=1,2)$ and d quantities, as functions of $(M_\bullet, a; E, L_z, C, r_o)$ are:

$$c_{11} = 4E(1-E^2)r_o^6 - 12M_\bullet E r_o^5 + 2E\left[a^2(1-E^2) + 3(C+L_z^2)\right] r_o^4 + 8M_\bullet\left[2a(L_z - aE) - E(C+L_z^2) + a^2E^3\right] r_o^3 + 2a\left[a^3E(1-E^2) + aE(C+L_z^2) + 6M_\bullet^2(aE - L_z)\right] r_o^2 - 4M_\bullet a^2 E\left[(aE-L_z)^2 + C\right] r_o + 4aM_\bullet^2(L_z - aE)\left[(aE-L_z)^2 + C\right] , \quad \text{(G1)}$$

$$c_{12} = 4(1-E^2)L_z r_o^4 - 16M_\bullet(1-E^2)(L_z - aE)r_o^3 + 2\left[6M_\bullet^2(L_z - aE) - L_z(C + L_z^2 + a^2(1-E^2)\right] r_o^2 + 4M_\bullet L_z\left[(aE-L_z)^2 + C\right] r_o - 4M_\bullet^2(L_z - aE)\left[(aE-L_z)^2 + C\right] , \quad \text{(G2)}$$

$$c_{21} = -2\left[E r_o^5 - 3M_\bullet E r_o^4 + 2a^2 E r_o^3 + aM_\bullet(L_z - 2aE)r_o^2 + a^4 E r_o - a^3 M_\bullet(L_z - aE)\right] , \quad \text{(G3)}$$

$$c_{22} = -2a\left[M_\bullet E r_o^2 - aL_z r_o - aM_\bullet(aE - L_z)\right] , \quad \text{(G4)}$$

$$d = 2(1-E^2)r_o^4 - 4M_\bullet(1-E^2)r_o^3 + \left[6M_\bullet^2 - C - L_z^2 + 5a^2(1-E^2)\right] r_o^2 + 2M_\bullet\left[a^2(E^2-3) - 2aL_z E + C + L_z^2\right] r_o + a^4(1-E^2) + a^2(C+L_z^2) - 2M_\bullet^2\left[(aE-L_z)^2 + C\right] . \quad \text{(G5)}$$

[1] C. M. Will, Living Reviews in Relativity, **9** (2006), arXiv:gr-qc/0510072.

[2] N. Yunes and F. Pretorius, Phys. Rev., **D80**, 122003 (2009), arXiv:0909.3328 [gr-qc].

[3] K. Danzmann and A. Rudiger, Class. Quant. Grav., **20**, S1 (2003); K. Danzmann, Advances in Space Research, **32**, 1233 (2003); T. Prince, American Astronomical Society Meeting, **202**, 3701 (2003).

[4] "Laser Interferometer Space Antenna," URLs: `www.esa.int/lisa`, `lisa.jpl.nasa.gov`.

[5] P. Amaro-Seoane *et al.*, Class. Quant. Grav., **24**, R113 (2007), arXiv:astro-ph/0703495.

[6] D. Hils and P. L. Bender, Astrophysical Journal Letters, **445**, L7 (1995); S. Sigurdsson and M. J. Rees, Monthly Notices of the Royal Astronomical Society, **284**, 318 (1997), arXiv:astro-ph/9608093.

[7] M. Freitag, P. Amaro-Seoane, and V. Kalogera, Astrophysical Journal, **649**, 91 (2006), arXiv:astro-ph/0603280; C. Hopman and T. Alexander, Astrophysical Journal Letters, **645**, L133 (2006), arXiv:astro-ph/0603324; D. Merritt, Reports on Progress in Physics, **69**, 2513 (2006), arXiv:astro-ph/0605070.

[8] K. Holley-Bockelmann, J. C. Mihos, S. Sigurdsson, L. Hernquist, and C. Norman, Astrophysical Journal, **567**, 817 (2002), arXiv:astro-ph/0111029; C. Hopman and T. Alexander, *ibid.*, **629**, 362 (2005), arXiv:astro-ph/0503672.

[9] K. P. Rauch and S. Tremaine, New Astronomy, **1**, 149 (1996), arXiv:astro-ph/9603018; C. Hopman and T. Alexander, Astrophysical Journal, **645**, 1152 (2006), arXiv:astro-ph/0601161.

[10] M. C. Miller, M. Freitag, D. P. Hamilton, and V. M. Lauburg, Astrophysical Journal Letters, **631**, L117 (2005), arXiv:astro-ph/0507133.

[11] Y. Levin, (2003), arXiv:astro-ph/0307084; Monthly Notices of the Royal Astronomical Society, **374**, 515 (2007), arXiv:astro-ph/0603583.

[12] N. Yunes, B. Kocsis, A. Loeb, and Z. Haiman, (2011), arXiv:1103.4609 [astro-ph.CO]; B. Kocsis, N. Yunes, and A. Loeb, Phys. Rev. D, **84**, 024032 (2011), arXiv:1104.2322 [astro-ph.GA].

[13] L. S. Finn and K. S. Thorne, Phys. Rev., **D62**, 124021 (2000), arXiv:gr-qc/0007074.

[14] N. Yunes *et al.*, Phys. Rev., **D83**, 044044 (2011), arXiv:1009.6013 [gr-qc].

[15] L. Barack and C. Cutler, Phys. Rev., **69**, 082005 (2004), arXiv:gr-qc/0310125.

[16] N. A. Collins and S. A. Hughes, Phys. Rev., **D69**, 124022 (2004), arXiv:gr-qc/0402063; K. Glampedakis and S. Babak, Class. Quant. Grav., **23**, 4167 (2006), arXiv:gr-qc/0510057; L. Barack and C. Cutler, Phys. Rev., **D75**, 042003 (2007), arXiv:gr-qc/0612029; N. Yunes, C. F. Sopuerta, L. J. Rubbo, and K. Holley-Bockelmann, Astrophys. J., **675**, 604 (2008), arXiv:0704.2612 [astro-ph]; J. Brink, Phys. Rev., **D78**, 102001 (2008), arXiv:0807.1178 [gr-qc]; S. J. Vigeland and S. A. Hughes, **D81**, 024030 (2010), arXiv:0911.1756 [gr-qc]; S. A. Hughes, (2010), arXiv:1002.2591 [gr-qc].

[17] C. F. Sopuerta, Gravitational Wave Notes, **4**, 3 (2010), arXiv:1009.1402 [astro-ph.CO].

[18] S. A. Hughes, AIP Conf. Proc., **873**, 233 (2006), arXiv:gr-qc/0608140.

[19] B. F. Schutz, Class. Quant. Grav., **26**, 094020 (2009).

[20] S. Babak, J. R. Gair, A. Petiteau, and A. Sesana, Class. Quant. Grav., **28**, 114001 (2011), arXiv:1011.2062 [gr-qc]; S. Vigeland, N. Yunes, and L. Stein, Phys. Rev., **D83**, 104027 (2011), arXiv:1102.3706 [gr-qc]; J. R. Gair and N. Yunes, (2011), arXiv:1106.6313 [gr-qc].

[21] J. R. Gair, L. Barack, T. Creighton, C. Cutler, S. L. Larson, E. S. Phinney, and M. Vallisneri, Class. Quant. Grav., **21**, S1595 (2004).

[22] C. L. MacLeod and C. J. Hogan, Phys. Rev., **D77**, 043512 (2008), arXiv:0712.0618 [astro-ph]; J. R. Gair, Class. Quant. Grav., **26**, 094034 (2009),

arXiv:0811.0188 [gr-qc].
[23] C. O. Lousto and Y. Zlochower, Phys. Rev. Lett., **106**, 041101 (2011), arXiv:1009.0292 [gr-qc]; H. Nakano, Y. Zlochower, C. O. Lousto, and M. Campanelli, (2011), arXiv:1108.4421 [gr-qc].
[24] Y. Mino, M. Sasaki, and T. Tanaka, Phys. Rev., **D55**, 3457 (1997), arXiv:gr-qc/9606018.
[25] T. C. Quinn and R. M. Wald, Phys. Rev., **D56**, 3381 (1997), arXiv:gr-qc/9610053.
[26] S. E. Gralla and R. M. Wald, Class. Quant. Grav., **25**, 205009 (2008), arXiv:0806.3293 [gr-qc].
[27] A. Pound, Phys. Rev., **D81**, 024023 (2010), arXiv:0907.5197 [gr-qc].
[28] A. Pound, Phys. Rev., **D81**, 124009 (2010), arXiv:1003.3954 [gr-qc].
[29] K. Glampedakis, Class. Quant. Grav., **22**, S605 (2005), arXiv:gr-qc/0509024.
[30] E. Poisson, Living Rev. Relativity, **7**, 6 (2004), arXiv:gr-qc/0306052.
[31] L. Barack, Class. Quant. Grav., **26**, 213001 (2009), arXiv:0908.1664 [gr-qc].
[32] L. Barack and N. Sago, Phys. Rev. Lett., **102**, 191101 (2009), arXiv:0902.0573 [gr-qc]; Phys. Rev., **D81**, 084021 (2010), arXiv:1002.2386 [gr-qc].
[33] L. Barack, T. Damour, and N. Sago, Phys. Rev., **D82**, 084036 (2010), arXiv:1008.0935 [gr-qc].
[34] L. Barack and N. Sago, Phys. Rev., **D83**, 084023 (2011), arXiv:1101.3331 [gr-qc].
[35] A. L. Tiec *et al.*, (2011), arXiv:1106.3278 [gr-qc].
[36] A. G. Shah, T. S. Keidl, J. L. Friedman, D.-H. Kim, and L. R. Price, Phys.Rev., **D83**, 064018 (2011), arXiv:1009.4876 [gr-qc].
[37] C. F. Sopuerta, P. Sun, P. Laguna, and J. Xu, Class. Quantum Grav., **23**, 251 (2006), gr-qc/0507112; L. Barack and D. A. Golbourn, Phys. Rev., **D76**, 044020 (2007), arXiv:0705.3620 [gr-qc]; L. Barack, D. A. Golbourn, and N. Sago, **D76**, 124036 (2007), arXiv:0709.4588 [gr-qc]; I. Vega and S. Detweiler, **D77**, 084008 (2008), arXiv:0712.4405 [gr-qc]; C. O. Lousto and H. Nakano, Class. Quant. Grav., **25**, 145018 (2008), arXiv:0802.4277 [gr-qc]; P. Canizares and C. F. Sopuerta, J. Phys. Conf. Ser., **154**, 012053 (2009), arXiv:0811.0294 [gr-qc]; Phys. Rev., **D79**, 084020 (2009), arXiv:0903.0505 [gr-qc]; S. E. Field, J. S. Hesthaven, and S. R. Lau, Class. Quant. Grav., **26**, 165010 (2009), arXiv:0902.1287 [gr-qc]; P. Canizares, C. F. Sopuerta, and J. L. Jaramillo, Phys. Rev., **D82**, 044023 (2010), arXiv:1006.3201 [gr-qc]; J. Thornburg, (2010), arXiv:1006.3788 [gr-qc]; P. Canizares and C. F. Sopuerta, Class. Quant. Grav., **28**, 134011 (2011), arXiv:1101.2526 [gr-qc]; N. Warburton and L. Barack, (2011), arXiv:1103.0287 [gr-qc]; S. R. Dolan, B. Wardell, and L. Barack, (2011), arXiv:1107.0012 [gr-qc].
[38] P. C. Peters and J. Mathews, Phys. Rev., **131**, 435 (1963); P. C. Peters, **136**, B1224 (1964).
[39] S. Babak, H. Fang, J. R. Gair, K. Glampedakis, and S. A. Hughes, Phys. Rev., **D75**, 024005 (2007), arXiv:gr-qc/0607007.
[40] N. Yunes, A. Buonanno, S. A. Hughes, M. Coleman Miller, and Y. Pan, Phys. Rev. Lett., **104**, 091102 (2010), arXiv:0909.4263 [gr-qc].
[41] N. Yunes, Gravitational Wave Notes (2010), arXiv:1003.5553 [astro-ph.CO].
[42] S. A. Hughes, Phys. Rev., **D61**, 084004 (2000).
[43] S. A. Hughes, Phys. Rev., **D64**, 064004 (2001).
[44] C. W. Misner, K. Thorne, and J. A. Wheeler, *Gravitation* (W. H. Freeman & Co., San Francisco, 1973).
[45] K. A. Arnaud *et al.*, Class. Quant. Grav., **24**, S551 (2007), arXiv:gr-qc/0701170.
[46] J. R. Gair and K. Glampedakis, Phys. Rev., **D73**, 064037 (2006), arXiv:gr-qc/0510129.
[47] K. S. Thorne, Rev. Mod. Phys., **52**, 299 (1980).
[48] A. Buonanno and T. Damour, Phys.Rev., **D59**, 084006 (1999), arXiv:gr-qc/9811091; **D62**, 064015 (2000), arXiv:gr-qc/0001013; T. Damour, **D81**, 024017 (2010), arXiv:0910.5533 [gr-qc].
[49] R. A. Isaacson, Phys. Rev., **166**, 1263 (1968); **166**, 1272 (1968).
[50] T. Damour, B. R. Iyer, and B. S. Sathyaprakash, Phys. Rev., **D57**, 885 (1998).
[51] T. Tanaka, H. Tagoshi, and M. Sasaki, Prog. Theor. Phys., **96**, 1087 (1996).
[52] Y. Mino *et al.*, Prog. Theor. Phys. Suppl., **128**, 1 (1997).
[53] M. Shibata, M. Sasaki, H. Tagoshi, and T. Tanaka, Phys. Rev., **D51**, 1646 (1995), arXiv:gr-qc/9409054.
[54] E. Poisson, Phys. Rev., **D47**, 1497 (1993).
[55] K. Glampedakis and D. Kennefick, Phys. Rev., **D66**, 044002 (2002), arXiv:gr-qc/0203086.
[56] S. Drasco and S. A. Hughes, Phys. Rev., **D73**, 024027 (2006), arXiv:gr-qc/0509101.
[57] S. Drasco, E. E. Flanagan, and S. A. Hughes, Class. Quant. Grav., **22**, S801 (2005), arXiv:gr-qc/0505075.
[58] S. A. Hughes, S. Drasco, E. E. Flanagan, and J. Franklin, Phys. Rev. Lett., **94**, 221101 (2005), arXiv:gr-qc/0504015.
[59] R. Lopez-Aleman, G. Khanna, and J. Pullin, Class. Quant. Grav., **20**, 3259 (2003), arXiv:gr-qc/0303054.
[60] G. Khanna, Phys. Rev., **D69**, 024016 (2004), arXiv:gr-qc/0309107.
[61] L. M. Burko and G. Khanna, Europhys. Lett., **78**, 60005 (2007), arXiv:gr-qc/0609002.
[62] P. A. Sundararajan, G. Khanna, and S. A. Hughes, Phys. Rev., **D76**, 104005 (2007), arXiv:gr-qc/0703028.
[63] P. A. Sundararajan, G. Khanna, S. A. Hughes, and S. Drasco, Phys. Rev., **D78**, 024022 (2008), arXiv:0803.0317 [gr-qc].
[64] L. Blanchet and T. Damour, Phys. Lett., **A104**, 82 (1984).
[65] A. Pound and E. Poisson, Phys. Rev., **D77**, 044013 (2008), arXiv:0708.3033 [gr-qc].
[66] Y. Mino, Phys. Rev., **D67**, 084027 (2003), arXiv:gr-qc/0302075.
[67] W. L. Burke, J.Math.Phys., **12**, 401 (1971).
[68] L. Blanchet and T. Damour, Phys.Rev., **D37**, 1410 (1988).
[69] L. Blanchet and T. Damour, Annales Poincare Phys. Theor., **50**, 377 (1989).
[70] T. Damour and B. R. Iyer, Ann. Poincare, **54**, 115 (1991).
[71] L. Blanchet, Phys.Rev., **D47**, 4392 (1993).
[72] O. Poujade and L. Blanchet, Phys. Rev. D, **65**, 124020 (2002), arXiv:gr-qc/0112057.
[73] E. E. Flanagan and T. Hinderer, (2010), arXiv:1009.4923 [gr-qc].
[74] E. Poisson, A. Pound, and I. Vega, (2011), arXiv:1102.0529 [gr-qc].

[75] L. Barack, Y. Mino, H. Nakano, A. Ori, and M. Sasaki, Phys. Rev. Lett., **88**, 091101 (2002), arXiv:gr-qc/0111001.

[76] S. Detweiler, Phys. Rev. Lett., **86**, 1931 (2001), gr-qc/0011039.

[77] S. E. Gralla, A. I. Harte, and R. M. Wald, Phys. Rev., **D80**, 024031 (2009), arXiv:0905.2391 [gr-qc].

[78] J. R. Gair, E. E. Flanagan, S. Drasco, T. Hinderer, and S. Babak, Phys.Rev., **D83**, 044037 (2011), arXiv:1012.5111 [gr-qc].

[79] R. P. Kerr, Phys. Rev. Lett., **11**, 237 (1963).

[80] R. Ruffini and J. A. Wheeler, Physics Today, **24**, 30 (1971).

[81] S. Chandrasekhar, *The mathematical theory of black holes* (Oxford University Press, New York, 1992).

[82] R. H. Boyer and R. W. Lindquist, J. Math. Phys., **8**, 265 (1967).

[83] B. Carter, Physical Review, **174**, 1559 (1968); B. Carter, Commun. Math. Phys., **10**, 280 (1968).

[84] J. M. Bardeen, W. H. Press, and S. A. Teukolsky, Astrophys. J., **178**, 347 (1972).

[85] W. Schmidt, Class. Quant. Grav., **19**, 2743 (2002), arXiv:gr-qc/0202090.

[86] S. Drasco and S. A. Hughes, Phys. Rev., **D69**, 044015 (2004), arXiv:astro-ph/0308479.

[87] R. Fujita and W. Hikida, Class. Quant. Grav., **26**, 135002 (2009), arXiv:0906.1420 [gr-qc].

[88] D. Kennefick and A. Ori, Phys. Rev., **D53**, 4319 (1996), arXiv:gr-qc/9512018.

[89] F. D. Ryan, Phys. Rev., **D53**, 3064 (1996), arXiv:gr-qc/9511062.

[90] E. E. Flanagan and T. Hinderer, Phys. Rev., **D75**, 124007 (2007), arXiv:0704.0389 [gr-qc].

[91] B. R. Iyer and C. M. Will, Phys. Rev. Lett., **70**, 113 (1993).

[92] B. R. Iyer and C. M. Will, Phys. Rev., **D52**, 6882 (1995).

[93] L. Blanchet, Phys. Rev., **D55**, 714 (1997), arXiv:gr-qc/9609049.

[94] W. L. Burke, J. Math. Phys., **12**, 401 (1971).

[95] K. G. Arun, L. Blanchet, B. R. Iyer, and M. S. S. Qusailah, (2007), arXiv:0711.0302 [gr-qc].

[96] L. Blanchet, A. Buonanno, and G. Faye, Phys. Rev., **D74**, 104034 (2006), arXiv:gr-qc/0605140.

[97] G. B. Cook and M. A. Scheel, Phys. Rev., **D56**, 4775 (1997).

[98] E. Ruiz, Gen. Rel. Grav., **18**, 805 (1986).

[99] M. Abe, S. Ichinose, and N. Nakanishi, Progress of Theoretical Physics, **78**, 1186 (1987).

[100] E. Poisson, "Post-Newtonian Theory for the Common Reader," Lecture Notes (2007).

[101] L. Blanchet, Living Rev. Relativity, **9**, 4 (2006), arXiv:gr-qc/0202016.

[102] L. E. Kidder, Phys. Rev., **D77**, 044016 (2008), arXiv:0710.0614 [gr-qc].

[103] A. Buonanno, G. B. Cook, and F. Pretorius, Phys. Rev., **D75**, 124018 (2007), arXiv:gr-qc/0610122.

[104] C. Cutler, Phys. Rev., **D57**, 7089 (1998).

[105] B. W. Kernighan and D. M. Ritchie, *The C Programming Language*, 2nd ed. (Prentice Hall, Inc., Englewood Cliffs, NJ, 1988).

[106] M. Galassi, J. Davies, J. Theiler, B. Gough, G. Jungman, M. Booth, and F. Rossi, *GNU Scientific Library Reference Manual*, 2nd ed. (Network Theory Ltd., Bristol, 2006).

[107] R. Bulirsch and J. Stoer, Num. Math., **8**, 1 (1966); J. Stoer and R. Bulirsch, *Introduction to Numerical Analysis* (Springer-Verlag, New York, 1993).

[108] T. Ito and T. Fukushima, Astronomical Journal, **114**, 1260 (1997); T. Fukushima, **112**, 1298 (1996).

[109] W. H. Press, B. P. Flannery, S. A. Teukolsky, and W. T. Vetterling, *Numerical Recipes: The Art of Scientific Computing* (Cambridge University Press, Cambridge (UK) and New York, 1992).

[110] K. Glampedakis, S. A. Hughes, and D. Kennefick, Phys. Rev., **D66**, 064005 (2002), arXiv:gr-qc/0205033.

[111] K. Ganz, W. Hikida, H. Nakano, N. Sago, and T. Tanaka, (2007), arXiv:gr-qc/0702054.

[112] F. D. Ryan, Phys. Rev., **D52**, 5707 (1995).

[113] S. W. Hawking and G. F. R. Ellis, *The Large scale structure of space-time* (Cambridge University Press, Cambridge, 1973).

[114] J. M. Aguirregabiria, L. Bel, J. Martin, A. Molina, and E. Ruiz, Gen. Rel. Grav., **33**, 1809 (2001), arXiv:gr-qc/0104019.

[115] D. C. Wilkins, Phys. Rev., **D5**, 814 (1972).

[116] M. Abramowitz and I. A. Stegun, *Handbook of Mathematical Functions with Formulas, Graphs, and Mathematical Tables* (Dover, New York, 1972).